UNIVERSIDADE FEDERAL DO CEARÁ
CENTRO DE TECNOLOGIA
DEPARTAMENTO DE ENGENHARIA QUÍMICA
PROGRAMA DE PÓS-GRADUAÇÃO EM ENGENHARIA QUÍMICA

FERNANDO JOSÉ SOARES BARROS

CATALYTIC APPLICATION OF LAYERED DOUBLE HYDROXIDES AND FLUOROPEROVSKITES IN GLYCEROL OLIGOMERIZATION

FORTALEZA

2019

FERNANDO JOSÉ SOARES BARROS

CATALYTIC APPLICATION OF LAYERED DOUBLE HYDROXIDES AND FLUOROPEROVSKITES IN GLYCEROL OLIGOMERIZATION

Tese apresentada ao Programa de Pós-Graduação em Engenharia Química da Universidade Federal do Ceará, como requisito parcial à obtenção do título de Doutor em Engenharia Química. Área de concentração: Processos Químicos e Bioquímicos.

Orientador: Prof. Dr. Rodrigo Silveira Vieira.
Coorientador: Prof. Dr. Francisco Murilo Tavares de Luna

FORTALEZA

2019

Dados Internacionais de Catalogação na Publicação
Universidade Federal do Ceará
Biblioteca Universitária
Gerada automaticamente pelo módulo Catalog, mediante os dados fornecidos pelo(a) autor(a)

B277c Barros, Fernando José Soares.

Catalytic application of layered double hydroxides and fluoroperovskites in glycerol oligomerization / Fernando José Soares Barros. – 2019.

120 f. : il. color.

Tese (doutorado) – Universidade Federal do Ceará, Centro de Tecnologia, Programa de Pós-Graduação em Engenharia Química, Fortaleza, 2019.

Orientação: Prof. Dr. Rodrigo Silveira Vieira.

Coorientação: Prof. Dr. Francisco Murilo Tavares de Luna.

1. Glycerol. 2. Oligomerization. 3. Diglycerol. 4. Layered double hydroxide. 5.Fluoroperovskite. - Produção. I. Título.

CDD 660

FERNANDO JOSÉ SOARES BARROS

CATALYTIC APPLICATION OF LAYERED DOUBLE HYDROXIDES AND FLUOROPEROVSKITES IN GLYCEROL OLIGOMERIZATION

Thesis submitted to the Graduate Program in Chemical Engineering as partial fulfillment of the requirements for the degree of Doctor in Chemical Engineering at Universidade Federal do Ceará.

Approved on: 01/02/2019.

DOCTORAL COMITEE

_____

Prof. Dr. Rodrigo Silveira Vieira (Thesis Advisor)
Universidade Federal do Ceará (UFC)

_____

Prof. Dr. Diana Cristina Silva de Azevedo
Universidade Federal do Ceará (UFC)

_____

Prof. Dr. Antoninho Valentini
Universidade Federal do Ceará (UFC)

_____

Prof. Dr. Rinaldo dos Santos Araújo
Instituto Federal de Educação, Ciência e Tecnologia do Ceará (IFCE)

_____

Prof. Dr. Moisés Bastos Neto
Universidade Federal do Ceará (UFC)

ACKNOWLEDGMENTS

Firstly, I would like to thank God and St. George for all the blessings and protection. All my gratitude to my parents Marlene Nascimento and José Barros Neto, my aunt Maria Gomes da Silva, my sister Val Barros and my cousin Deilson Gomes who supported me throughout my academic trajectory.

I would like to thank my dear friends, Camila Trigueiro, Larissa Viana, Wanna Guedes, Paula Beatricy, Denyse Gaspar, Jonathan Wallace, Heriverto Nunes, Janailton Santos, Madson Santos, Lice Rabelo, Ediane Karlésia, Isaque Felix, Joaquim Lopes, Niedja Vasconcelos and Rayane Claudino for encouraging me through this venture.

I wish to express my sincere thanks to my advisor, Professor Rodrigo Vieira, for the valuable guidance and encouragement over the period of this research.

I am also grateful to Professor Johannes Lercher, from Technische Universität München, for the supervision during my period in Munich. My gratitude to the TCII team members for their scientific contributions, specially Eszter Barath and Yue Liu.

My acknowledgements to Professor Enrique Castellón (University of Malaga), Ramón Tost and Juan Cecilia for the suggestions and support.

I am also grateful to all PGEQ faculty members for their contributions over disciplines and internships. Special thanks to Professor Diana Azevedo, Professor Alcinéia Oliveira and Professor Murilo Luna for the contributions to this work.

I gratefully acknowledge the staff of the laboratory of lubricants, NPL, who helped me get results of better quality. Special mention to Jane Eloi, Rosy Arcanjo, Aurélia Oliveira and my undergraduate students: Matheus Oliveira, Clarissa Dantas, Lara Timbó and Cammilla Benício.

My deepest gratitude to the UFC laboratories: LRX, *Central Analítica*, LPA-CO_2, Infrared Laboratory and Laboratory of Adsorption and Catalysis (LANGMUIR). I am also thankful to Embrapa Agroindústria Tropical for the ICP-OES analysis.

I gratefully acknowledge the funding received towards my doctoral research from Funcap. I am also grateful to Facepe for the support for my period at CETENE and the Erasmus SMART2 program for funding my period at TUM.

“If something is perfect, then there is nothing left. There is no room for imagination. No place left for a person to gain additional knowledge or abilities. Do you know what that means? For scientists such as ourselves, perfection only brings despair. It is our job to create things more wonderful than anything before them, but never to obtain perfection. A scientist must be a person who finds ecstasy while suffering from that antimony.”

Tite Kubo

RESUMO

O glicerol tornou-se um importante insumo para as indústrias devido seu baixo preço, alta disponibilidade e à possibilidade de produzir diversos compostos de valor agregado. Os seus oligômeros, diglicerol e triglicerol, encontram aplicações em polímeros, alimentos e cosméticos. Neste estudo, hidróxidos duplo lamelares (HDLs) e fluoroperovskitas ambos contendo Mg/Al, Zn/Al e Co/Al foram obtidos por coprecipitação e utilizados como catalisadores na oligomerização do glicerol. Foi avaliada a modificação dos HDLs por reidratação via ultrassom e agitação mecânica. Foram preparados também, catalisadores usando os materiais anteriores como suportes para o acetilacetonato de cobalto (II). Os sólidos foram caracterizados por espectrometria de emissão óptica por plasma acoplado indutivamente (ICP-OES), difração de raios X, espectroscopia de infravermelho com transformada de Fourier, análise termogravimétrica (ATG), propriedades texturais por adsorção de N_2, microscopia eletrônica de transmissão e de varredura (MET e MEV) e espectroscopia de fotoelétrons excitados por raios X (XPS). A basicidade foi estudada por dessorção termoprogramada de CO_2 e por adsorção irreversível de ácidos fortes medida com espectroscopia no ultravioleta visível. A influência da quantidade de catalisador, tempo de reação e temperatura foram avaliadas. Os produtos foram analisados por cromatografia gasosa e a ocorrência de lixiviação foi verificada por ICP-OES. Os catalisadores pós uso reacional foram estudados por ATG e XPS. Para o HDL de Mg/Al, foi definida uma estratégia de modificação por meio de adição de ácido acético. O melhor desempenho alcançado neste grupo levou a 64% de conversão do glicerol (X_{Gly}), 37% de seletividade para diglicerol (S_{di}) e 4 ciclos de reação (reação com 4% de cat., a 240 °C por 8 horas). Para o grupo Zn/Al, o uso de fluoroperovskita foi mais efetivo, levando a 68% de X_{Gly}, 27% de S_{di} e uso por 4 ciclos (4% de cat., a 230 °C e 18 horas). Dentre os materiais impregnados com acetilacetonato de cobalto(II), o suporte de HDL de Mg/Al apresentou melhor desempenho com 68% X_{Gly}, 27% de S_{di} e 4 ciclos reacionais (4% de cat., 240 °C e 8 horas). A desativação dos catalisadores está relacionada as severas condições reacionais que acarretaram a perda espécies ativas ou ao bloqueio destas por impurezas. Apesar disso, as diversas estratégias adotadas mostraram ser viável produzir oligômeros do glicerol por catálise heterogênea.

Palavras-chave: Glicerol. Oligomerização. Diglicerol. Hidróxido duplo lamelar. Fluoroperovskita.

ABSTRACT

Glycerol has become an important feedstock for industries due to its low price, high availability and the possibility of producing several value-added compounds. Its oligomers, diglycerol and triglycerol, find applications in polymers, foods and cosmetics. In this study, layered double hydroxides (LDHs) and fluoroperovskites, both containing Mg/Al, Zn/Al and Co/Al were obtained by coprecipitation and used as catalysts in glycerol oligomerization. Modification of LDHs by rehydration via ultrasound and mechanical agitation was evaluated. Catalysts using the above-mentioned materials as support for cobalt(II) acetylacetonate were prepared as well. The solids were characterized by inductively coupled plasma optical emission spectrometry (ICP-OES), X-ray diffraction, Fourier transform infrared spectroscopy, thermogravimetric analysis (TGA), textural properties by nitrogen adsorption, transmission electron microscopy (TEM), scanning electron microscopy (SEM) and X-ray photoelectron spectroscopy (XPS). Basicity was studied by temperature-programmed desorption of CO_2 and irreversible adsorption of strong acids measured with ultraviolet-visible spectroscopy. The influence of catalyst loading, reaction time and temperature were evaluated. The products were analyzed by gas chromatography and the occurrence of leaching was verified by ICP-OES. The spent catalysts were studied by TGA and XPS. For Mg/Al LDH, a modification strategy was developed with the addition of acetic acid. The best performance achieved in this group led to 64% of glycerol conversion (X_{Gly}), 37% of diglycerol selectivity (S_{di}) and 4 reaction cycles (reaction with 4% cat., at 240 °C for 8 hours). For Zn/Al group, the use of fluoroperovskite was more effective, leading to 68% of X_{Gly}, 27% S_{di} and 4 cycles (4% cat., at 230 °C and 18 hours). Among the materials impregnated with cobalt(II) acetylacetonate, the Mg/Al LDH support showed better performance with 68% X_{Gly}, 27% S_{di} and 4 cycles (4% cat., 240 ° C and 8 hours). Catalyst deactivation was related to the harsh reaction conditions, that led to the loss of active species or their blockage by impurities. Nevertheless, the several strategies adopted showed that it is viable to produce glycerol oligomers with heterogeneous catalysis.

Keywords: Glycerol. Oligomerization. Diglycerol. Layered double hydroxide. Fluoroperovskite.

LIST OF FIGURES

LIST OF TABLES

LIST OF SYMBOLS AND ABBREVIATIONS

BET	Brunauer, Emmet e Teller
BJH	Barrett-Joyner-Halenda
BSTFA	N,O-Bis(trimethylsilyl)trifluoroacetamide
CEG	CaO from calcined eggshell
CD	Calcined dolomite
CO_2- TPD	Temperature-Programmed Desorption of Carbon Dioxide
CoAS	Co/Al layered double hydroxide
CoAC450	CoAS calcined at 450 °C for 24 hours
CoAC700	CoAS calcined at 700 °C for 24 hours for 6 hours
$Co(acac)_2$	Cobalt(II) acetylacetonate
Co/FPMAC	$Co(acac)_2$ impregnated over FPMAC
Co/FPZAC	$Co(acac)_2$ impregnated over FPZAC
Co/MAS	$Co(acac)_2$ impregnated over FPMAS
Co/ZAC	$Co(acac)_2$ impregnated over ZAC
DTG	Differential Thermogravimetric Analysis
D_P	Average diameter of pores
EDX	Energy Dispersive X-ray Spectroscopy
FPCoAC	FPCoAS calcined at 450 °C, 24 hours.
FPCoAS	solid obtained by coprecipitation of $Co(NO_3)_2.6H_2O$, $Al(NO_3)_3.9H_2O$, KF and K_2CO_3
FPCuAC	FPCuAS calcined at 450 °C,24 hours
FPCuAS	solid obtained by coprecipitation of $Cu(NO_3)_2.6H_2O$, $Al(NO_3)_3.9H_2O$, KF and K_2CO_3
FPMAC	FPMAS calcined at 450 °C, 24 hours
FPMAS	solid obtained by coprecipitation of $Mg(NO_3)_2.6H_2O$,$Al(NO_3)_3.9H_2O$, KF and K_2CO_3
FPZAC	FPZAS calcined at 450 °C,24 hours

FPZAS	solid obtained by coprecipitation of $Zn(NO_3)_2.6H_2O$, $Al(NO_3)_3.9H_2O$, KF and K_2CO_3
FTIR	Fourier-Transform Infrared Spectroscopy
GC-FID	Gas Chromatography with Flame Ionization Detector
ICP-OES	Inductively Coupled Plasma - Optical Emission Spectrometry
IUPAC	International Union of Pure and Applied Chemistry
JCPDS	Joint Committee on Powder Diffraction Standards
k	Reaction rate constant
LDH	Layered double hydroxide
MAC	MAS calcined at 450 °C for 24 hours
MAM24	MAC rehydrated under mechanic stirring for 24 hours
MAM60	MAC rehydrated under mechanic stirring for one hour
MAS	Mg/Al layered double hydroxide
MAU30	MAC rehydrated under ultrasound for one 30 minutes
MAU30P	MAU30 after addition of acetic acid
MAU60	MAC rehydrated under ultrasound for one hour
S_{BET}	Surface area by BET method
S_{di}	Selectivity to diglycerol
SEM	Scanning Electron Microscopy
S_{tri}	Selectivity to triglycerol
TGA	Thermogravimetric Analysis
TEM	Transmission Electron Microscopy
UFC	Universidade Federal do Ceará
UV-Vis	Ultraviolet-visible spectroscopy
V_P	Average volume of pores
XRD	X -Ray Diffraction
XPS	X-Ray Photoelectron Spectroscopy
X_{Gly}	Glycerol conversion

Y_{di}	Yield of diglycerol
Y_{tri}	Yield of triglycerol
ZAC	ZAS calcined at 450 °C for 24 hours
ZAM24	ZAC rehydrated under mechanic stirring for 24 hours
ZAM60	ZAC rehydrated under mechanic stirring for one hour
ZAS	Zn/Al layered double hydroxide
ZAU30	ZAC rehydrated under ultrasound for 30 minutes
ZAU60	ZAC rehydrated under ultrasound for one hour

CONTENTS

1 INTRODUCTION

The changes in the fossil fuels scenario that arises from the depleting of petroleum reserves allied with the increasing concern over the effects of the emission of hazardous substances into the atmosphere have brought attention to renewable energies. The production of biodiesel appears as an interesting option, usually this fuel is produced by transesterification of vegetable oils or animal fats , resulting in at least 10% of glycerol as by-product (ANITHA; KAMARUDIN; KOFLI, 2016; HE; MCNUTT; YANG, 2017). The increased biodiesel production results in a surplus of glycerol, thus the search for routes for its valorization is of utmost importance.

Glycerol chemical structure makes it suitable for several reactions. The production of glycerol oligomers by etherification has a growing interest in recent years due to their potential of replace petrochemical-based glycol ether, being a bio based alternative with similar physicochemical properties and reduced toxicity (SUTTER *et al.*, 2015). Glycerol oligomers are also used in cosmetics, polymers, food, lubricants and drug delivery systems due to properties such as biocompatibility and thermal stability (CIRIMINNA *et al.*, 2015; SIVAIAH *et al.*, 2012).

Typically, basic homogeneous catalysis in this reaction for instance K_2CO_3, Na_2CO_3 and $CsHCO_3$ have been employed, (SUTTER *et al.*, 2015). The search for heterogeneous catalysts with high activity and selectivity to the oligomers is a major challenge. The heterogeneous processes have several advantages, such as ease of separation, recycling of catalytic systems and high selectivity (ZHOU *et al.*, 2008).

Layered double hydroxides (LDH) are being widely studied in several chemical reactions as solid catalysts. This layered material is also known as hydrotalcite or anionic clay and is composed of positively charged double hydroxide layers with interlayer charge-balancing anions and water molecules. The thermal decomposition of LDH leads to the formation of mixed oxides. This material exhibit the property of "memory effect", which is the reconstruction of the layered structure after its collapse by calcination, this process can be performed by putting the mixed oxides in contact with aqueous solution of several anions (TAKEHIRA, 2017; WANG *et al.*, 2016).

Perovskites is another class of materials that have attracted attention in catalysis, it has the chemical formula ABO_3, where A is the larger cation and B is the smaller cation. Their application as catalysts takes advantage of their good thermal stability and the possibility of tuning their properties by partial or full substitution of A

or B by a large number of chemical elements. Several closely related layered structures or defective structures are also referred as perovskite-type materials. Among the non-oxide ones , there are the halide perovskites ABX_3 (X, halide) such as fluoroperovskites (KUBICEK; BORK; RUPP, 2017; POLO-GARZON; WU, 2018).

1.1 Objective

The main objective of this study is to evaluate the use of layered double hydroxides and fluoroperovskites containing Mg, Al, Zn, Co or Cu as catalysts for glycerol oligomerization.

The specific objectives are:

• To synthesize base heterogeneous catalysts from layered double hydroxide containing Mg, Co or Zn as divalent cation and Al as trivalent cation;

• Evaluate the impact of the rehydration of Mg/Al and Zn/Al LDH's on its catalytic activity for glycerol oligomerization;

• Compare the activity of LDHs and fluoroperovskites;

• Evaluate the use of LDHs and fluoroperovskites as support for Cobalt (II) acetylacetonate;

• Characterize the properties of the catalysts (structural, thermal, textural and acidity-basicity);

• Evaluate the reuse and stability of the catalysts;

1.2 Outline

This thesis is comprised by a literature review, "Material and methods" (catalysts synthesis and characterization, tests of activity for glycerol oligomerization, characterization of reaction products, reusability and stability of the catalysts), followed by "Results and discussion" (divided in three Sections) and conclusion. The literature review addresses the relevant aspects that have motivated this research. Initially, the impacts of the increasing amount of glycerol from the biodiesel industries on the market will be discussed..Also, the different reactional routes for the valorization of glycerol will be presented with emphasis in glycerol oligomerization. The properties and uses of glycerol oligomers will be highlighted, as well as recent advances related to this reaction via homogeneous or heterogenous catalysis. Finally, the structure and the main properties

of layered double hydroxides and fluoroperovskites will be presented alongside with recent works regarding their application in catalysis.

The Section 4.1, "Enhancing the catalytic activity of Mg/Al layered double hydroxide for glycerol oligomers production", will discuss the changes in the materials properties and activity for glycerol oligomerization arising from the LDH modification through calcination followed by rehydration, via mechanic stirring or ultrasound. Based on these results, the development of a modification strategy to adjust the properties of the catalyst is reported. Section 4.2, "Catalytic application of Zn/Al layered double hydroxides and fluoroperovskites in glycerol oligomerization" will report the influence of rehydration in Zn/Al LDH activity for glycerol etherification, in contrast with the results obtained in Section 4.1. Then, to assess the effect of fluorine , in opposition to the hydroxyls and carbonate anions of the previous sections, a series of fluorinated materials (with Mg/Al, Zn/Al, Co/Al and Cu/Al) will be discussed**.** Section 4.3 "Oligomerization of glycerol catalyzed by Co/Al LDH and $Co(acac)_2$ supported on LDH and fluoroperovskites" comprises the preparation, characterization and catalytic application of mixed oxides derived from Co/Al LDH, as well as cobalt (II) acetylacetonate supported on Mg/Al and Zn/Al in the forms of LDH, mixed oxide and fluoroperovskite.

2 LITERATURE REVIEW

2.1 Glycerol market: surplus and valorization opportunities

Glycerol, or propan-1,2,3triol (Figure 2.1), is a colorless, odorless and viscous liquid. It has three hydroxyl groups, which are responsible for its solubility in water and in different polar compounds, such as methanol, ethanol and pyridine. Glycerol backbone is the main component of all lipids, known as triglycerides, present on vegetable oils and animal fats (HEJNA *et al.*, 2016).

Figure 2. 1 - Molecular structure of glycerol.

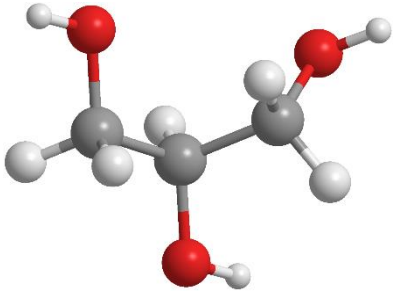

Source: Author.

A versatile material, glycerol can be used as a humectant in meats and cheeses, and also as a solvent, sweetener and preservative in beverages and foods, (MONTEIRO *et al.*, 2018). Use on personal care formulations and drugs/pharmaceutics takes an expressive share of glycerol market, besides minor amounts in explosives and tobacco industries. Glycerol can also be added to animal food, where it reduces the emission of dust and keeps the food in a moist state. It has some beneficial influence on the taste and promotes the food intake (MARTIN; RICHTER, 2011).

It is important to notice that glycerol produced in the biodiesel industry is known as “crude glycerol”, it displays a dark coloration, water content and contains impurities such as methanol, fatty acid methyl esters and salts. The amount of these undesired compounds can vary from 20% to 60%, depending on the raw material, reaction process and purification steps. Due to such impurities, the refining cost of crude glycerol is very high, which turns its use in the traditional industries infeasible, despite its low market price (HE; MCNUTT; YANG, 2017; MONTEIRO *et al.*, 2018).

In 2016 more than 30.8 million m^3 of biodiesel were produced, an increase of 7.5% in comparison to 2015 and the largest producers were the United States and Brazil,

followed by Germany, Indonesia and Argentina. The boom in the biodiesel industry means an increase in surplus production of glycerol. In 2011, it was estimated that from a total of 5.1 million tons of glycerol just 2 million tons (or just 40%) of it were used, therefore a surplus of 3 million tons. Among European Commission directives is a goal of increasing the proportion of biofuels in use, which has led to estimates that global production of glycerol will reach 7.66 million tons in 2020 (MONTEIRO *et al.*, 2018). The glycerol market is intricate because of its price fluctuations, the high number of applications and a complex supply market. With biodiesel industry being the leading source, glycerol market is expected to reach USD 2.52 billion by 2020 (ANITHA; KAMARUDIN; KOFLI, 2016; HE; MCNUTT; YANG, 2017).

The economic feasibility of biodiesel industry faces the challenge of dealing with the glycerol surplus. Transforming the conventional biodiesel industry into an integrated biorefinery, by producing valuable chemicals and fuels from crude glycerol offers an excellent opportunity to improve economic viability and also to provide a replacement for fossil-based products (CHEN; LIU, 2016; GARGALO *et al.*, 2016; HE; MCNUTT; YANG, 2017).

2.2 Glycerol oligomerization

Glycerol is suitable for several chemical reactions, such as oxidation, dehydration, transesterification, acetalization, esterification and etherification. Table 2.1 summarizes a series of glycerol valorization routes and recent works on each of them. A large portfolio of compounds for pharmaceutical application, cosmetics, additives, surfactants and polymers can be produced by the chemical conversion of glycerol.

The etherification of glycerol is possible via three different reactions, leading to alkyl ethers of glycerol, alkenyl ethers of glycerol and glycerol oligomers (BEHR *et al.*, 2008). In their comprehensive review Martin and Richter (2011) pointed out that the reaction of glycerol with itself to form oligomers can be designated as oligomerization to avoid confusion, since the other paths are most often understood as etherification. Is important to notice that the designation of oligomers obtained via condensation of 2, 4, or 6 glycerol molecules as “polyglycerols” was used for long time in the chemical industry and leads to confusion with truly polymeric polyglycerol formed by hyperbranched polymerization of glycidol (CIRIMINNA *et al.*, 2015).

Table 2. 1 - Chemical routes for the valorization of glycerol.

Product	Process	Applications	References
Latic acid	Oxidation	Acidulant and/or a conservative for food; Pharmaceuticals; Cosmetics; Textiles and leather; Biodegradable polymers.	ARCANJO *et al.*, (2017); MARQUES *et al.*, (2015)
Acrolein	Dehydration	Aquatic biocide to control the growth of algae; Precursor of acrylic acid, acrylic acid esters and detergents.	CECILIA *et al.*, (2015); SANCHO *et al.*, (2015)
Glycerol carbonate	Transesterification with dimethyl carbonate	Solvent in the cosmetics industry; Coatings and detergents; Polycarbonate; Polyurethane.	ALGOUFI; KABIR; HAMEED, (2017); STEFANUS *et al.*, (2011)
Acetals and ketals	Acetalization	Biodiesel additive; Surfactants, flavors and scents; Low-toxic solvent; Water-based inks.	CHEN *et al.*, (2017); SONAR *et al.*, (2017)
Glycerine acetate	Esterification with acetic acid	Additive for biodiesel and gasoline; Cosmetics and medicines Biodegradable polyesters	LENG *et al.*, (2016); POPOVA *et al.*, (2014)

Source: Author.

2.2.1 Application and uses of glycerol oligomers

The properties of glycerol and its oligomers are summarized in Table 2.2. The increase of molecular weight changes the polarity, thus low oligomers are more hydrophilic than the higher ones and have a better solubility in polar solvents. The higher

degree of oligomerization is often followed by changes in coloration, from colorless (glycerol) to dark yellow, and is presumably due to side reactions. The oligomers have higher refractive index than glycerol, which represents benefits for the formulation of clear gels (MARTIN; RICHTER, 2011).

Table 2. 2 - Physical data of glycerol, diglycerol and triglycerol.

	Molecular formula	**Molecular weight ($g.mol^{-1}$)**	**Refractivity n^{20}_D (-)**	**Density ($g.cm^{-3}$)**	**Boiling point (ºC) /(Pa)**
Glycerol	$C_3H_8O_3$	92	1.4720	1.2560	290
Diglycerol	$C_6H_{14}O_5$	166	1.4897	1.2790	205/133
Triglycerol	$C_9H_{20}O_7$	240	1.4901 (40ºC)	1.2646 (40ºC)	> 250/13.3

Source: Adapted from (MARTIN; RICHTER, 2011).

The applications of glycerol oligomers include lubricants, dispersants and drug delivery systems. In cosmetics, diglycerol is responsible for enhancing fragrance, flavor impact and longevity. The food industry includes diglycerol in the production of emulsifiers, due to the possibility of controlling their hydrophilic–lipophilic balance. Diglycerol is used on the polymer industry in the production of plasticizer, thermoplastic, polyurethanes and polyesters. (MARTIN; RICHTER, 2011; SIVAIAH *et al.*, 2012) .

According to Sutter *et al.* (2015) , the interest for glycerol oligomers has grown in recent years due to their potential to replace petrochemical-based glycol ethers. The latter are widely used in paints, solvents and cleaning formulations. However, some of them are toxic such as short ethylene glycols.

2.2.2 Recent developments in catalyzed glycerol oligomerization

Studies of glycerol oligomerization in homogeneous phase found for acid catalysts, e.g H_2SO_4, fast routes with a lack of selectivity (MEDEIROS *et al.*, 2009). On base catalysis side, a loss on diglycerol selectivity at complete glycerol conversion was observed for $CsHCO_3$ (RICHTER *et al.*, 2008). Selectivity is an issue in both cases, since acid catalysts present side reactions, such as dehydration to acrolein, and base catalysts displays low selectivity in higher conversions rates.

Heterogeneous catalysts application in glycerol oligomerization is an emerging research topic due to advantages such as less purification steps and recyclability. Basic heterogeneous catalysts, such as alkaline earth oxides (CaO, SrO and BaO) and Cs supported on MCM-41, have been studied (POUILLOUX *et al.*, 2002;

RUPPERT *et al.*, 2008). Acid heterogeneous catalysis was also tested by using materials such as zeolites (COTTIN *et al.*, 1998; ESHUIS; LAAN; POTMAN, 1997).

Ruppert *et al.* (2008) have proposed a mechanism for glycerol oligomerization (Figure 2.2), in which Lewis basic site (oxygen anions) attacks a hydroxyl group of a glycerol molecule, extracting a proton. Then, an unsaturated metal site (Lewis acid site) located on the surface of the alkaline earth oxide is able to activate a hydroxyl group of another glycerol molecule, which is attacked by the nucleophilic oxygen obtained in the first step, leading to a diglycerol molecule. The formation of triglycerol and higher oligomers are consecutive reactions.

Figure 2. 2 - Mechanism for glycerol etherification.

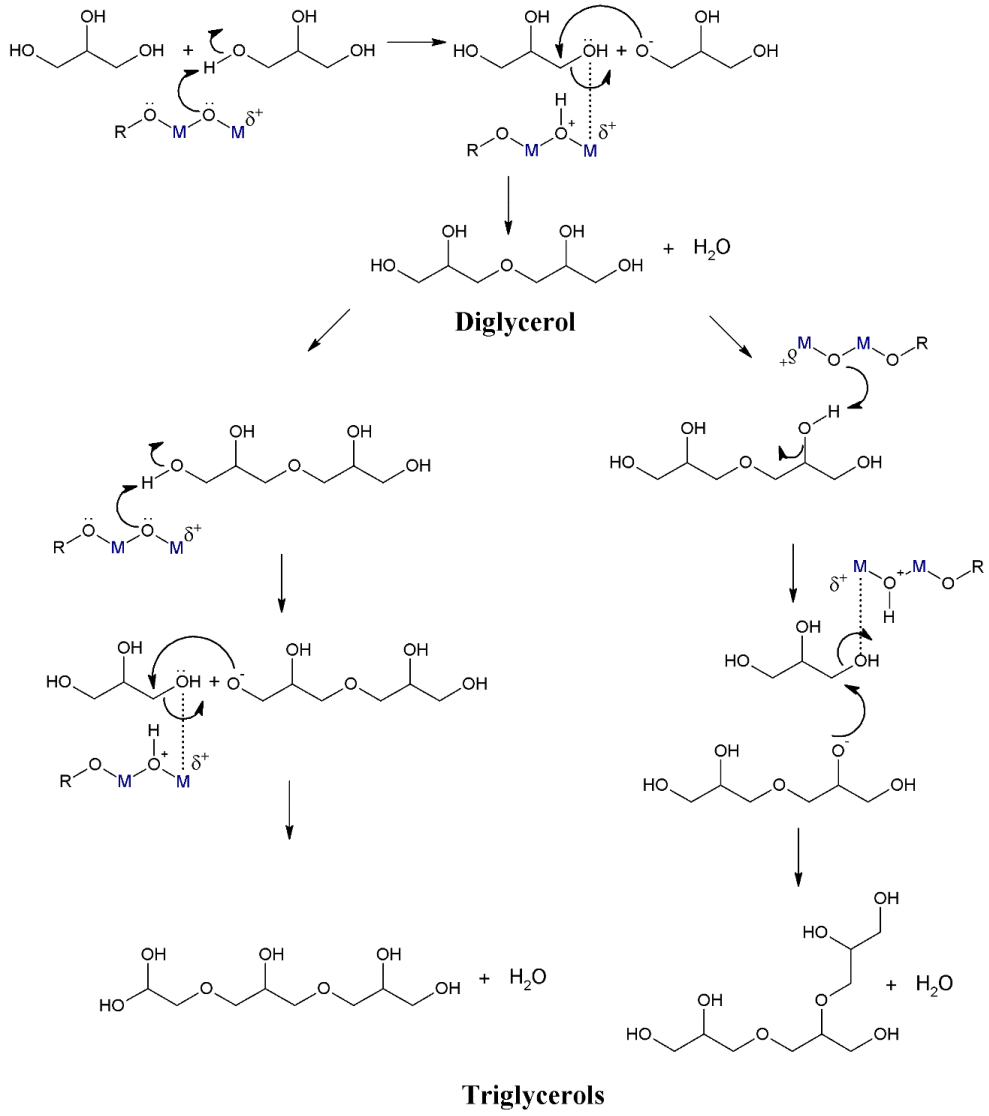

Source: BARROS *et al.* (2018) based on RUPPERT *et al.*(2008).

According to Sutter *et al.* (2015), the main difficulty for the direct oligomerization of glycerol is to control the degree of polymerization and regioselectivity (linear, branched, cyclic polymers) to form a well-defined oligomer.

In our previous works, low cost catalysts were employed by using calcium natural sources, such as waste eggshells and dolomite (BARROS *et al.* 2017; BARROS *et al.* 2018). Both materials displayed glycerol conversions around 80% and high oligomers yield. However, leaching of Ca species was expressive for the material derived from eggshells, and was responsible for calcined dolomite deactivation over recycling.

The development of catalysts with attractive price, activity and stability is a challenge to the production of glycerol oligomers. Recent works have proposed new approaches to deal with these issues. However, most of the works with heterogeneous catalysts did not present recycling tests.

Sayoud *et al.* (2015) studied homogeneous acid catalysts (metal triflates and triflimidates) for the oligomerization of glycerol. They report that under optimized conditions (150 °C, 6 h, 1.4 mol%), $Al(TFSI)_3$ led to a glycerol conversion of 80% with selectivity to oligoglycerols higher than 90%.

Kirby *et al.* (2015) reported the selective etherification of glycerol to higher oligomers in the presence of Ca colloidal particles synthesized by dispersing CaO as nanoparticles or thin films onto a carbon nanofiber support. The authors addressed that at Ca loadings of 5 mmol Ca and higher, calcium colloids were present and contributed to catalysis on top of the homogeneous reaction.

The synthesis of glycerol oligomers in a continuous flow reactor using K_2CO_3 as homogeneous catalyst was studied by Galy *et al.* (2017). Cyclic mode combined with short path distillation, afforded a mixture of oligomers with the distribution: glycerol dimer (20 wt%), trimer (21 wt%), tetramer (16 wt%) and pentamer (11 wt%).

The use of microwaves as a heat source for the etherification of glycerol to polyglycerols with sodium carbonate as a catalyst was demonstrated by Bookong,Ruchirawat and Boonyarattanakalin (2015). Under optimized conditions (270 °C, 1 h, 3 wt% cat.), glycerol conversion was of 97%, the combined yield of diglycerols, triglycerols, and tetraglycerols was 70% and the selectivity to diglycerol 7%.

Lee *et al.*(2018) recently addressed the catalytic activities of alkali metal-acetate salts (LiOAc, NaOAc, and KOAc) for glycerol oligomerization. The less basic catalysts showed higher selectivity to the oligomers. A half mol % of LiOAc (reaction at

260 °C and 6 h) exhibited selectivity to di and triglycerol as 52.5 and 30.4% for glycerol conversion of 66.7%.

2.3 Layered double hydroxides

Layered double hydroxides (LDHs) represented in Figure 2.3, have the general formula $[M^{II}_{1-x}M^{III}_{x}(OH)_2]^{x+}[A_{x/n}{}^{n-}\cdot yH_2O]^{x-}$, where x usually has values between 0.25 and 0.33, M^{II} and M^{III} are the divalent and trivalent metal cations and A^{n-} is the n-valent anion (ZHANG *et al.*, 2015). Their layered structure is composed of positively charged metal hydroxide sheets compensated by charge-balancing anions and water present in the interlayer spaces. In the past years, these compounds have been used in the form of catalysts, adsorbents and ionic exchangers (DAS; DAS; PARIDA, 2003; LIMA *et al.*, 2012; MEHER *et al.*, 2009).

Figure 2. 3 - Structure of a layered double hydroxide (LDH).

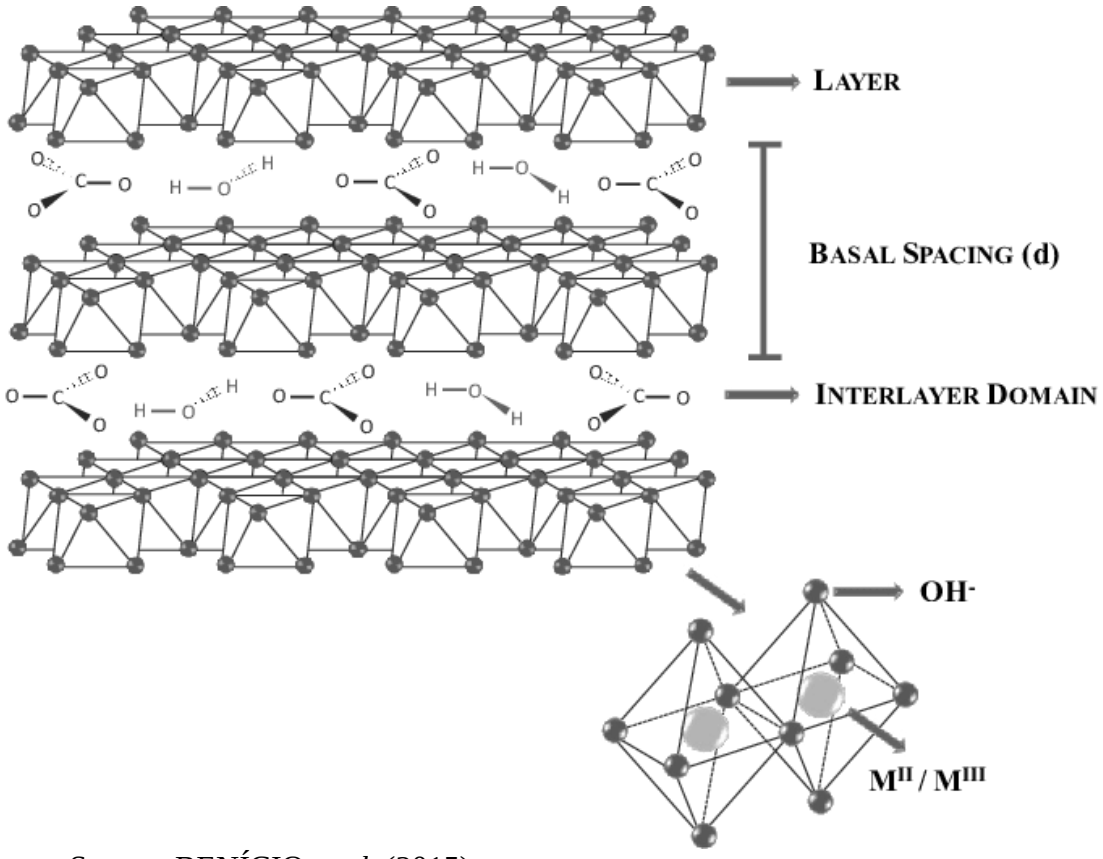

Source: BENÍCIO *et al.* (2015).

LDHs and their derivatives have been intensively investigated in recent years as catalysts and catalyst supports. This mineral has a large surface area and its acidic/basic properties can be tuned by modifying its composition. LDHs can be used as catalysts

support either by adsorbing the catalyst in the anionic form on the surface of the material or in a second form by inserting the catalyst between the lamellae. They may also serve as precursors, and the most common way of preparing a catalyst from a LDH is by calcination, to form an oxyhydroxide or a double oxide, (CREPALDI; VALIM, 1998; ZHANG *et al.*, 2015).

The mixed-metal oxides derived from layered double hydroxides after calcination presents high surface area, acidic-basic and redox properties. For glycerol oligomerization, previous studies have used mixed oxides from Mg/Al, Ca/Al and Mg/Fe LDH (GARCÍA-SANCHO *et al.*, 2011; GUERRERO-URBANEJA *et al.*, 2014; PÉREZ-BARRADO *et al.*, 2015). All of them have reported successful conversion of glycerol into the oligomers, however data on the catalyst reusability is still missing in the literature.

Mixed oxides are commonly able to recover the layered structure upon contact with water or an anionic aqueous solutions, in a feature frequently referred as "memory effect" (LIMA *et al.* 2012; PÉREZ-RAMÍREZ; ABELLÓ; PERS, 2007). Reconstitution of Mg/Al LDH structure from the oxide by contact with water vapor or by immersion in decarbonated water leads to formation of mexinerite ($Mg_6Al_2(OH)_{18}\cdot 4H_2O$), an structure similar to hydrotalcite with OH^- groups as compensating anions in the interlayer instead of carbonates (PÉREZ-RAMÍREZ; ABELLÓ; PERS, 2007). Using this phenomenon as a strategy to improve activity through the changes on the physicochemical properties has been reported for aldol condensation (ABELLÓ *et al.* 2005), isomerization of glucose (LEE *et al.* 2014) and transesterification of glycerol (ÁLVAREZ *et al.* 2012).

The use of LDHs with zinc and cobalt as divalent cations is being reported as well. Liu *et al.* (2014) has used Zn/Al LDH as catalyst for biodiesel production. Prakruthi, Prakash and Bhat (2015) studied Zn/Al LDH for microwave assisted conversion of glycerol to glycerol carbonate. To recover the catalyst after deactivation , the reconstruction of the thermally treated catalyst was done through rehydration via microwave irradiation , which recovered the structure and restored the catalytic activity.

Álvarez *et al.* (2013) has investigated the reconstruction of mixed oxides resulting from the thermal decomposition of Zn/Al and Zn/Mg/Al LDHs using mechanical stirring or ultrasonic treatment. Their catalytic behavior was tested for the carbonylation of glycerol with urea .

Baskaran *et al.* (2014) studied the catalytic activity of synthesized Co/Al LDH and silicate anion intercalated LDH for the oxidation of various primary and secondary

alcohols using t-butyl hydro peroxide (TBHP) as co-oxidant. Wang *et al.*(2016) prepared composites of Co/Al LDH and reduced graphene oxide by growing the LDHs on the surface of graphene oxide *in situ* via coprecipitation and hydrothermal treatment. And tested their activity for the electrocatalytic reduction of oxygen.

The use of LDH as support is another approach reported in the literature. Gennequin *et al.*(2010) has prepared a catalyst of cobalt supported on Mg/Al LDH using the property of "memory effect". The lamellar structure was regenerated after calcination by dipping the solid in a Co nitrate aqueous solution.

The interactions between transition metal acetylacetonates and layered double hydroxides or their corresponding mixed oxides is a relatively unexplored field. Zăvoianu *et al.* (2010) has compared the activity of Co, Cu and Ni acetylacetonates supported on Mg/Al LDH for cyclohexene epoxidation. Cobalt(II) acetylacetonate catalyst was the most active and stable.

2.5 Perovskites

Perovskites also have attracted attention in catalysis, especially due to their good thermal stability and the possibility of tuning their properties by substitution of their cations. They are complex metal oxides with general formula ABX_3, in which A and B are cations and X is an anion, Figure 2.4. The term was originally named for $CaTiO_3$, however many different cations can have similar crystal structures (CHEM; POLO-GARZON, 2018; YIN *et al.*, 2018).

Figure 2. 4 - The ideal cubic $Pm\bar{3}m$ structure of an ABX_3 perovskite.

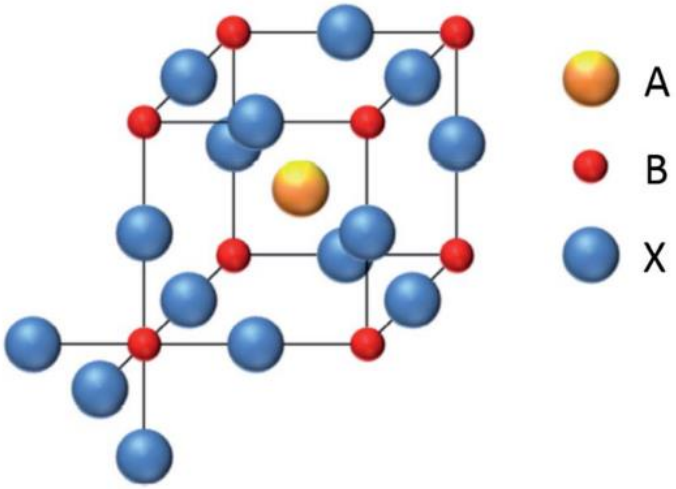

Source: Kubicek, Bork; Rupp, (2017).

Several similar layered or defective structures are referred as perovskite-type materials, such as the Ruddlesden–Popper-series $A_{n+1}B_{n}X_{3n+1}$ or the double perovskite structures $A_2B_2X_{5+\sigma}$. Non-oxide perovskites also exist, such as halide perovskites (X = halide), or anti-perovskites where A and B are anions and X are cations. The large variety of electronic, ionic or magnetic properties achieved with perovskites is a consequence of the large number of chemical elements and different cations that can be selected (KUBICEK; BORK; RUPP, 2017).

According to Zeng *et al.* (2007) , fluoroperovskite compounds are of great scientific interest because most of the perovskites are ferroelectrics and may be desirable for certain applications in electronics and optics. Fluoroperovskites are of stable structure and are inert to oxygen and moisture.

POLO-GARZON and WU (2018) have recently published comprehensive reviews over acid-base catalytic properties of perovskites. Yin *et al.*(2018) have summarized a series of works with oxide perovskites for applications on electrocatalysis, photocatalysis, and photovoltaics.

IIDA and coworkers (2018), have evaluated the catalytic activity of several fluoroperovskites supported on activated carbon to produce diethyl carbonate from ethylene. $KCaF_3$/C catalyst was found to be effective, since it maintained conversion over recycling without expressive leaching. The $KMgF_3$/C catalyst had superior catalytic activity, however there was a higher potassium leaching.

Use of fluoroperovskites for photocatalytic removal of various pollutants under visible light is reported by HU *et al.*(2013). Their results demonstrated that photocatalytic activities of $KMgF_3$ synthesized by microemulsion method were superior to those of sol–gel method and that the excellent photocatalytic activities achieved by $KMgF_3$ have a close relation to the crystal defects of fluorine vacancies.

3 MATERIAL AND METHODS

3.1 Synthesis and characterization of catalysts

3.1.1 Layered double hydroxides

Mg/Al, Co/Al and Zn/Al LDHs, with molar ratios of 3, 3 and 2 respectively, were synthetized by the coprecipitation method, following the procedure described by Carvalho *et al.* (2015) . An aqueous precipitating solution of $NaOH/Na_2CO_3$, was slowly added to the metallic solutions of $X(NO_3)_2.6H_2O$ (X = Mg, Co or Zn) and $Al(NO_3)_3.9H_2O$. Figure 3. 1 - Synthesis of X/Al LDH by coprecipitation (X=Mg, Zn or Co).

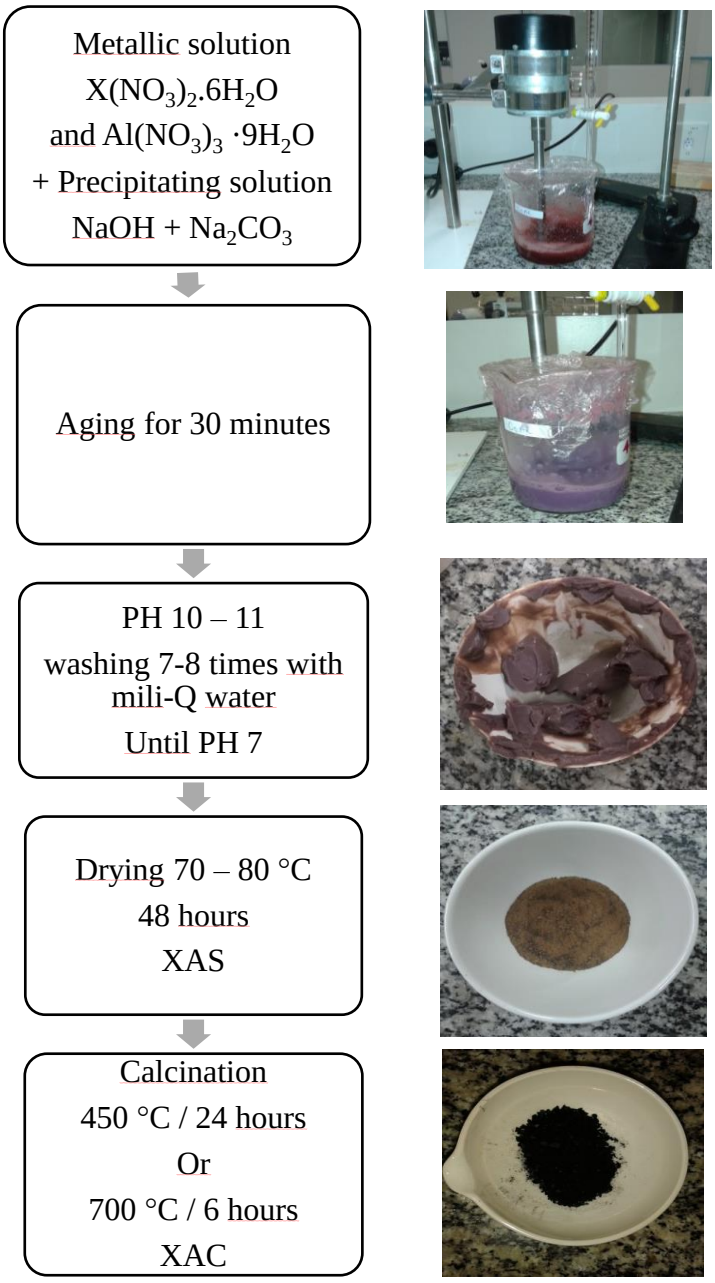

Source: Author.

The mixture was aged under mechanical stirring for 30 minutes at room temperature. The precipitates were separated by centrifugation and then washed extensively with deionized water (until pH 7). The resulting material was dried at 70 °C for 48 hours and named XAS. On some catalytic tests, calcination conditions were different, either with 450 °C for 24 hours or 700 °C, 6 hours, samples were labeled XAC, where X can be Mg, Co or Zn, A is aluminum, S stands for dried and C for calcinated samples. Figure 3.1 summarizes this process.

3.1.2 Rehydration of Mg/Al and Zn/Al LDHs

From the dry Mg/Al and Zn/Al LDH, mixed oxides were obtained by calcination at 450 ºC for 24 hours (XAC), figure 3.2. Two different types of rehydration

Figure 3. 2 - Scheme for the preparation of LDH, mixed oxide and rehydrated samples (X=M for Mg or Z for Zn).

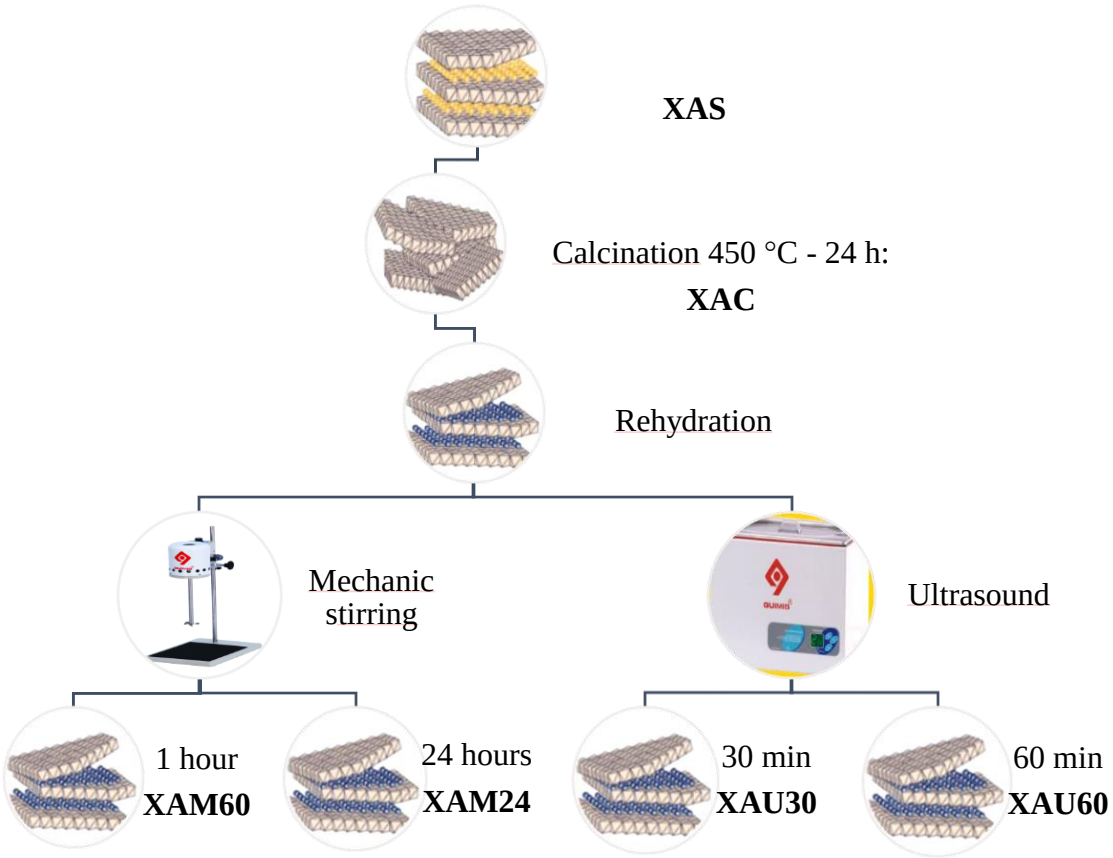

Source: Author.

were used on the mixed oxides: ultrasound or mechanical agitation. For tests with ultrasound, 0.6 g of sample were added to 100 mL of deionized water, in 30 or 60 minutes of agitation, samples were labeled XAU30 and XAU60. In mechanical stirring tests, the same proportion of sample/deionized water was stirred for one or 24 hours (labeled as XAM60 and XAM24, respectively).

3.1.3 Fluorine-containing catalysts

To investigate the activity of fluorine in glycerol oligomerization, Mg/Al/F, Co/Al/F, Cu/Al/F and Zn/Al/F systems were synthetized by coprecipitation. In this case, the precipitating solution was KF/K_2CO_3, the same nitrates described above composed the metallic solutions. Mixture, aging, separation, washing, drying and calcination followed the previous procedure. Samples were labeled as FPXAS and FPXAC, where X can be Mg, Co, Cu or Zn, A is aluminum, S stands for dried and C for calcinated samples.

Figure 3. 3 - Cobalt (II) acetylacetonate impregnation on LDH and perovskites.

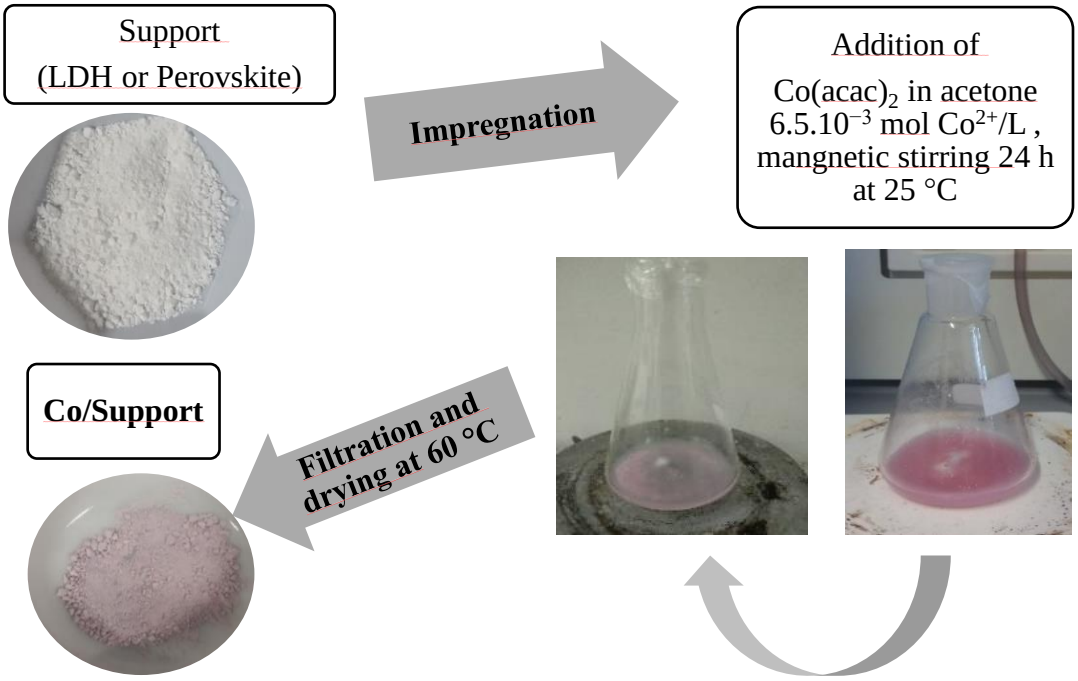

Source: Author.

3.1.4 $Co(acac)_2$ impregnation on LDH and fluoroperovskites

Cobalt(II) acetylacetonate impregnation over LDH and fluorine-containing materials was based on the method described by Zăvoianu *et al.* (2010). The impregnation

of the samples MAS, FPMAC, ZAC and FPZAC was performed by contacting the support with a solution of cobalt(II) acetylacetonate and acetone, $6.5.10^{-3}$ mol Co/L, under magnetic stirring for 24 h at room temperature (figure 3.3). By the end of this period, colored liquid phase became colorless and the solid supports turned to a pink-violet color. Solids were filtered and dried overnight at 60 °C and labeled as Co/Support Name.

3.1.5 Catalyst characterization

Lamellar structure formation and changes after the thermal and rehydration processes were evaluated by X-ray diffraction (XRD) on a Bruker D8 Advanced diffractometer, using Cu Kα (40 kV, 40 mA) radiation. The diffractograms were collected in $2\theta = 2°– 90°$ range with a step of 0.05° and a counting time of 1 s per step. Diffraction peaks recorded at 40 kV and 40 mA. Results were compared to that of the Joint Committee on Powder Diffraction Standards (JCPDS).

FTIR-ATR Spectroscopy (VERTEX70, BRUKER), was used to monitor changes in functional groups. Samples were analyzed in the range of 600 - 4400 cm^{-1}, with spectral resolution of 4 cm^{-1}.

The textural analyses were performed with the ASAP 2420 equipment (Micrometrics). Samples were pretreated at 120 °C for 12 hours with N_2 and the nitrogen adsorption-desorption measurements were carried out at -196 °C. The surface area was determined with the Brunauer-Elmmett-Teller (BET) method (S_{BET}). The cumulative volume of pores (V_P) and the average pore diameter (D_P) were calculated from the adsorption branch of isotherms by the Barrett–Joyner–Hallenda (BJH) method.

The morphology of samples was observed by transmission electron microscopy (TEM), Morgagni 268D 100 kV (FEI). Scanning electron microscopy (SEM) was used for fluorine-containing solids, using energy dispersive X-ray spectroscopy (EDX) to assess fluorine content, these measurements were carried out with the Quanta 450 FEG (FEI) microscope.

For Mg/Al, Zn/Al, Co/Al LDHs and rehydrated samples, the thermogravimetric analysis/differential thermal analysis (TG/ DTG) was carried out in a STA 449 F3 – JUPITER/ NETZSCH analyzer operating under the following conditions: 20 mg of sample, nitrogen flow of 80 ml. min^{-1}; heating rate of 5 °C min^{-1}; temperature range of 40 to 800 ºC. For fluoroperovskites and materials impregnated with cobalt

acetylacetonate, the analysis was performed with a TG/DSC 3+ (Mettler Toledo), under the following conditions: 20 mg of sample, air flow of 80 ml. min^{-1}; heating rate of 5 °C min^{-1}; temperature range of 40 to 800 ºC.

Temperature-programmed desorption of CO_2 was used to evaluate the basicity. Tests were performed in two different set-ups, as follows. Catalysts from Mg/Al LDH study and CoAC (450 And 700 ºC) were analyzed in a self-constructed 6-fold TPD unit., set-up 1. The analysis procedure consisted on filling one tube with 50 mg of $NaHCO_3$ (Sigma Aldrich) as standard; the other tubes were filled with the same amount of samples to be measured and they all were pretreated in vacuum at 100 °C for 1 hour. The reaction temperature was lowered to 50 °C and pure CO_2 stream was subsequently introduced into the reactor for 1 hour. Then, the thermal desorption of CO_2 was conducted from 50 to 770 °C (10 °C min^{-1}) and was registered using a mass spectrometer Pfeiffer QMS 200 (Pfeiffer Vacuum), that monitored the weight of CO_2 during the experiment. The mass of samples was measured at the end of process, to calculate basicity.

For selected samples of fluorine-containing materials and with $Co(acac)_2$ impregnation, the CO_2-TPD set-up had a single quartz reactor, set-up 2. An amount of sample was activated, for 1 hour at 100 °C for $Co(acac)_2$ supported material and 450 °C for 30 min for fluoroperovskite. On the next step, CO_2 adsorption was performed at 40 °C for half an hour, and then 30 min of He stream was used to remove the excess of CO_2 prior desorption. Desorption was performed from 30 to 770 °C (10 °C min^{-1}), under He flow, a thermal conductivity detector (TCD) was used to monitor this process. System had an ice trap in order to eliminate any trace of water.

For comparative purposes, sample MAU30 was measured in both set-ups. Also, a blank experiment was carried out with this sample (without CO_2 adsorption), in which the solid was activated at 100 °C for 1 hour. And next, the desorption was performed from 30 to 770 °C (10 °C min^{-1}), under He flow .

For Zn/Al LDH, fluorine-containing materials and $Co(acac)_2$ impregnated solids, the surface basicity was studied by the irreversible adsorption of noninteracting acids, based on a methodology reported by LEE *et al.* (2014) and Parida and Das (2000). Acrylic acid (pK_a = 4.3) was used as probe molecule for total basicity and phenol (pK_a = 9.9) for strong base sites. The number of weak base sites was calculated by the difference between strong basicity and total basicity. Samples were dried at 60 °C overnight, then 0.02 g were added to 4 mL of standard solution of organic acid (phenol/acrylic acid) in cyclohexane, next they were mixed for 2h at room temperature on a tube rotator.

Concentration of organic acid was determined by UV-vis spectrometer (Biomate 3S, Thermo Scientific), using calibration curves derived from standard solutions.

The contents of Mg, Co, Zn, Cu , K and Al in the solids were determined by ICP-OES. Solids were analyzed after dissolving 10 mg of sample in 50 mL of a 2% HNO_3 aqueous solution, which was then filtrated through a syringe filter with a pore diameter of 0.45 μm and then 2 mL of this solution was diluted into 20 mL. The calibration curves were prepared on a nitric acid aqueous solution by using a multielemental standard solution (SpecSol).

3.2 Activity tests

Glycerol oligomerization was carried out in a batch reactor (Parr) under nitrogen flow, typically, tests used 50 g of glycerol. The autoclave was equipped with a system to collect the water formed, Figure 3.4.

Figure 3. 4 - Reaction system for glycerol oligomerization: left: controller of temperature and stirring, right: batch reactor (attached to nitrogen flow and water collection system).

Source: Author.

For Section 4.1, with Mg/Al LDH catalysts, the influence of reaction parameters was tested with MAC, calcinated at 450 °C. First, the effect of reaction temperature (210 - 240 °C) was evaluated for reaction of 24 hours with 2 wt% of catalyst.

Next, the influence of catalyst load (1 - 4 wt%). was studied. Then, for comparative purposes reaction time was lowered to 8 hours. Rehydrated LDH (MAU30, MAU60, MAM60 and MAM24) were tested over the best set of reaction conditions.

In Section 4.2, the study of Zn/Al LDH had the same experimental design of previous section. The fluorine-containing catalysts were tested under the optimal conditions observed.

For Section 4.3, first the effect of calcination temperature (450 and 700 °C) on the activity of Co/Al LDH was evaluated for reactions with 2% of catalyst, at 220 °C for 24 hours. Then, for the same reaction time, influence of reaction temperature (220 - 240 °C) and catalyst load (2- 4%) were assessed. Catalytic application of materials impregnated with $Co(acac)_2$ was studied for the best set of conditions.

To study glycerol conversion (X_{gly}) and oligomers production versus time, a reaction under the best set of conditions was performed and samples were taken periodically without opening the reactor, using a sample collection vessel.

Product analysis was measured by gas chromatography with flame ionization detector GC-FID (Agilent) and a CP-SIL 5CB column (Agilent). Samples were silylated with BSTFA, using pyridine as solvent, following the same methodology reported by Barros *et al.*, (2017). The following equations were used to quantify X_{Gly}, di and triglycerol selectivity (S_{di} and S_{tri}) and the yield of oligomers (Y_{di} and Y_{tri}.):

$$X_{Gly} = \frac{n_0 - n_f}{n_0} 100 \quad (1)$$

Where, n_0 is the initial amount of glycerol mols and n_f is the final amount in mol.

$$S_{olig} = \frac{n_{olig}}{n_0 - n_f} 100 \quad (2)$$

Where n_{olig} is the amount of each oligomer in mol.

$$Y_{olig} = \frac{X_{Gly} \sum S_{olig}}{100} \quad (3)$$

Oligoglycerols higher than triglycerol could not be resolved by this analytical procedure. Therefore, once the percentage of glycerol and the selectivity to diglycerol and triglycerol were calculated, the missing fraction was assumed to be the selectivity to higher oligomers and other products (S_{ho}), Kirby *et al.*(2015) has used a similar approach.

Acrolein detection was performed on the water collected in each reaction, with GC-FID and a DB-Wax column (Agilent), following the methodology described by Atia, Armbruster and Martin (2011). Hydroquinone and 1-Butanol were used as polymerization inhibitor and internal standard, respectively.

3.3 Catalyst reuse and stability

Reusability tests were performed for catalysts with the best activity in each case. Procedure for catalysts separation comprises a first decanting step, followed by water addition (to remove remaining glycerol and oligomers) and then the mixture was filtered and the solid dried at 80 °C overnight.

To observe changes related to the presence of adsorbed species, thermogravimetric analysis of spent catalysts was carried out following the same procedure describe for fresh solids.

The surface of fresh and spent catalysts was studied by X-Ray Photoelectron Spectroscopy (XPS). The analysis was performed with a spectrometer (Physical Electronics PHI 5700) equipped with a non-monochromatic Mg Kα radiation (1253.6 eV) with a multichannel detector. Each spectrum was registered in the constant-pass energy mode at 29.35 eV, using a 720 mm diameter analysis area. Charge referencing was done against adventitious carbon (C 1s at 284.8 eV). Data acquisition and analysis was performed with PHI ACCESS ESCA-V6.0F software package. The signals were subtracted using a Shirley-type background and fitted with Gaussian–Lorentzian curves to determine more accurately the binding energies of the different element core levels. Samples were outgassed for 12 hours prior analysis.

To understand catalysts stability, the reaction products were analyzed by ICP-OES to detect any trace of metal leached from catalysts to the reaction medium. For sample preparation, one mg of product was diluted on 10 mL of ultrapure water and then filtrated through a syringe filter with a pore diameter of 0.45 μm. Calibration curves were prepared under the same conditions of catalyst analysis.

.

4 RESULTS AND DISCUSSION

4.1 Enhancing the catalytic activity of Mg/Al layered double hydroxide for glycerol oligomers production

4.1.1 Catalysts characterizations

The several analyses performed in the material as-synthesized (MAS), after calcination (MAC), rehydrated by ultrasound (MAU30 and MAU60) and mechanical stirring (MAM60 and MAM24) are presented and discussed in the following paragraphs. First, ICP measurements, Table 4.1, confirmed that as-synthesized material, MAS, had Mg/Al molar ratio close to the theoretical amounts, and that this value was not significantly changed across calcination and rehydration steps.

Table 4. 1 - ICP - OES analysis (Mg/Al molar ratio) and structural data (d spacing, unit cell dimensions, ISF and FWHM) for LDH (MAS), mixed oxide (MAC) and rehydrated samples (MAU30, MAU60, MAM60 and MAM24).

Sample	Mg/Al	d_{003}	d_{110}	a (Å)	c (Å)	IFS (Å)	I_{006}/I_{003}	$FWHM_{110}$	$FWHM_{003}$
MAS	2.90	7.800	3.913	7.826	23.400	3.00	0.47	0.541	0.637
MAC	3.09	-	-	-	-	-	-	-	-
MAU30	3.18	7.605	1.528	3.056	22.815	2.81	0.35	0.492	0.541
MAU60	3.28	7.814	1.533	3.066	23.442	3.01	0.33	0.394	0.689
MAM60	3.17	7.740	1.529	3.058	23.22	2.94	0.28	0.590	0.541
MAM24	3.05	7.801	1.535	3.070	23.403	3.00	0.36	0.394	0.541

*d_{003} and d_{110} : d spacing;

*a and c (Å): unit cell dimensions;

* ISF (Å) : Interlayer free space;

*I_{006}/I_{003} : relative intensities;

*$FWHM_{110}$ and $FWHM_{003}$: Full width at half maximum.

Lamellar structure formation and the changes after thermal and rehydration processes were evaluated by XRD (Fig.4), MAS exhibits a single phase, which corresponds to the typical structure of a hydrotalcite, according to JCPDS 70-2151, with well-defined and symmetric peaks in (0 0 3), (00 6), (110) and (113) and wide asymmetric peaks at (0 1 2), (0 1 5) and (0 1 8). Calcination led to the formation of a mixed oxide of periclase type (JCPDS 45-0946), with the characteristic reflections on (2 0 0) and (2 2 0), pointing to the total collapse of lamellar structure on MAC (ANGELESCU *et al.*, 2008). Rehydrated samples showed the typical pattern for LDH, although lamellar structure is recovered some differences can be noticed on the diffractograms. Higher times of ultrasound and mechanic stirring presented slightly higher and better-defined basal peaks than MAS, whereas the planes (0 1 2), (0 1 5) and (0 1 8) become more symmetrical for all rehydrated samples.

Figure 4. 1 - XRD for MAS, MAC, MAU30, MAU60, MAM60 and MAM24.

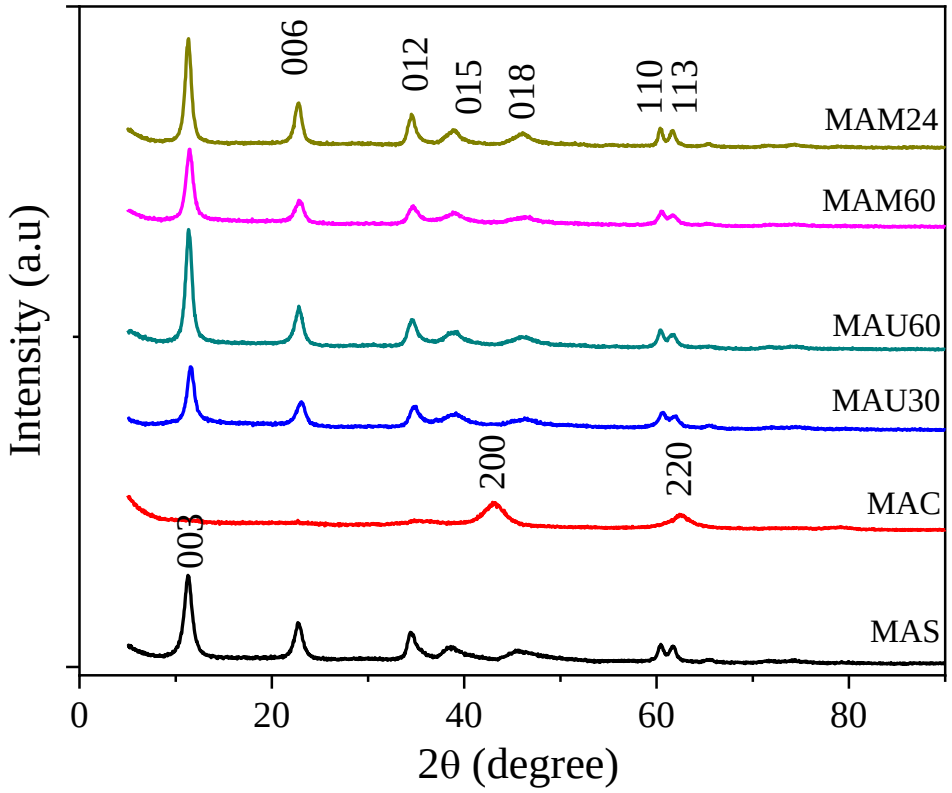

Reduction of relative intensities of main diffraction peaks (I_{006}/I_{003}) in comparison with MAS, presented in Table 4.1, suggests lower crystallinity and presence of defects on rehydrated samples. The reduction of carbonate amount, as a result of the change on interlamellar composition, can be noticed by the decrease of lattice parameter a. The interlayer free space (IFS) was calculated using the expression ISF=(c/3) - 4.8,

where the thickness of brucite-like layer is considered as 4.8 Å (PAVEL *et al.*, 2008), this parameter has reduced significantly on lower rehydration times, MAU30 and MAM60, in agreement with the findings of previous works, where calcination and rehydration steps are considered as aging procedures that improve crystallinity (ANGELESCU *et al.*, 2008).

FTIR results were used to monitor functional groups changes, (Figure 4.2) the band assigned to hydroxyl group, around 3500 cm^{-1}, present in the lamellae and on interlamellar water, has a strong presence in MAS and rehydrated samples; MAC exhibited a reduction of this band due to the water exit after thermal process (450 °C), the same behavior was observed for the band related to interlayer water bending vibration at 1630 cm^{-1}. Presence of a reduced band related to the carbonate group at around 1350 cm^{-1} in MAC, suggests that the calcination temperature did not eliminate completely hydroxyls and carbonates, although LDH phase collapse confirmed by XRD. The band at around 630 cm^{-1} is characteristic of carbonate in-plane bending (ABELLÓ *et al.*, 2005).

Figure 4. 2 - FTIR for MAS, MAC, MAU30, MAU60, MAM60 and MAM24.

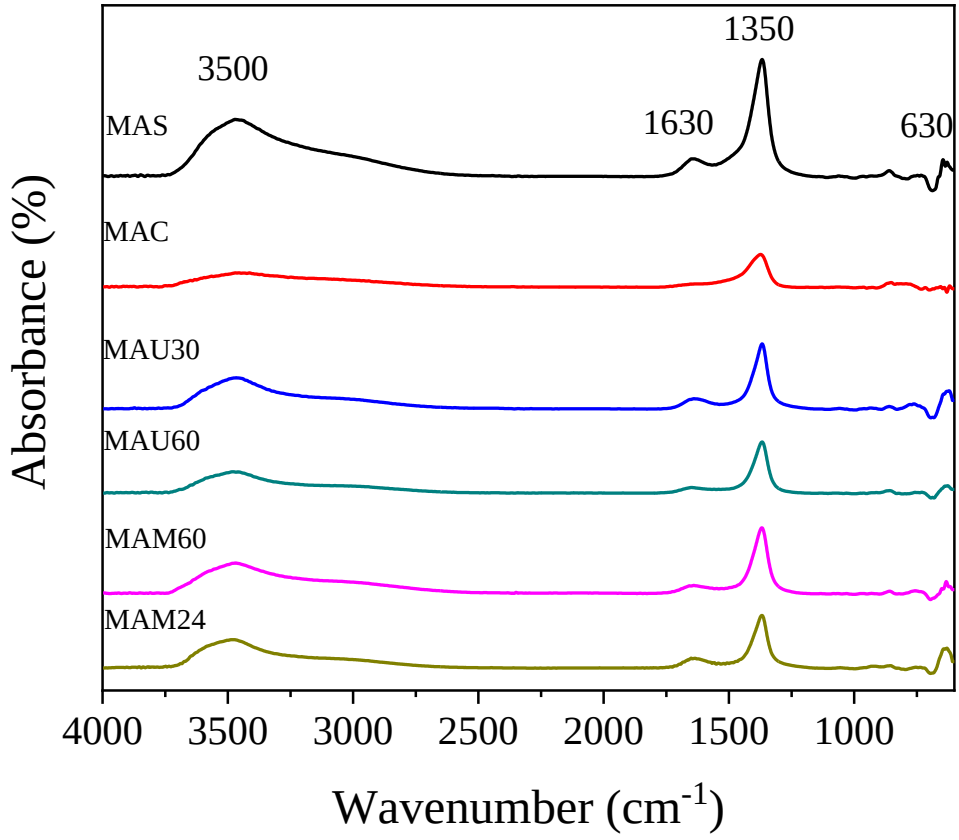

Thermogravimetric analysis, Fig. 4.3, shows that MAS and the reconstructed materials present two steps of weight loss. In the first one, from room temperature to 200

°C, loss of adsorbed and interlamellar water occurs. Values of weight loss for this step are quite similar for rehydrated samples MAU30 and MAM60, Table 4.2, indicating that they have similar amounts of water molecules. For both ultrasound and mechanic stirring, this first weight loss increased on higher reconstruction times. On the second event, from 200 to 450 °C, the loss is related to removal of condensed water molecules and carbon dioxide from carbonate anions present in the interlayer space of LDH. The lower weight loss for MAC suggests that during calcination LDH was transformed into periclase (CHIMENTÃO *et al.*, 2007; SHARMA; PARIKH; JASRA, 2010).

Figure 4. 3 - a) TGA and b) DTG for MAS, MAC, MAU30, MAU60, MAM60 and MAM24.

a)

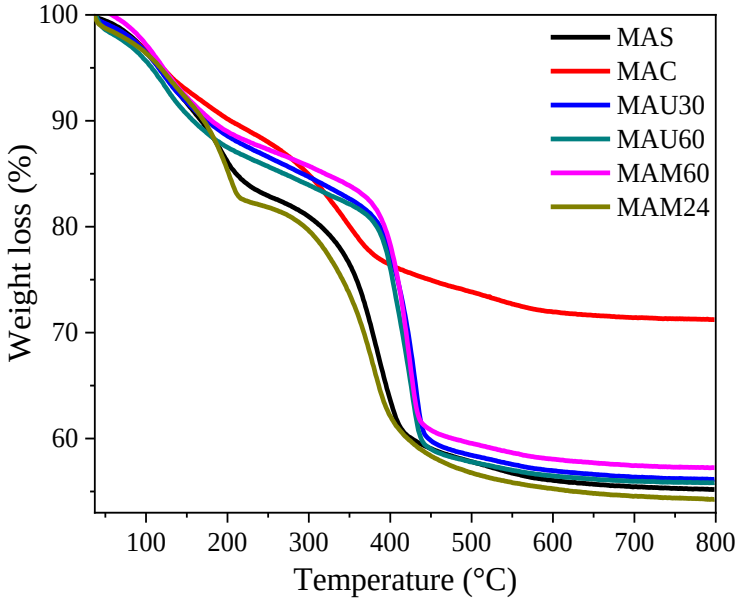

b)

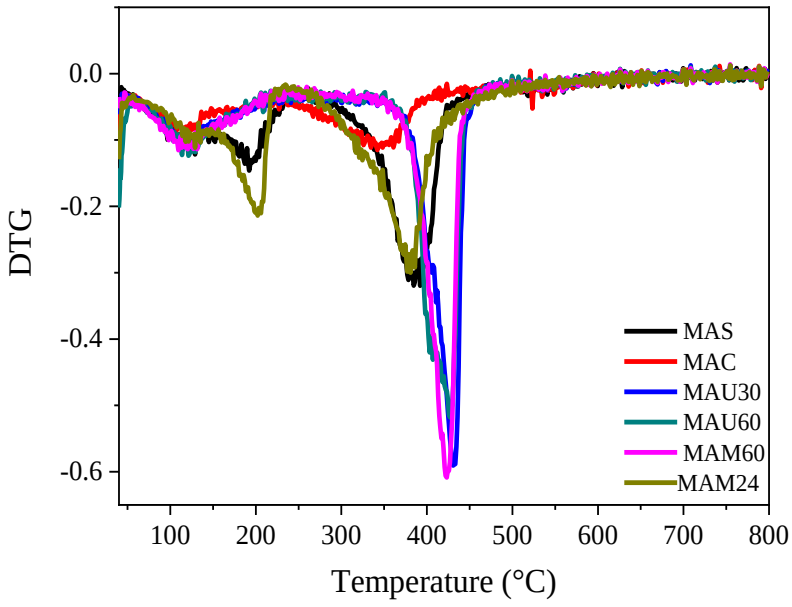

Table 4. 2 - Thermogravimetric analysis of MAS, MAC, MAU30, MAU60, MAM60 and MAM24.

Sample	W_1 (%)	W_2 (%)	W_{Total} (%)
MAS	13.93	30.75	44.68
MAC	9.95	18.83	28.78
MAU30	11.26	32.61	43.87
MAU60	12.49	31.71	44.2
MAM60	11.04	31.64	42.68
MAM24	14.8	30.94	45.74

Calcined material, MAC, exhibited similar textural properties to MAS, table 4.3. The LDH and their mixed oxides have presented a large range of textural properties on the literature. These differences can be explained by several factors such as the different synthesis methods (by coprecipitation or urea hydrolysis) and aging procedures, where time and temperature of process, e.g at room temperature or heating with microwave, plays an important role (BERGADÀ *et al.*, 2006; GARCÍA-SANCHO *et al.*, 2011) .

It is also possible to notice in Table 4.3 that rehydration by ultrasound led to the reduction of all textural properties, and this behavior was increased with time of treatment, since MAU30 presented S_{BET} 1.7 times higher, than MAU60. Álvarez *et al.* (2012) have also observed the reduction of S_{BET} after one hour of ultrasound for reconstruction of a similar LDH in comparison to its respective mixed oxide, attributing this alteration to the formation and growth of mexinerite particles, as well as to the high surface tension of water , which may lead to the formation of a platelet agglomeration, which provokes the closure of small mesopores, and thus a substantial loss of S_{BET}.

For samples obtained via mechanical stirring, MAM60 presented similar surface area to MAC, and all textural properties increased substantially for MAM24, reaching approximately the double of S_{BET} of MAS and MAC, conversely to the results found with ultrasound. Previous studies of LDH rehydration observed a similar behavior, pointing that during the reconstruction process, mechanical stirring in liquid phase can break and exfoliate the hydrotalcite-like platelets, increasing the specific surface area (ABELLÓ *et al.*, 2005; SHARMA; PARIKH; JASRA, 2010). Some previous works also report that a reduction on the surface area is noticed for rehydration without stirring, Pavel *et al.* (2008) observed a reduction on S_{BET} for parenting LDH from 112 to 6.6 m^2/g ,

sample was rehydrated by immersion in decarbonized water and dried in air at 90 °C for 24 hours. Angelescu *et al.* (2008) reported a drop from 99 (as-synthesized LDH) to 2.7 m^2/g for the material obtained by dipping a mixed oxide in water for 24 h at 25 °C.

Table 4. 3 - Textural properties and basicity (CO_2-TPD set-up 1) for Mg/Al catalysts.

Sample	S_{BET} ($m^2\ g^{-1}$)	V_P ($cm^3\ g^{-1}$)	D_P (nm)	Basicity (mmol g^{-1})			Intrinsic Basicity[a] ($mmolm^{-2}$)
				Medium	Strong	Total	
MAS	58	0.13	19.57	8.68	4.72	13.40	0.23
MAC	62	0.17	19.42	7.16	2.61	9.77	0.16
MAU30	44	0.04	3.30	4.33	2.66	6.99	0.16
MAU60	26	0.03	3.31	3.99	2.16	6.15	0.24
MAM60	56	0.05	3.29	5.24	3.34	8.58	0.15
MAM24	112	0.33	16.40	4.90	3.12	8.02	0.07

[a] Intrinsic basicity is calculated as total CO_2 desorbed per unit of surface area.

Figure 4. 4 - N_2 isotherms for MAS, MAC, MAU30, MAU60, MAM60 and MAM24.

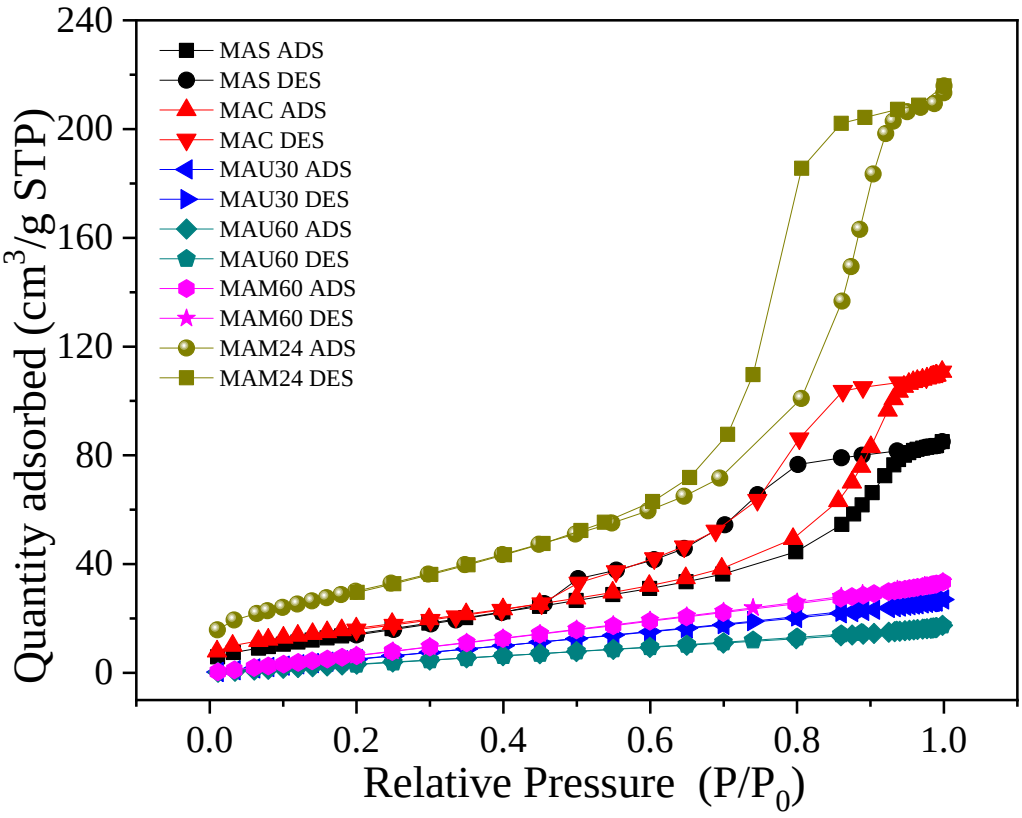

The isotherms of MAS, MAC and the solid rehydrated by mechanical stirring for 24 hours (MAM24) resembles type IV isotherm, Figure 4.4, with the presence of a

hysteresis loop (type H2b) caused by capillary condensation, indicating the mesoporous nature of the catalysts with relatively lower specific surface area (MITTA *et al.*, 2018). MAU30, MAU60 and MAM60 isotherms resembles type II, the differences on the initial part of the isotherm can be due to operational reasons. Mesoporous character of all samples was confirmed by its pore size distribution in Figure 4.5, MAM24 was the only one to present similar D_p to MAS and MAC, in agreement with the increasing on the other textural properties.

Figure 4. 5 - BJH pore size distribution for MAS, MAC, MAU30, MAU60, MAM60 and MAM24.

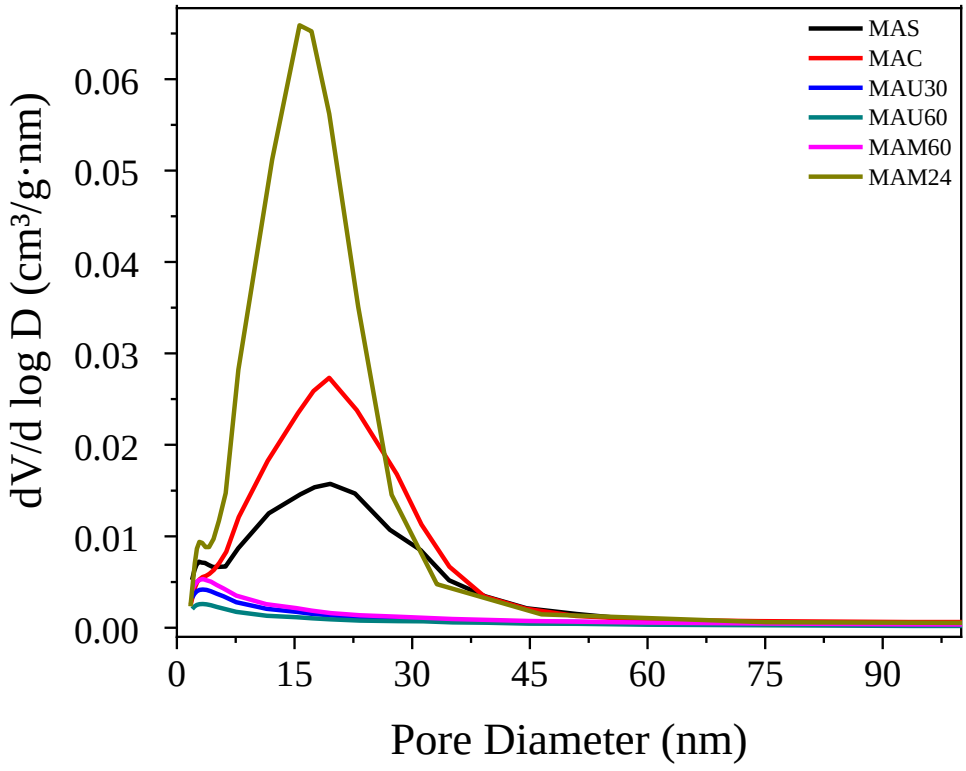

The basicity was studied by temperature-programmed desorption of CO_2, using set-up 1. All materials presented similar profiles, Figure 4.6, with two desorption peaks at around 450 °C (medium strength) and at around 650 °C (strong basic sites). The first peak can be ascribed to the contribution of mainly bidentate carbonates and bicarbonate species (ABELLÓ *et al.*, 2005). The second peak has pronounced intensity on MAS and the rehydrated samples MAU30, MAM60 and MAM24 in comparison with MAC and MAU60, pointing that the type and time of rehydration can induce changes in the population of basic sites. This difference can also be inferred in Table 4.3, which

shows the intrinsic basicity in mmol m^{-2}, from these data the following trend is observed: MAU60 > MAS >MAC = MAU30 >MAM60> MAM24.

Figure 4. 6 - CO_2-TPD profiles (set-up 1) of MAS, MAC, MAU30, MAU60, MAM60 and MAM24.

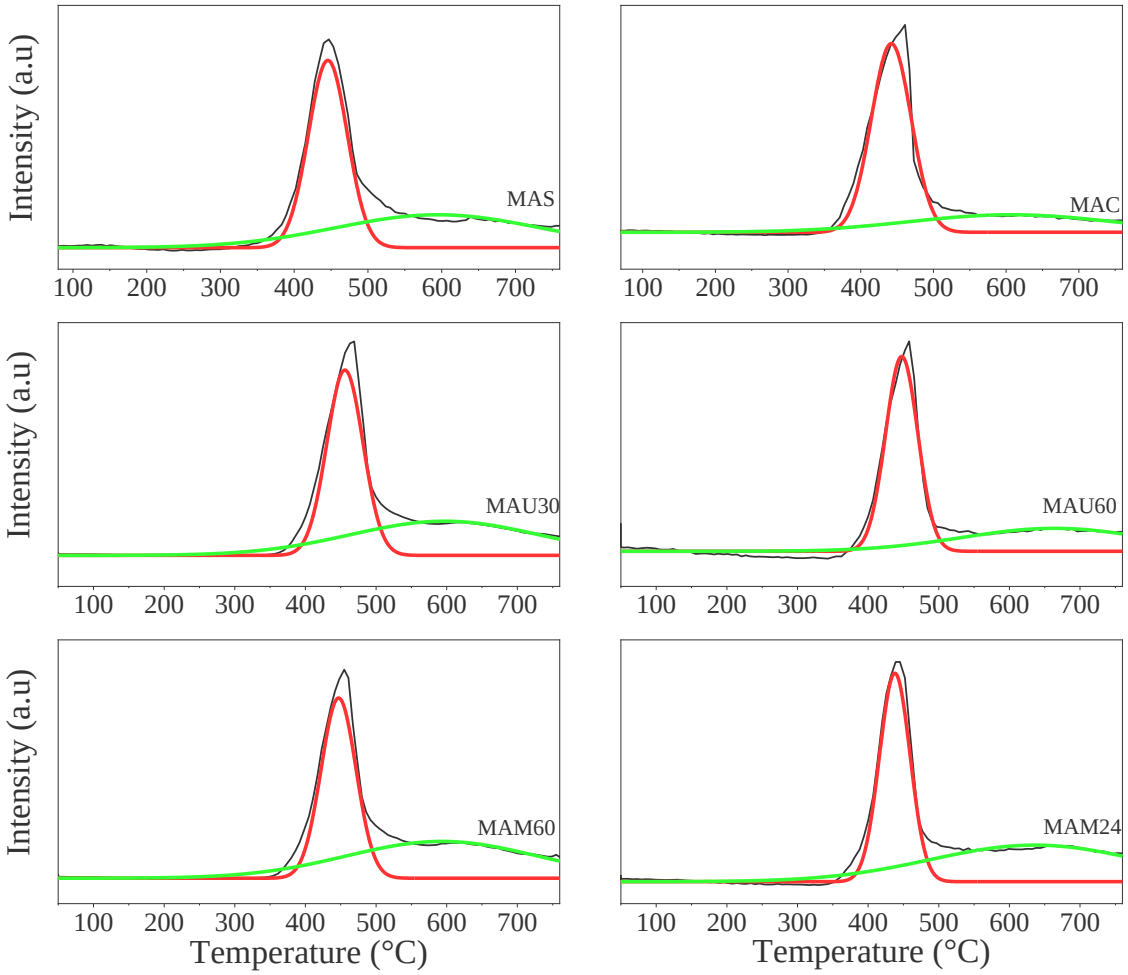

Figure 4.7 a) exhibits the analysis of MAU30 in set-ups 1 and 2, there are no relevant differences in both graphs, allowing comparisons between results. The blank test performed in set-up 2, Figure 4.7 b), showed that without previous CO_2 adsorption on MAU30 the main peak at around 450 °C was recorded, and should correspond to CO_2 adsorbed from atmosphere, what evidences the high reactivity of rehydrated material. This fact in agreement with the findings of Reyero *et al.* (2013). Furthermore, for the test with MAU30 after saturation with CO_2, presence of strong sites (at around 650 °C) was observed showing that the solid contains reactive strong basic sites.

Figure 4. 7 - CO_2-TPD studies a) Comparison of set-ups 1 and 2 for MAU30 and b) Test of MAU30 with and without CO_2 adsorption.

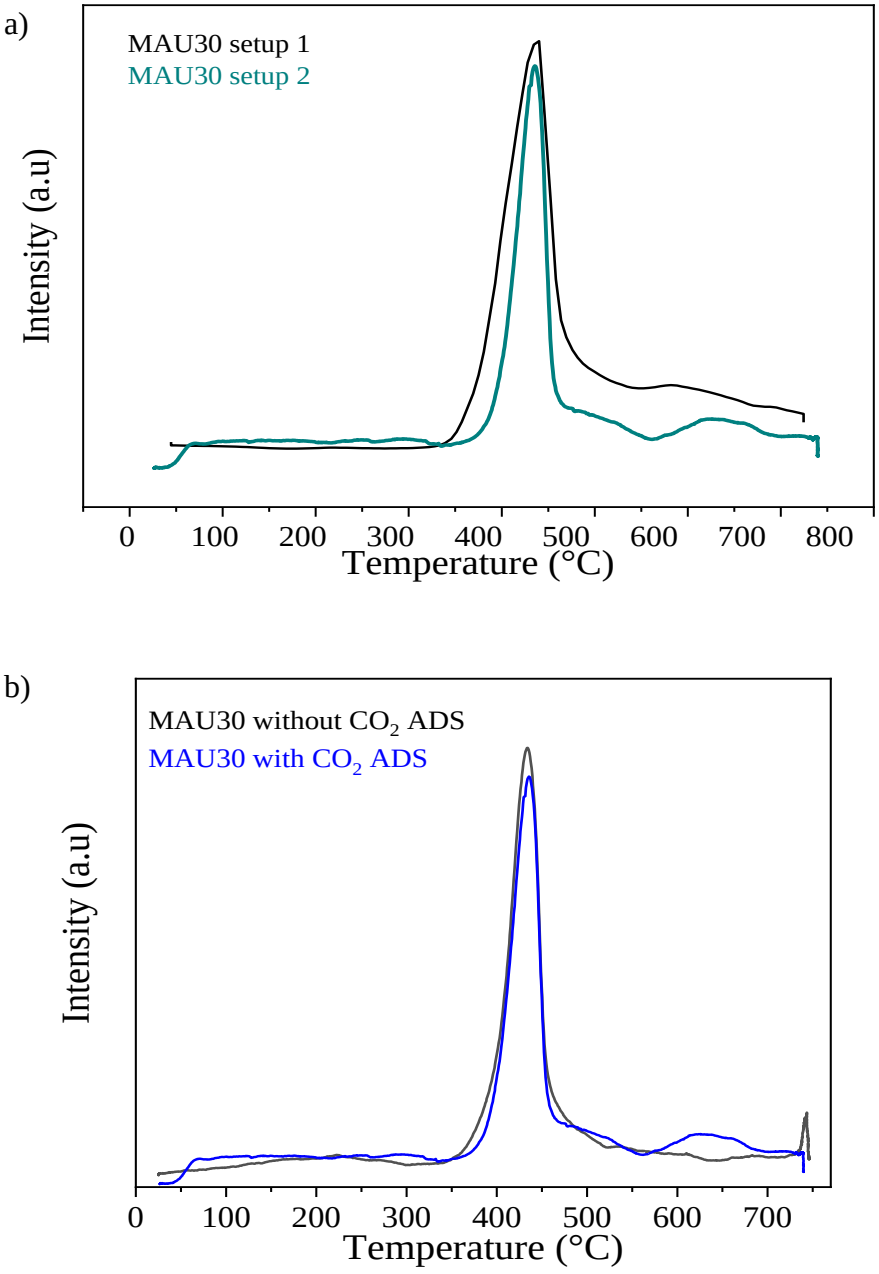

TEM micrographs are shown in Figure 4.8, MAS exhibits irregular morphology and dark areas that indicates the presence of dense agglomerations of particles. These features are maintained after calcination. The rehydrated materials MAU30, MAU60 and MAM60 displayed several thin layered crystals, which are typical from LDHs. For samples rehydrated upon lower times, the agglomeration of these thin platelets is responsible for modifying the adsorption properties and can explain their lower surface areas (44, 26 and 56 m^2g^{-1}) in comparison with MAM24 (112 m^2g^{-1}) in

accordance with previous works (ANGELESCU *et al.*, 2008; PAVEL *et al.*, 2008). MAM24 presented hexagonal like crystallites, characteristic of LDH structures, and fewer agglomerates of platelets. This result combined with XRD measurements supports the hypothesis that the use of mechanical stirring for longer times improves crystallinity of LDH.

Figure 4. 8 - TEM images (scale bar 0.1 µm) for MAS, MAC MAU30, MAU60, MAM60 and MAM24.

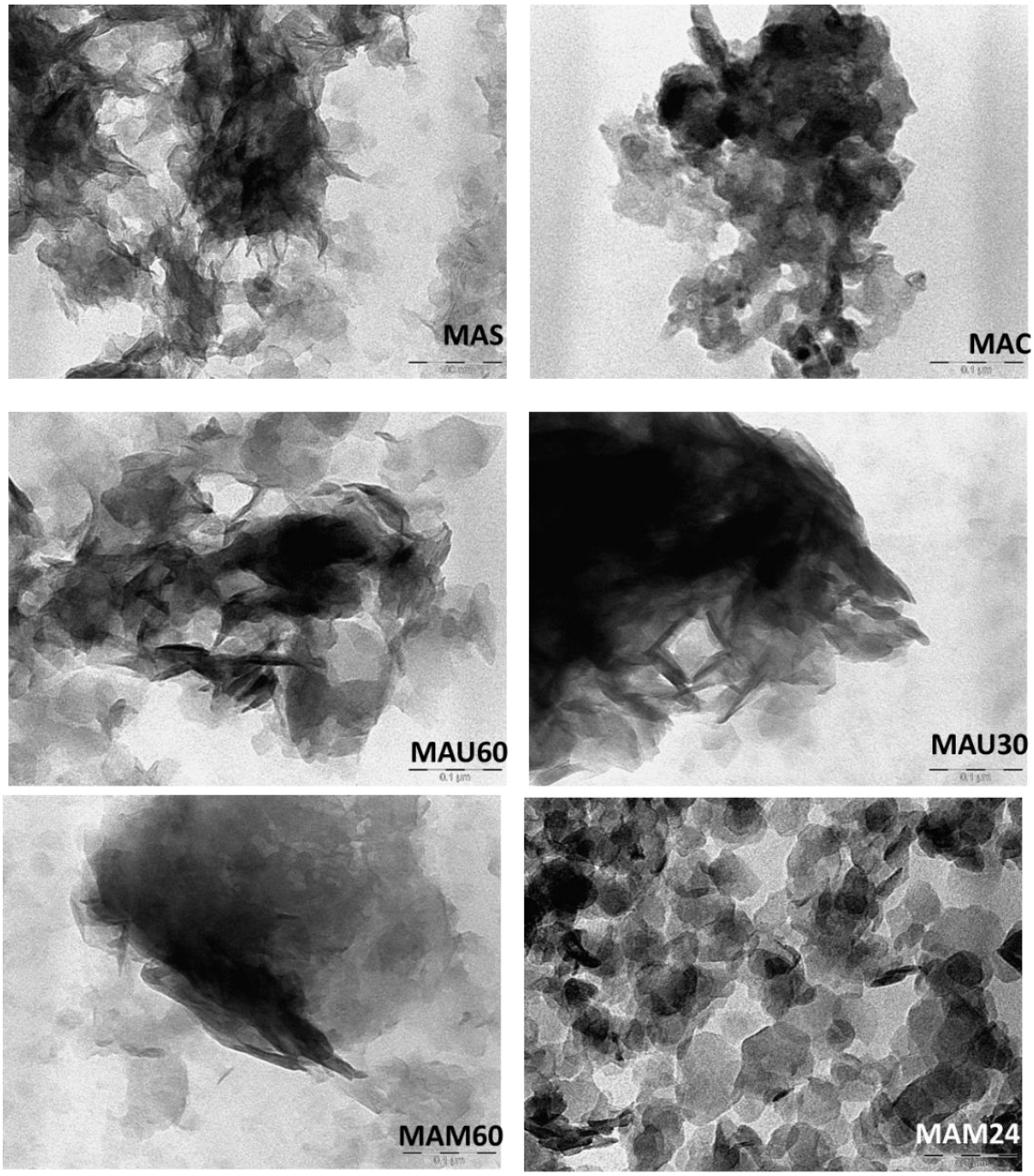

4.1.2 Catalytic application

To start the evaluation of reaction parameters, Figure 4.9, 2 %wt of MAC, calcined at 450 °C, was tested in reaction temperatures from 210 to 240 °C, for 24 hours. The reaction at 210 °C led to very low glycerol conversion (X_{Gly}) and yield of diglycerol (Y_{di}) , 3.68 and 1.40% respectively. By increasing temperature to 220 °C, X_{Gly} raises up to 15%. At 230 °C, reaction had similar X_{Gly} (17%) and better selectivity to diglycerol (S_{di}) was reached (44% in comparison with 30%). At 240 °C, X_{Gly} reached 49% and the highest yield of oligomers was obtained, 19% Y_{di} and 13%Y_{tri}, and therefore this temperature was used in the next tests.

Figure 4. 9 - Influence of the reaction temperature for glycerol oligomerization (reaction conditions: 2 wt% of MAC and 24 h) in terms of: Glycerol conversion (XGly); Selectivity to diglycerol (Sdi), triglycerol (Stri) and for high oligomers and other products (Sho);Yield of diglycerol (Ydi) and triglycerol yield (Ytri) .

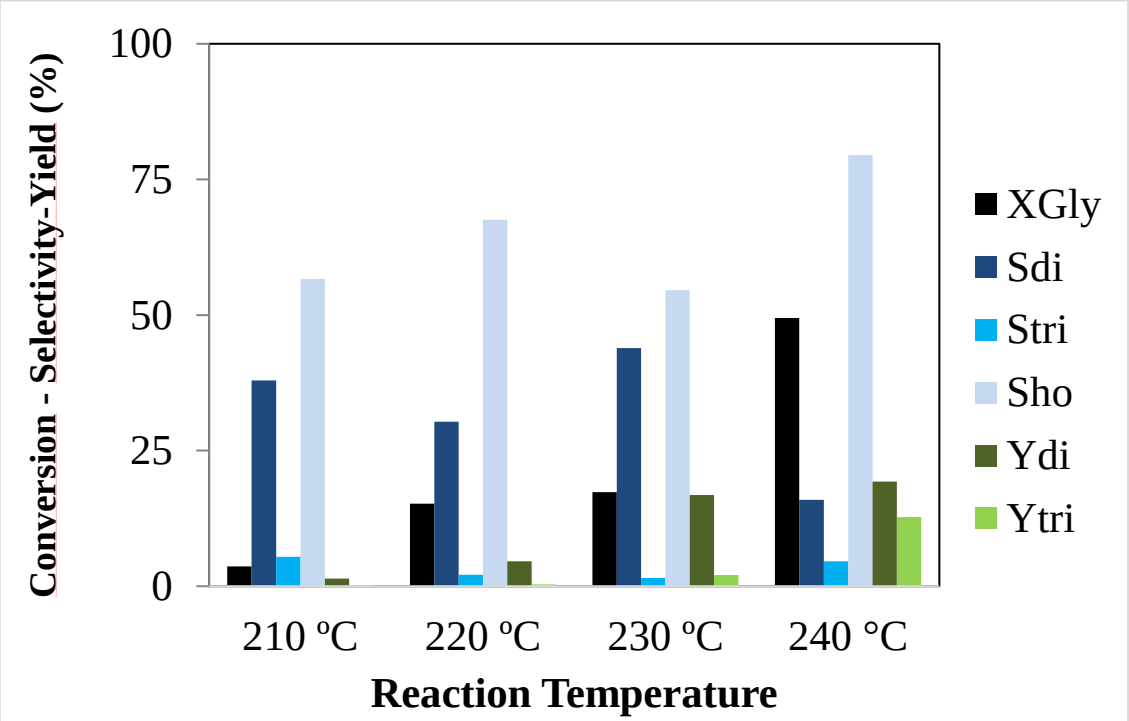

In our previous study, glycerol oligomerization at 245 °C with the use of catalysts obtained from calcined eggshells (BARROS *et al.*, 2017) and calcined dolomite, $CaCO_3 \cdot MgCO_3$, (BARROS *et al.*, 2018) had almost full X_{Gly} (100 and 91%, respectively) and high Y_{di} (38 and 23%, respectively), however in both cases there was a major homogeneous contribution, thus making unfeasible the recovery of catalyst, what did not

Figure 4. 10 - Influence of a) Catalyst loading (reaction conditions: 240°C and 24 h) b) Reaction time (reaction conditions: 4% wt and 240°C).

a)

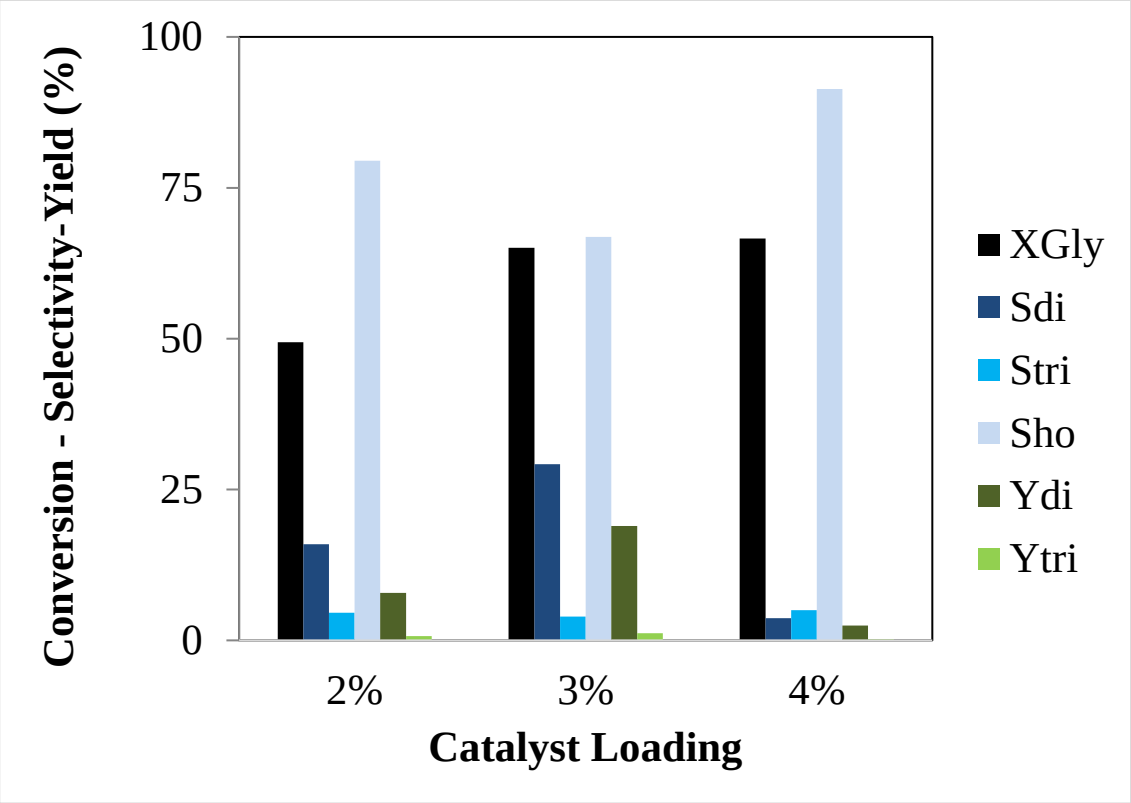

b)

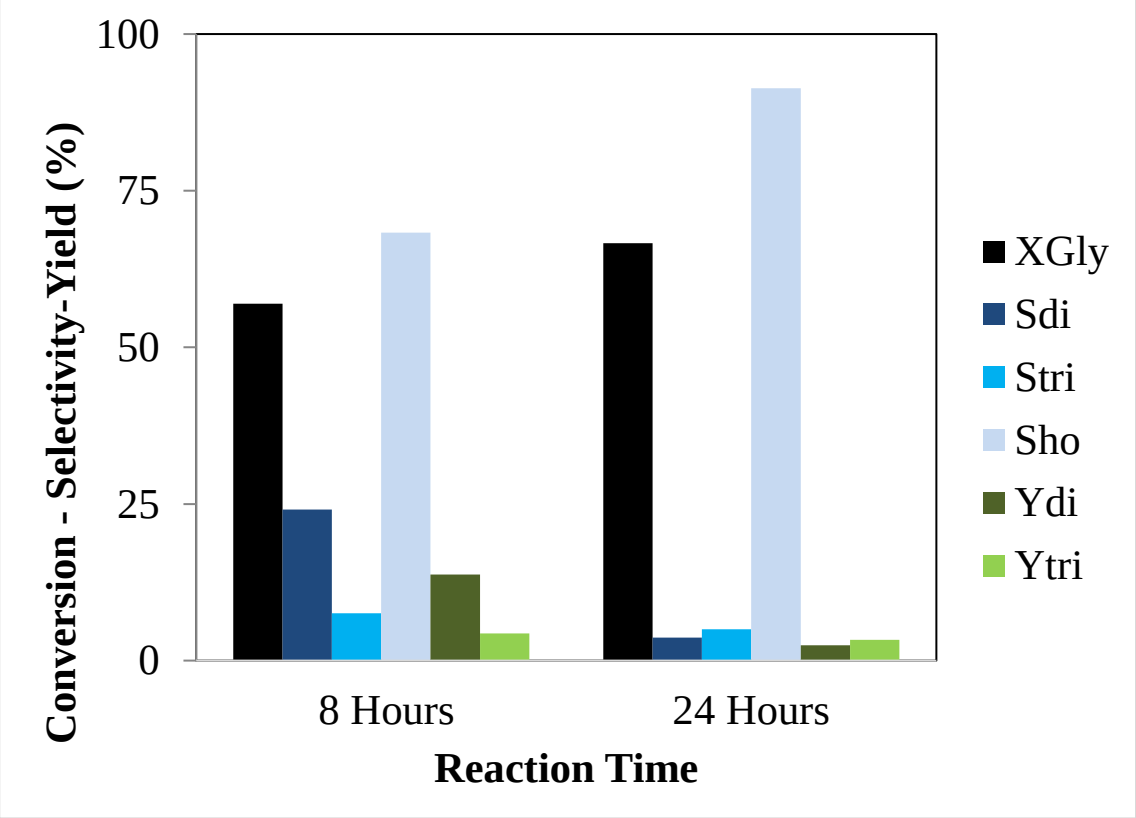

happen with MAC. For catalyst load tests, Figure 4.10 a), from 2 to 3% of MAC it was noticed an expressive increase of X_{Gly} (from 49 to 65%), however for an amount of 4% of catalyst there was a similar conversion and an expressive drop in selectivity to diglycerol (from 29 to 4%), pointing to the consumption of diglycerol by its oligomerization, thus increasing the formation of high oligomers (S_{ho} of 91%), which is in agreement with previous works (BARROS *et al.*, 2017; GHOLAMI; ABDULLAH; LEE, 2015; RICHTER *et al.*, 2008). This behavior can be explained by the higher number of basic sites available, which favors the consecutive steps of glycerol oligomerization.

Considering the longer time used in both reactions and the X_{Gly} achieved, the test with 4% of catalyst probably has reached similar selectivity to that of 3% in a lower time. To verify this hypothesis, (Figure 4.10 b) , a test for 8 hours was performed, at which X_{gly} was only 10% less than for 24 hours, and higher di and triglycerol selectivity (24 and 8%) was obtained, indicating that at this point diglycerol and triglycerol probably were not involved on the consecutive reactions.

Acrolein production was extremely low in all tests, with selectivity (S_{Acr}) lower than 0.5%, Table 4.4. Acrolein formation is more expressive with acidic catalysts, Peréz-Barrado *et al.* (2015), used a mixed oxide derived from Ca/Al LDH for glycerol oligomerization and has noticed that despite the presence of medium basic sites, high acidic content favored the formation of acrolein rather than di and triglycerol.

Table 4. 4 - Selectivity to acrolein for reactions with MAC and rehydrated catalysts.

Test	**Sample**	**S_{Acr} (%)**
Reaction Temperature	210 ºC	0.42
(4 wt% MAC and 24 hours)	220 ºC	0.17
	230 ºC	0.07
	240 °C	0.15
MAC Loading	2%	0.15
(240 °C and 24 h)	3%	0.02
	4%	0.15
Reaction time	8 h	0.11
(4 wt% MAC and 240 °C)	24 h	0.13
Rehydrated LDH	MAC	0.11
(4 wt%, 240 °C and 8 h)	MAU30	0.11
	MAU60	0.06
	MAM60	0.12
	MAM24	0.06

The activity of rehydrated materials was tested over the best set of reaction conditions observed (4 wt% of catalyst, at 240 °C and 8 hours of reaction), Figure 4.11 a). MAU30, MAM60 and MAM24 led to higher X_{Gly} than MAU60 (62, 64 and 73%, respectively, against 50%), in a correlation with their higher basicity and S_{BET} (Table 4.2). Such relation was also observed in Garcia-Sancho *et al.* (2011) , which compared a series of mixed oxides derived from Mg/Al LDH obtained with different precipitating agents ($NaOH/Na_2CO_3$, KOH/K_2CO_3 and NH_3 aqueous solution/$(NH_4)_2CO_3$).

Figure 4. 11 - a) Effect of rehydrated catalysts (reactions conditions: 4 wt% cat., 240 ºC and 8 h) b) Surface area and basicity versus Sdi.

a)

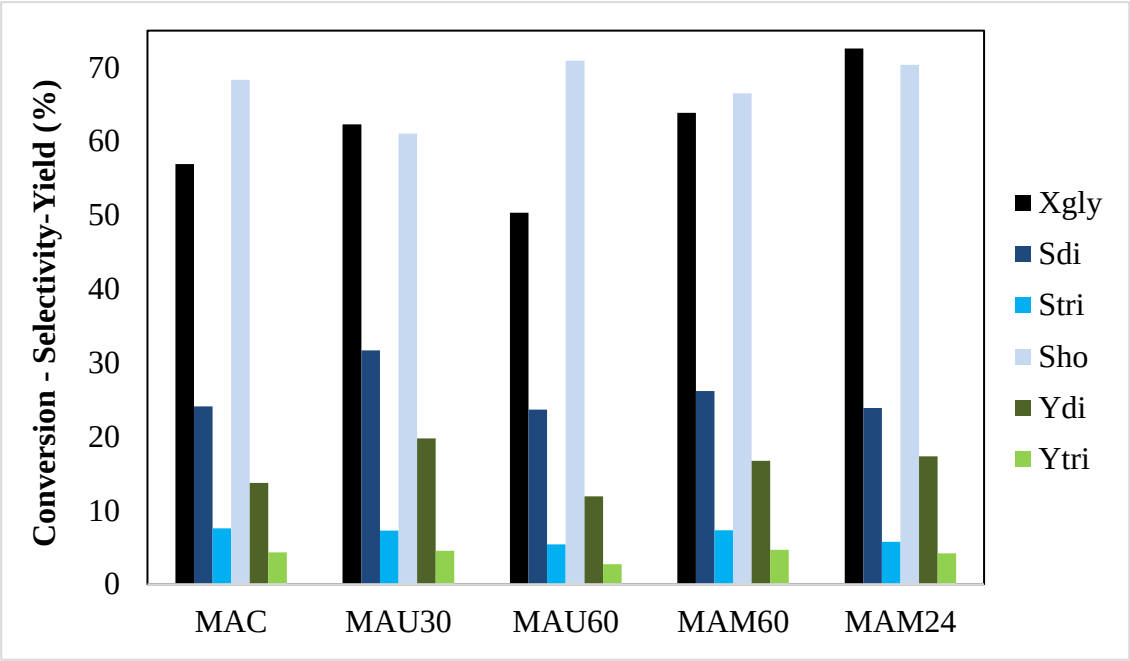

b)

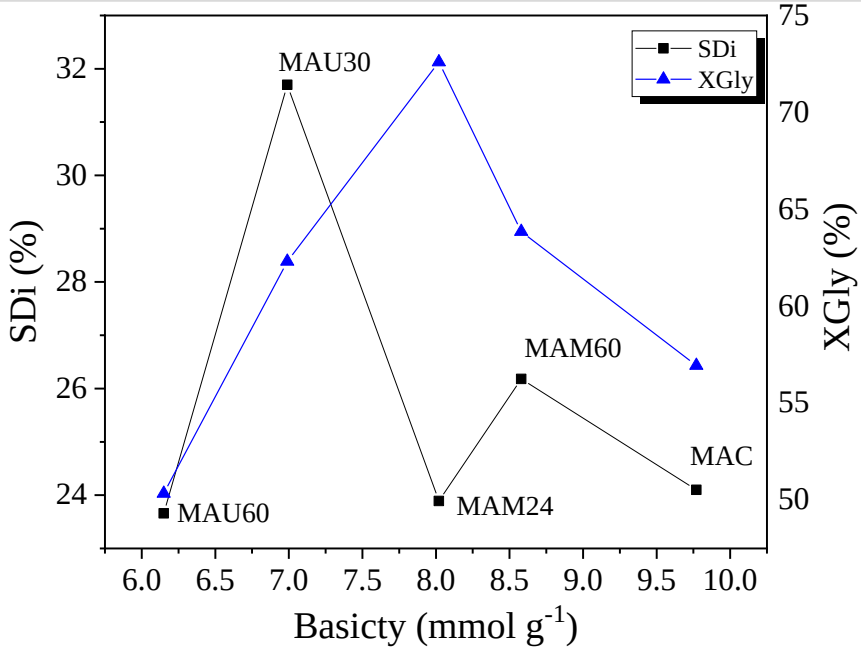

In terms of selectivity to diglycerol, it is necessary a deeper look into its correlation with basicity, Figure 4.11 b), above 8 mmol.g^{-1} the S_{di} is reduced for MAC, MAM60 and MAM24, indicating that from this value onwards production of higher oligomers and other compounds is favored; for ultrasound rehydrated samples, MAU60 had a much lower yield of diglicerol (12%) than MAU30 (20%), given the similar value of total basicity , this behavior could be explained by the distribution of strong basic sites, Table 4.2, which appear in higher amounts in MAU30.

Considering these hypotheses, it was decided to implement one more modification step in MAU30 to change it basic sites population. For this purpose, addition of acetic acid was chosen due to its weak character. The material was prepared by adding 20 mL of acetic acid to 1.4g of MAU30, with magnetic agitation for half an hour. Prior reaction, material was dried overnight at 120 °C and labeled as MAU30P.

Figure 4. 12 - MAU30P characterizations: a) XRD b) FTIR.

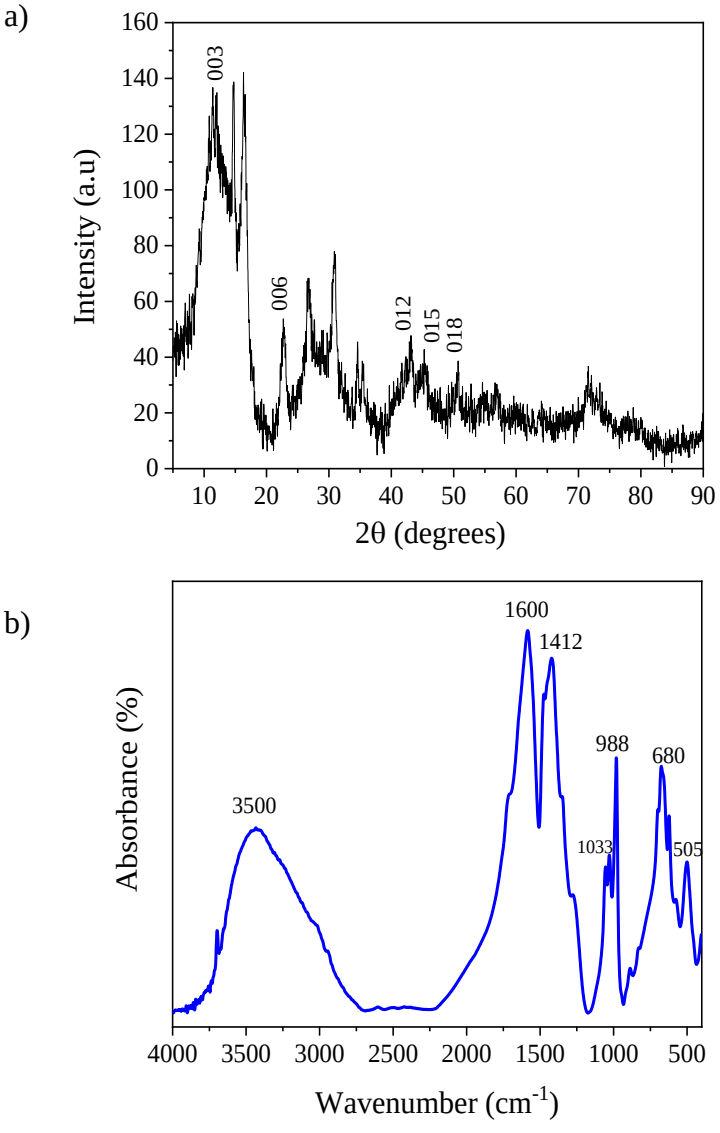

The characterization of MAU30P with XRD and FTIR is shown in Figure 4.12. Addition of acetic acid led to a material with the same diffractogram peaks of MAU30. However, increase of noise points to a lower crystallinity. Regarding FTIR, Figure 4.12 b), the main difference in comparison with MAU30 is the presence of bands characteristic of acetic acid from 1300 to 500 cm^{-1}, indicating that some amount of acid remains after drying.

Figure 4.13 a) shows nitrogen isotherm, before the addition of acetic acid material was type II and after that became type IV, suggesting the appearance of mesoporosity. Textural properties have changed as well, S_{BET} dropped from 44 to 24 m^2g^{-1}, V_P went from 0.04 to 0.05 $cm^3\ g^{-1}$ and D_P increased from 3.33 to 7.58 nm. Pore size distribution highlights this change of D_p, Fig 4.13ba).

Figure 4. 13 - MAU30P characterizations: a) N_2 isotherm and pore size distribution b) TEM (0.1 µm) c) TGA/DTG.

a)

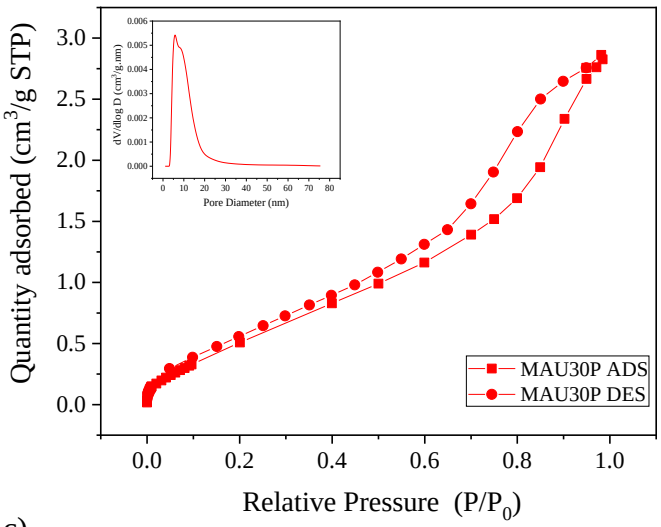

b)

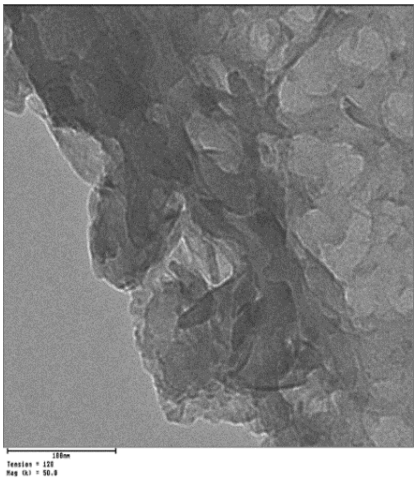

c)

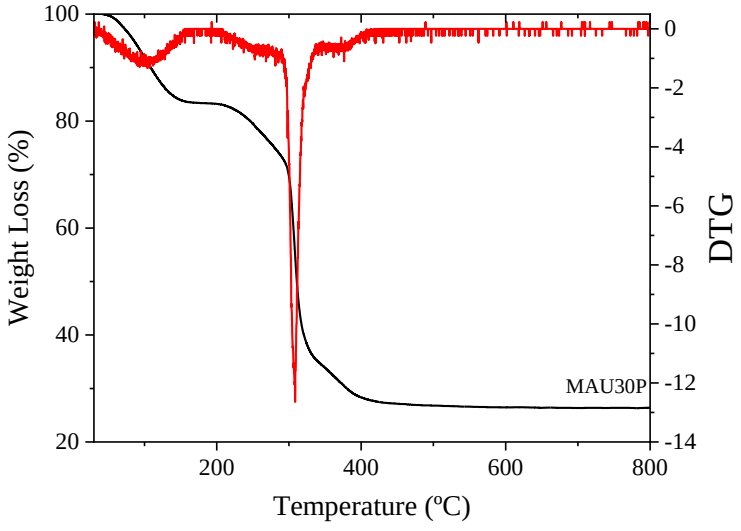

TEM image, Figure 4.13 b), suggests that morphology was not affected by the addition of acetic acid, since characteristic agglomerates of platelets are still present. TGA is presented in Figure 4.13 c), values of weight loss for this material are 16.9% for the first step (adsorbed water) and 56.68% for the second, compared to 11.3% and 32.61% for MAU30, respectively. Such behavior must be related to the presence of acetic acid .

Figure 4.14 shows a change in the distribution of basic sites after poisoning with acetic acid, displaying now two medium strength basic sites, the first with an intense and sharp peak at around 350 °C and the second at around 400 °C. Strong basic sites are present as can be notice by the peak at around 600 °C.

Figure 4. 14 - CO_2-TPD profiles (set-up 2) for a) MAU30P and b) MAU30.

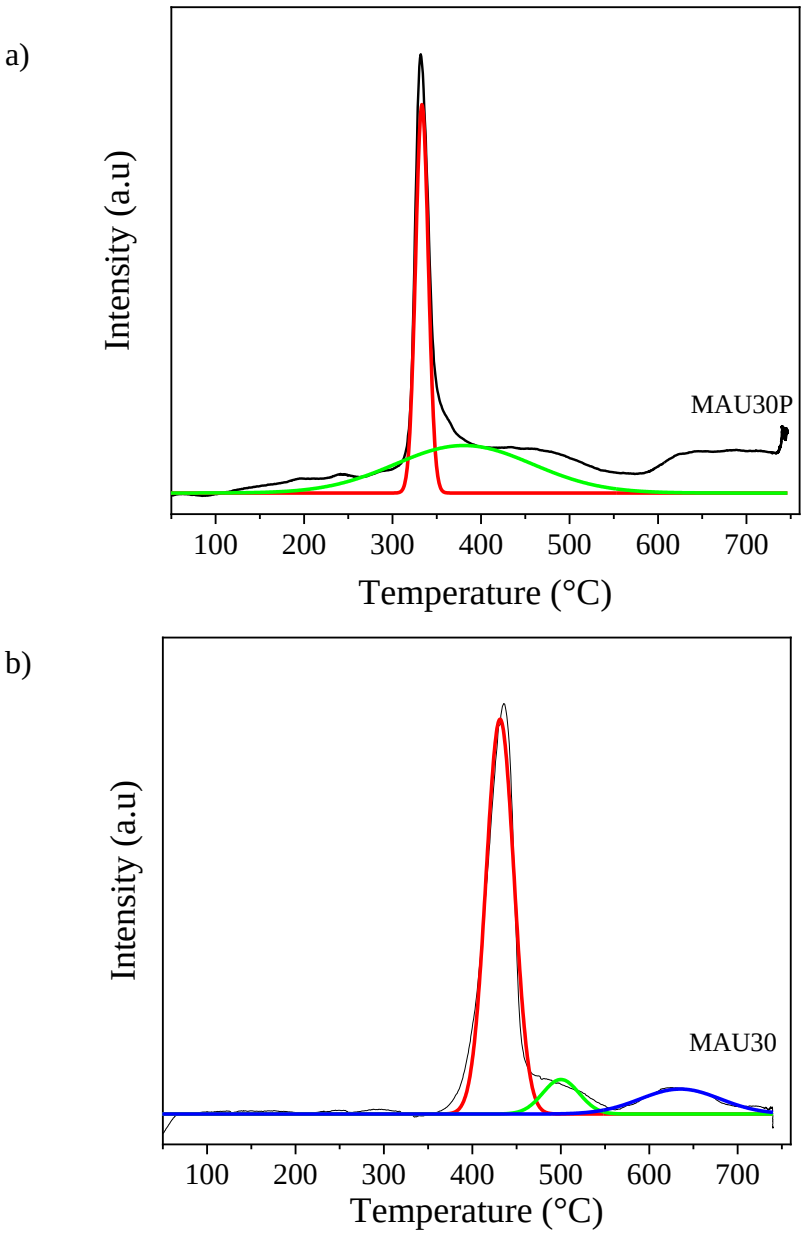

The reaction with MAU30P, Figure 4.15 a), led to X_{Gly} (64%) very similar to MAU30 (63%), Figure 4.15 b). However, the treatment was effective on increasing diglycerol selectivity (from 31% using MAU30 to 37% with MAU30P).

The catalytic performance MAU30P is interesting in comparison with previous works using Mg/Al LDH for glycerol oligomerization, since reached similar conversion in a lower time. Is important to notice that some of these works use different expressions to calculate selectivity. Mixed oxides from Mg/Al LDH coprecipitated with NaOH and Na_2CO_3 reported by Garcia-Sancho *et al.* (2011) led to 51% of X_{Gly} (reactions at 220 °C for 24 hours), the selectivity was calculated as the weight ratio of the respective product to the sum of products formed, being 84.8% for S_{di} and 15.2% for S_{tri} ; using this same approach in MAU30P data, S_{di} and S_{tri} would be 82.43 and 17.57% respectively. Anuar, Abdullah and Othman (2013) used the previous expressions as well, and their calcined Mg/Al LDH led to 78% of X_{Gly}, and approximately 80% of S_{di} and 20% of S_{tri} (reaction at 240 °C for 16 hours). Whereas Pérez-Barrado *et al.* (2015) studied calcined LDH (coprecipitated with $NH_3/(NH_4)_2CO_3$) and had a 60% of X_{Gly} (reaction at 235°C for 16 hours), in their work the selectivity term included a stoichiometric constant (2 for diglycerol and 3 for triglycerol), reaching 44% S_{di} and 11% S_{tri}. Application of this expression to the data in the present work results in 73.38% of S_{di} and 17.27% of S_{tri}.

MAU30P has shown to be more resistant to deactivation in comparison to MAU30 , Figure 4.15. MAU30 had an expressive drop on X_{Gly} already after the first reuse (from 63 to 21%), and only two reuses were possible, presenting a very low activity on 3rd run (9% of X_{Gly} and Y_{di} 4%). For MAU30P, X_{Gly} reaches 31% in the second run, with 62% of S_{di}; For the third run, there is an unexpected growing of X_{gly} to 61%, with a drop of S_{di} to 29%; For the fourth run, conversion goes to a minimum of 6%.The selectivity to acrolein , Table 4.5, was low until 3rd reaction cycle, and reached almost 2% in the last reaction, overall is a small amount, since X_{Gly} was only 6%.

Table 4.5 - Selectivity to acrolein for the reusability test of MAU30P.

Test	**Sample**	**SAcr (%)**
MAU30P	1st run	0.03
(4%wt, 240 °C and 8 h)	2nd run	0.29
	3rd run	0.25
	4th run	1.82

Figure 4. 15 - Reusability test (reaction conditions: 4 wt%, 240 °C and 8 h): a) MAU30P b) MAU30.

a)

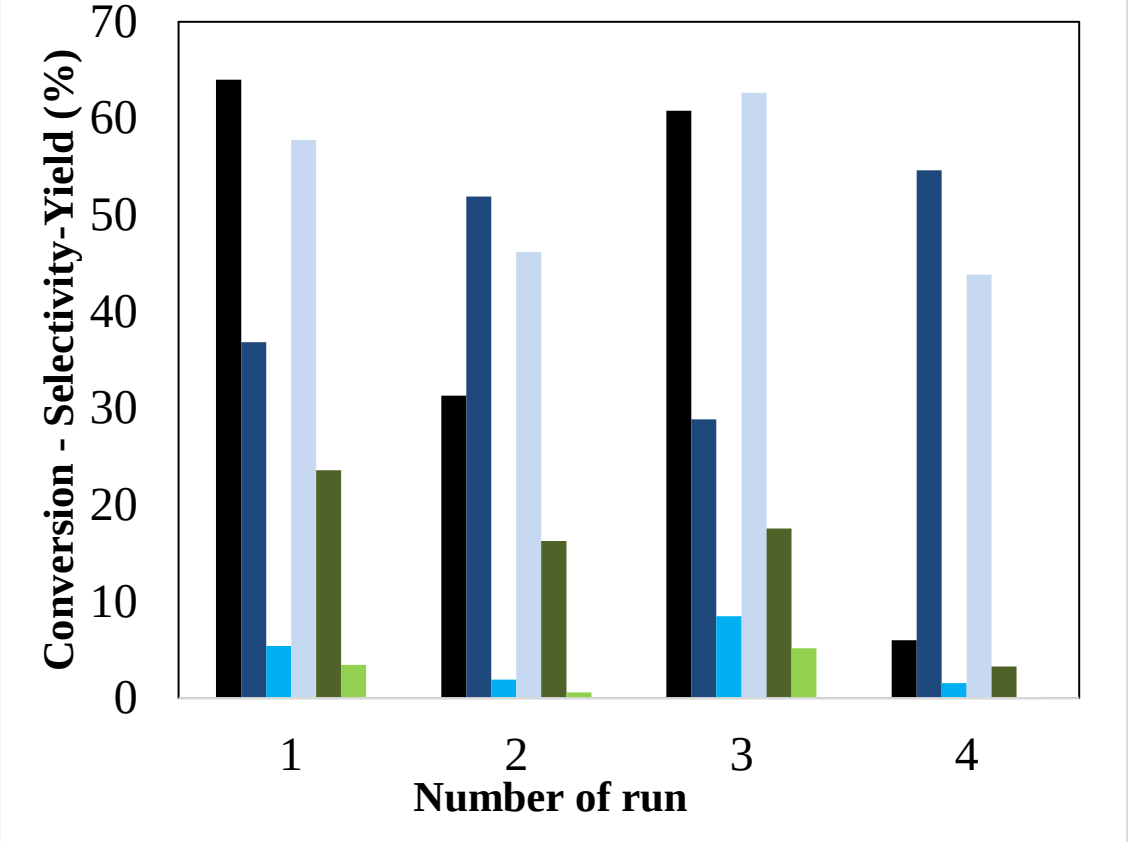

b)

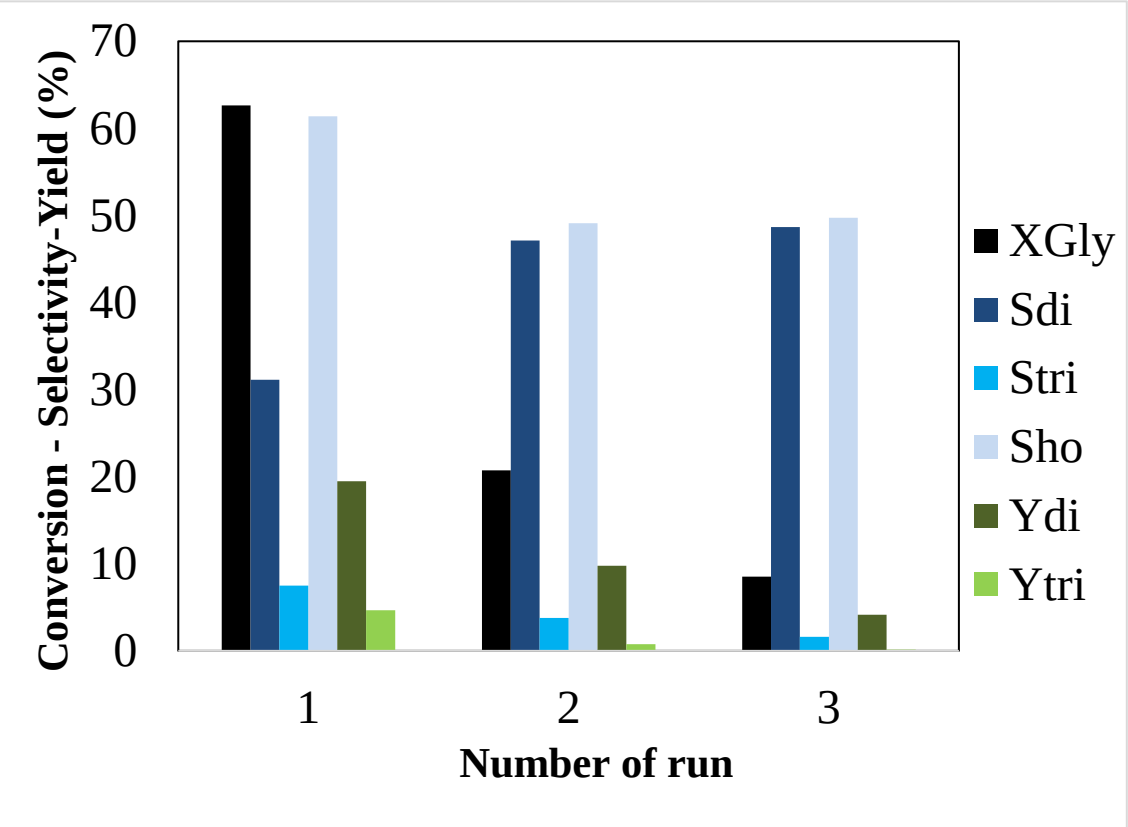

To understand catalyst deactivation, spent catalysts were characterized by TGA and XPS. Also, reaction products were analysed by ICP, to verify the occurrence of leaching of metallic species from catalysts to the reaction mixture. Catalyst was recovered as follows: solids and reaction medium were diluted in deionized water and then separated by vacuum filtration on a porous plate. In the next step, spent catalyst was dried at 80 °C overnight prior the new reaction cycle.

Following TGA and DTG profiles, Figure 4.16, spent catalysts have shown a first weight loss until 100 °C, and a second one between 200 and 500 °C, the latter can be divided in two parts for 2nd run spent catalyst. Comparing the total weight loss, 1st cycle spent catalyst has 46%, whereas the 2nd and 4th runs have 66% and 63% respectively, a major contribution of the second step can be noticed (Figure4.16b),

Figure 4. 16 - Thermogravimetric analysis of spent catalysts from reusability test of MAU30P: a) TGA and b) DTG.

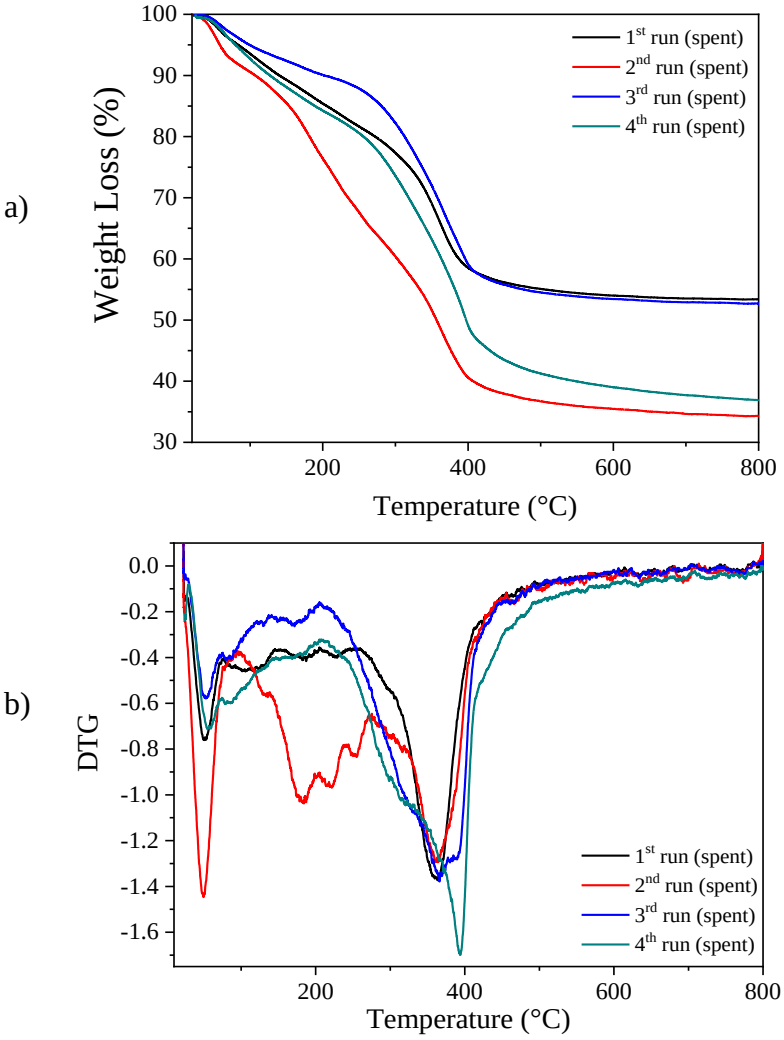

indicating the presence of species (20 and 17%, respectively) from unreacted glycerol or adsorbed products, which are responsible for decreasing the accessibility to basic centers and thus activity (ABELLÓ; VIJAYA-SHANKAR; PÉREZ-RAMÍREZ, 2008). The third cycle have almost the same total weight loss (48%) of the first and similar X_{gly} (61 % , against 64% of 1st cycle). However, deactivation affects S_{di} , reducing this value 8%.

The surfaces of MAU30 (fresh and spent from 3rd run) and MAU30P (fresh and spent from 1st run) were studied by XPS , Table 4.6 and Figure 4.17. Initially is important to notice a difference regarding the surface atomic ratio of Mg/Al, the material after acid treatment presents a higher ratio (2.59 compared to 1.75), due to the concentration of Mg.

Table 4. 6 - XPS results for fresh and spent catalysts MAU30 and MAU30P.

Sample	**Binding energy (eV)**				**Atomic concentration (%)**				**Molar ratio**
	C 1s	**O1s**	**Mg 2p**	**Al 2p**	**C**	**O**	**Mg**	**Al**	**Mg/Al**
MAU30(fresh)	284.84 (82.81%) 287 (13.6) 289.57 (3.6)	532.5	50.7	75	54.30	33.46	6.75	4.29	1.75
MAU30 3rd run (spent)	284.62 (75.85%) 286.55 (22.53%) 289 (1.62%)	530 (9.54%) 532.24 (90.46%)	50.5	74.6	56.04	30.43	5.06	6.01	0.99
MAU30P(fresh)	284.7 (68.71) 285.73 (8.82%) 288.83 (22.47%)	531.7	50.4	73.6	56.72	31.69	8.12	3.48	2.59
MAU30P1st run (spent)	284.74 (74.49%) 286.86 (20.76%) 288.98 (4.75%)	532.5	50.7	75	50.02	36.55	7.18	5.62	1.42

Surface Mg/AL molar ratios are lower than the ratio on the bulk determined by ICP-OES, table 4.1, suggesting the presence of a higher proportion of Al species on the catalyst surface. This superficial enrichment of aluminum was also observed by Garcia-Sancho *et al.* (2011) preparing Mg/Al LDH by coprecipitation. Spent catalysts had a reduction of this ratio, to 0.93 after 3 reaction cycles for MAU30 and to 1.42 for MAU30P after the first cycle, as a consequence of the decrease of Mg atomic concentration, these results can be related to the reduction on X_{Gly} observed in reusability test, Figure 4.15. Guerrero-Urbaneja *et al.* (2014) has also found similar correlation between catalytic behavior and structural stability (inferred from the superficial M^{II}/M^{III} atomic ratio) of mixed oxides derived of Mg/Fe LDH for glycerol oligomerization. Catalysts with reduction of the exposed iron after reaction had lower performance than the one where Mg/Fe atomic ratio was not affected.

Figure 4. 17 - XPS spectra for fresh and spent MAU30 and MAU30P: a) C 1s, b) O 1s, c) Mg 2p and d) Al 2p regions.

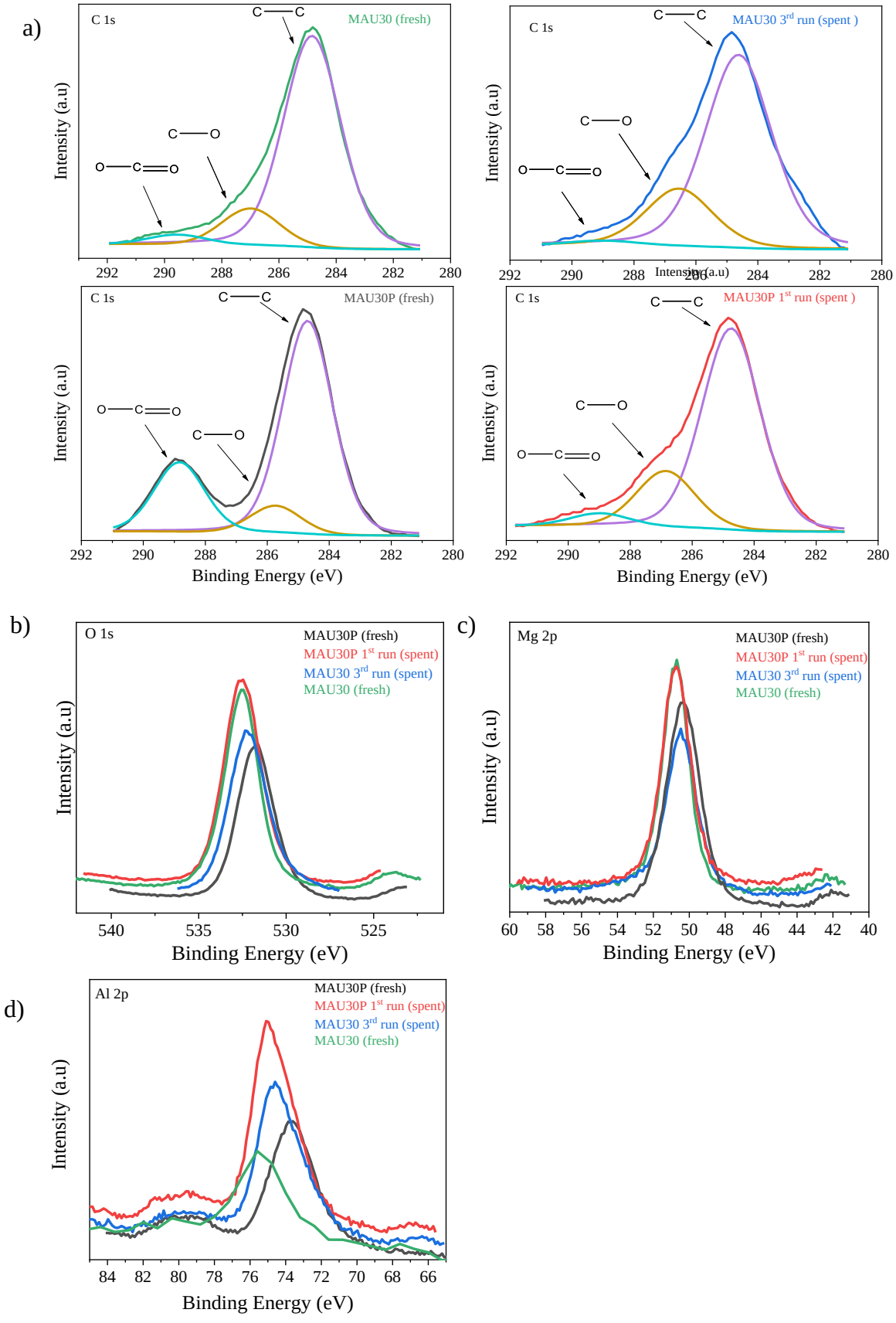

The C 1s core level spectra of fresh and spent catalysts displays three contributions, Figure 4.17a). The main binding energy located at 284 eV and the second contribution at 286 eV are attributed to adventitious carbon (C-C and C-O, respectively). Third band, at 298 eV, is related to the presence of carbonate. Distribution of these bands are markedly different for MAU30 and MAU30P, the later having 22% of carbonate, probably arising from the treatment with acetic acid. After the first reaction cycle, MAU30P displays a reduction of carbonate band to 4.75%. Increase of the band at 286 eV (C-O) is noticeable in the recycling of both catalysts, and can be related to unreacted glycerol or oligomers at the surface.

For the O 1s signal, MAU30 displays a band at around 532.5 eV, related to the hydroxide form. After three reaction cycles, the signal can be deconvoluted into two contributions, the main band has the binding energy reduced to 532.24 eV and the second at 530 eV, is ascribed to the presence of O^{2-} (GUERRERO-URBANEJA *et al.*, 2014; PADMASRI *et al.*, 2002). MAU30P presents a single band at around 531.7, related to the carbonate group. Conversely, the spent catalyst recovered from first run has this band shifted to 532.5 eV, indicating change of composition from carbonate to hydroxide.

Regarding the Mg 2p region, in all samples there is a single contribution ranging from 50.4 to 50.7 eV. For Al 2p signal, binding energy values are from 73.3 to 75 eV. Both results are related to the hydroxide form, these findings are supported by the O 1s core level spectra (PADMASRI *et al.*, 2002).

ICP-OES analysis has showed that the reaction products from the reuse of MAU30P did not have Mg and Al contents arising from catalysts, discarding possible leaching contribution for catalyst deactivation. In our previous work , glycerol oligomerization catalyzed by calcined dolomite (at 220 °C, with 2% of catalyst and 24 hours) presented Mg^{2+} concentrations of 160 ppm for the first reaction cycle, 190 ppm to for the second and 240 ppm for the third (BARROS *et al.*, 2018). Thus, Mg/Al rehydrated LDH has proved to be a more stable catalyst for this reaction.

The conversion of glycerol and the yield of oligomers versus time were monitored for the best set of reaction conditions, Figure 4.18. Within the first 3 hours, 8% of glycerol conversion is achieved with yield of diglycerol and triglycerol of 3% and 0.14%, respectively. The production of diglycerol is directly proportional to X_{Gly}, while triglycerol production is very low, starting to increase after 4 hours of reaction. Our previous work with CaO from waste eggshells has shown a similar profiles, for reaction at 220 °C with 2 wt% of catalyst (BARROS *et al.*, 2017).

Figure 4. 18 - X_{Gly} and oligomers yield versus time for MAU30P (reaction conditions: 4 wt% cat., 240 °C and 8 h).

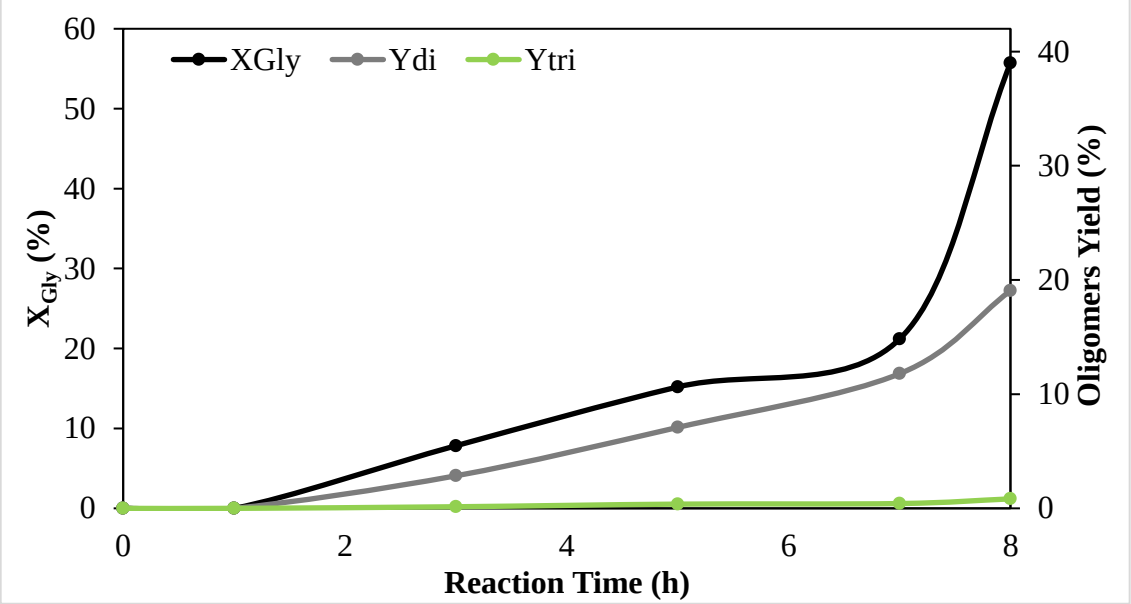

4.1.3 Partial Conclusion

Characterization of rehydrated Mg/Al LDHs by XRD, FTIR and TGA has shown the modification of interlamellar composition, with reduction of carbonate and differences in water content. Presence of defects on the structure was noticed as well. Treatment by ultrasound or mechanic stirring induced changes in the basic sites and thus in the activity for glycerol oligomerization. After evaluating reaction parameters, the best set of conditions was used for rehydrated materials (4 wt% of catalyst, at 240 °C for 8 hours) and MAU30 led to the best response (X_{Gly} of 63%, S_{di} of 31% and S_{tri} of 7.5%). A modification procedure for the catalyst was developed after these findings.

Addition of acetic acid to the LDH reconstructed by ultrasound for 30 minutes, has changed its distribution of base sites. Catalytic application of MAU30P led to X_{Gly} of 64%, S_{di} of 37% and S_{tri} of 5.4%. XPS results indicated that MAU30P had more structural stability than MAU30, assuring lower deactivation in catalyst recycling. Leaching of metallic species from catalysts to the reaction products was not observed. However, there was reduction in the molar ratio of Mg/Al on the surface upon recycling. The presence of unreacted glycerol and adsorbed products contributed to deactivation. MAU30P has increased the selectivity to diglycerol, reaching 37%, and exhibited good catalytic performance at relatively low reaction time (8 hours) in comparison to previous studies, together with recyclability up to 3 reuses.

4.2 Zn/Al layered double hydroxides and fluoroperovskites catalytic application in glycerol oligomerization

4.2.1 Zn/Al LDH derived materials

4.2.1.1 Catalysts characterizations

ICP-OES was used to confirm the presence of Zn and Al, and their ratio on as-synthesized LDH , mixed oxide and rehydrated samples, Table 4.7. Molar ratio was close to the theoretical value of 2, and no expressive change was noticed through the modification steps.

Table 4. 7 - ICP - OES analysis and structural data (d spacing, unit cell dimensions, ISF and relative intensity) for Zn/Al catalysts.

Sample	Zn/Al[a]	d_{003}	d_{110}	a (Å)	c (Å)	IFS(Å)	I_{006}/I_{003}
ZAS	2.14	7.562	1.537	3.074	22.686	2.76	0.29
ZAC	2.15	-	-	-	-	-	-
ZAU30	2.22	7.456	1.533	3.066	22.369	2.66	0.43
ZAU60	2.19	7.451	1.531	3.062	22.352	2.65	0.37
ZAM60	2.29	7.522	1.536	3.071	22.566	2.72	0.38
ZAM24	2.11	7.477	1.625	3.251	22.431	2.68	0.41

[a] ICP-OES;

*d_{003} and d_{110} : d spacing;

*a and c (Å): unit cell dimensions;

* ISF (Å) : Interlayer free space, ISF=(c/3) - 4.8 (PAVEL *et al.*, 2008);

*I_{006}/I_{003}: relative intensity.

Figure 4.19 shows the diffractograms of dried Zn/Al LDH (ZAS), its mixed oxide (ZAC) and rehydrated samples (ZAU30, ZAU60, ZAM60 and ZAM24). As in our previous work, with rehydrated Mg/Al, lamellar structure was recovered upon the different stirring processes and times. According to JCPDS 70-2151 the characteristic planes of layered double hydroxides, (0 0 3), (00 6), (110),(113),(0 1 2), (0 1 5) and (0 1 8) are present in ZAS and rehydrated samples. The change in the relative intensity of basal peaks (I_{006}/I_{003}) and the reduction of interlayer free space (related to d_{003}), presented in Table 4.7, suggests that rehydrated materials have lower crystallinity and present differences in the interlayer composition. According to Thomas *et al.*(2006) the relative

intensities of (003) and (006) reflections depend on the electron density in the interlayer region. Furthermore, the complete loss of water understandably results in a decrease in the interlayer spacing from d_{003} of 7.6 to 6.5 Å.

Calcined material, ZAC, presented a similar diffractogram profile to previously reported results, in which ZnO peaks were larger than those of pure ZnO (JCPDS 01-075-1533), suggesting that Al^{3+} cations are incorporated into the lattice of ZnO, implying that this calcination temperature led to the transformation of Zn/Al LDH into well-dispersed Zn/Al mixed oxides (LIU *et al.*, 2014) .

Figure 4. 19 - XRD for ZAS, ZAC, ZAU30, ZAU60, ZAM60 and ZAM24.

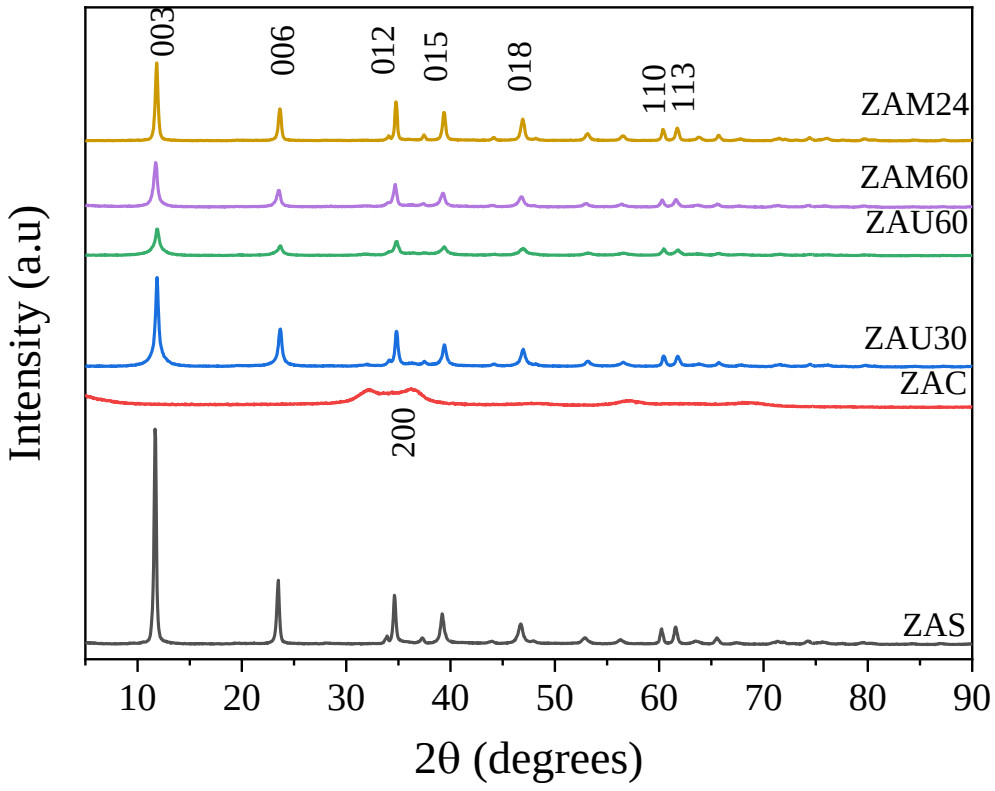

FTIR was used to verify possible changes in functional groups after calcination and rehydration, Figure 4.20. The broad and intense band centered on 3500 cm^{-1} is attributed to O-H stretching vibration in water molecules from brucite-like layers and interlamellar region. The band at around 1350 cm^{-1} is related to carbonate. These bands nearly disappear after calcination, and exhibits different intensities in rehydrated samples, suggesting differences in the composition of lamellar interspace of sonicated and mechanically stirred samples, for instance ZAU60 displays the lowest intensity in both of them, in accordance with the changes on its structural data reported in Table 4.7. The bands between 1000 and 500 cm^{-1} can be related to Zn and Al oxides. ZAU30 and

ZAU60, did not present this band, whereas the ones rehydrated by mechanic agitation exhibited higher intensity (DAS; DAS; PARIDA, 2003; ELHALI *et al.*, 2018).

Figure 4. 20 - FTIR for ZAS, ZAC, ZAU30, ZAU60, ZAM60 and ZAM24.

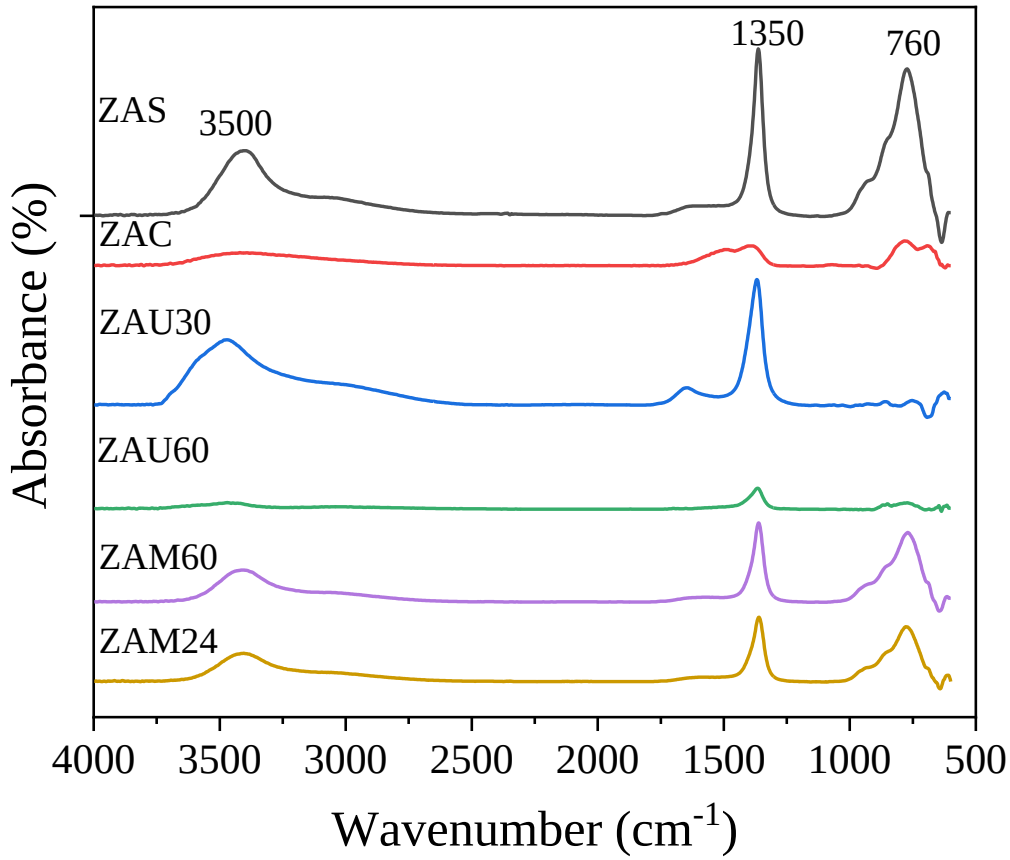

The thermogram of Zn/Al LDH and rehydrated samples shows weight loss up to 360 °C, corresponding to one peak in the DTA curve, Figure 4.21 b). Unlike the case of Mg/Al LDH in Section 4.1, loss of adsorbed and interlamellar water and the decomposition of OH^- and CO_3^{-2} takes place in one step, in agreement with the findings reported by Das *et al.*, (2003). For ZAC weight loss is up to 240 °C. Rehydrated materials recovered the aspect presented by ZAS thermogram, confirming reconstruction of lamellar structure after calcination at 450 °C , in accordance with XRD results. Their smaller total weight loss, Table 4.8, supports the differences in composition pointed by FTIR analysis, since samples submitted to mechanic stirring have higher total weight loss and more intense bands for -OH and carbonate in comparison to the sonicated ones. The reconstructed samples contained fewer hydroxides and carbonate ions in comparison with ZAS, which is in accordance with previous works (STARUKH; ROZOVIK; ORANSKA, 2016).

Figure 4. 21 - a) TGA b) DTG for ZAS, ZAC, ZAU30, ZAU60, ZAM60 and ZAM24.

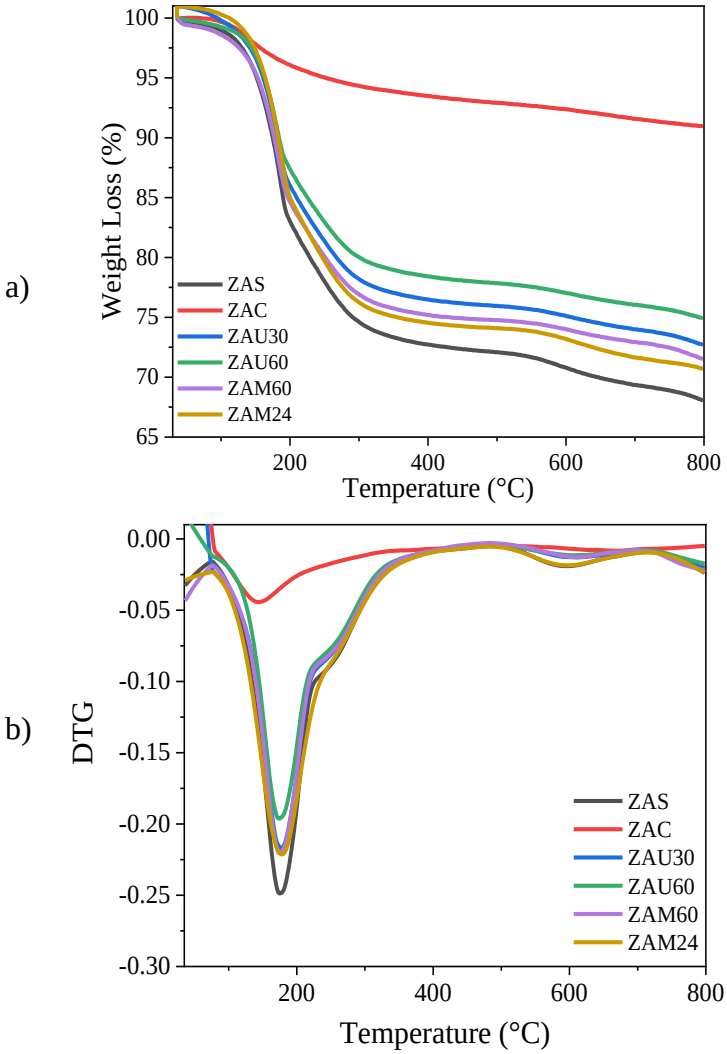

Table 4. 8 – Total weight loss for ZAS, ZAC, ZAU30, ZAU60, ZAM60 and ZAM24.

Sample	**W_{Total} (%)**
ZAS	32.07
ZAC	9.08
ZAU30	27.22
ZAU60	25.13
ZAM60	28.43
ZAM24	29.26

Textural properties are summarized in Table 4.9, it is possible to notice that calcination resulted in higher surface area in comparison to ZAS. Both ultrasound and mechanic stirring rehydrated samples presented surface area in the range of values of ZAC. Absence of correlation between these same rehydration modes and the textural properties of Zn/Al LDH was also reported by Prakruthi, Prakash and Bhat (2015).

Table 4. 9 - Textural properties and surface basicity for Zn/Al catalysts.

Sample	S_{BET} ($m^2\ g^{-1}$)	V_P ($cm^3\ g^{-1}$)	D_P (nm)	Base sites ($mmol.g^{-1}$)		
				Total [a]	Strong [b]	Weak [c]
ZAS	44	0.12	2.33	0.92	0.14	0.78
ZAC	59	0.15	2.28	0.54	0.03	0.51
ZAU30	50	0.12	2.20	0.92	0.15	0.78
ZAU60	57	0.15	2.22	1.46	0.14	1.31
ZAM60	38	0.09	2.28	0.74	0.15	0.59
ZAM24	57	0.15	2.24	1.33	0.13	1.19

[a] Acrylic acid was used as a probe molecule;
[b] Phenol was used as a probe molecule;
[c] Weak base site = Total base site − Strong base site.

The N_2 physisorption isotherms are shown in Figure 4.22. The adsorption isotherms are type II according to the IUPAC classification; nitrogen uptake monotonically increases with P/P_0 values due to sorption in LDH. The same aspect for

Figure 4. 22 - N_2 isotherms for ZAS, ZAC, ZAU30, ZAU60, ZAM60 and ZAM24.

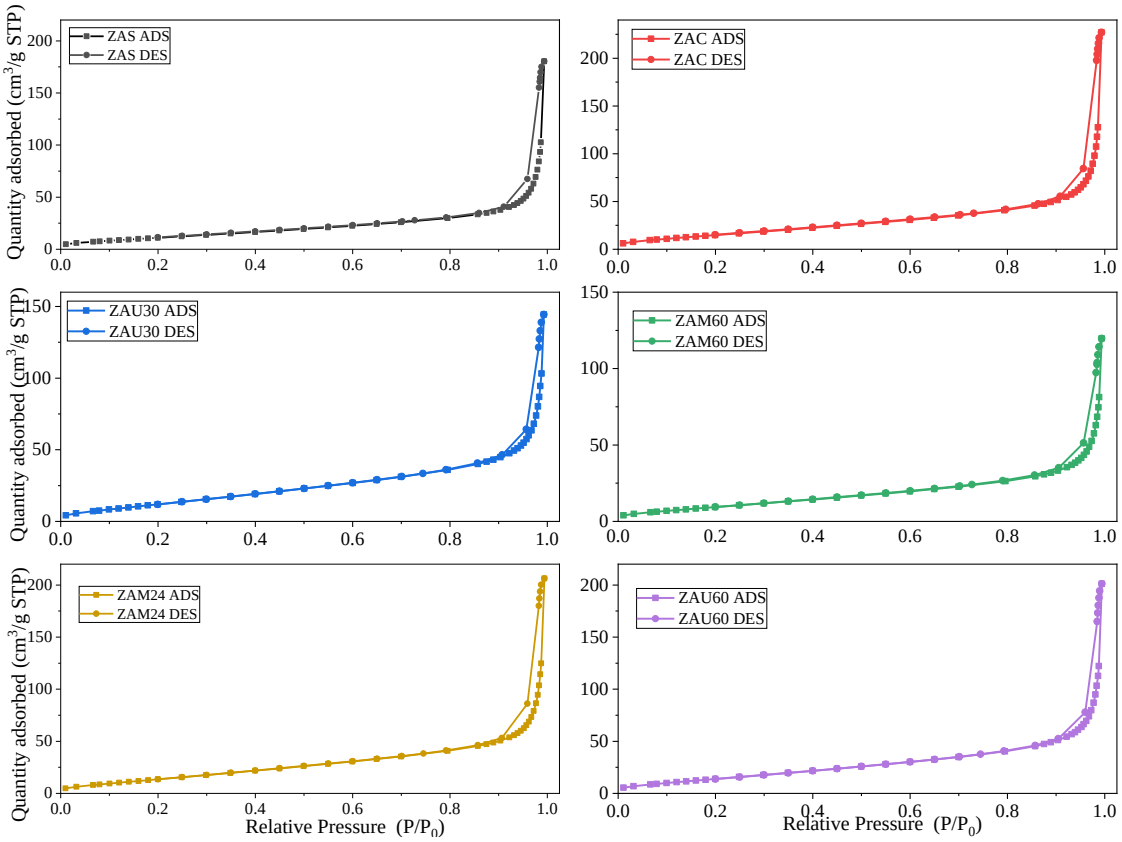

Zn/Al LDH isotherm was observed by Angelescu *et al.* (2008), with the presence of a narrow hysteresis of type H3, characteristic of aggregates of platelike particles forming slit-like pores. According Rouquerol *et al.*(2013) , this isotherms are present on a number of powders or aggregates, such as clays and cements. The pore size distributions, shown in Figure 4.23, has the same profile for all solids. Thus, rehydration did not have effect in this textural property. The average diameter of pores was around 2 nm.

Figure 4. 23 - BJH pore size distribution for ZAS, ZAC, ZAU30, ZAU60, ZAM60 and ZAM24.

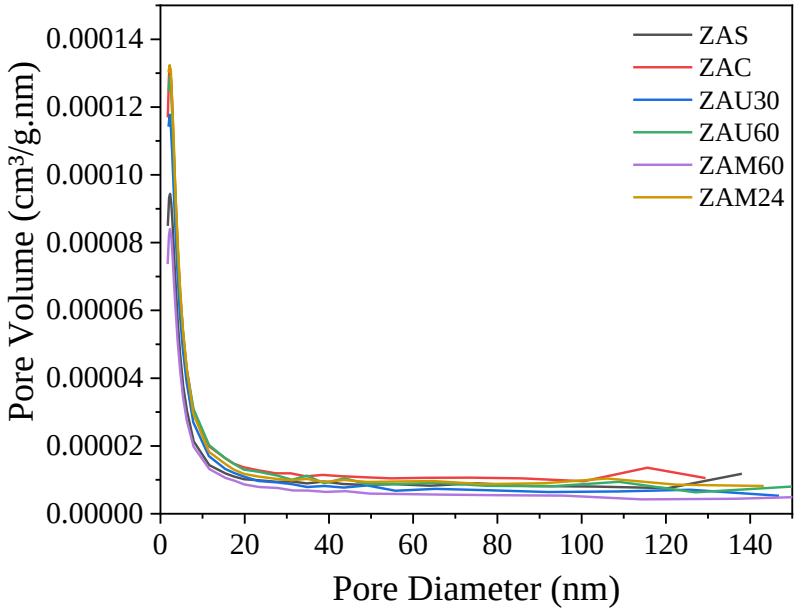

The micrographs in figure 4.24, shows very clear hexagonal crystals for ZAS and this aspect is partially maintained for calcined form (ZAC), solids rehydrated by ultrasound or mechanic agitation. The darker regions suggests the presence of aggregate crystallites which probably were obtained from a dense agglomeration of LDH particles (ELHALIL *et al.*, 2017). Porous appearance is in evidence for ZAC,ZAU60 and ZAM24 with small and uniform spaced craters. The scape of CO_2 through holes at the crystal surface can explain the development of porosity on ZAC (PAVEL *et al.*, 2008) . This effect is responsible for its higher surface area in comparison with ZAS, Table 4.9.

Basicity plays an important role in glycerol oligomerization., Table 4.9 presents total, strong and weak base sites determined by irreversible adsorption of acids (acrylic acid for total and phenol for strong sites). For Zn/Al LDH rehydration study, both methods of stirring were successful in recover/increase base sites after calcination, and it is possible to notice a correlation between time of rehydration and the total of base sites. Sonication assisted rehydration was more favorable to obtaining abundant weak base sites

than mechanical stirring, ZAU60 had he highest number of weak sites, 1.31 mmol.g^{-1}. Lee *et al.* (2014) has observed similar trends by using this same approach to calculate total basicity of Mg/Al LDH and derived rehydrated materials using ultrasound and mechanic stirring as well. Prakruthi, Prakash and Bhat (2015), reported that despite surface area values of as-synthesized Zn/Al LDH and rehydrated samples (using the same stirring mode as in this work) were in the same range, the base sites distribution (obtained by CO_2-TPD in this case) was different.

Figure 4. 24 - TEM images (scale bar 0.2 µm) for ZAS, ZAC, ZAU30, ZAU60, ZAM60 and ZAM24.

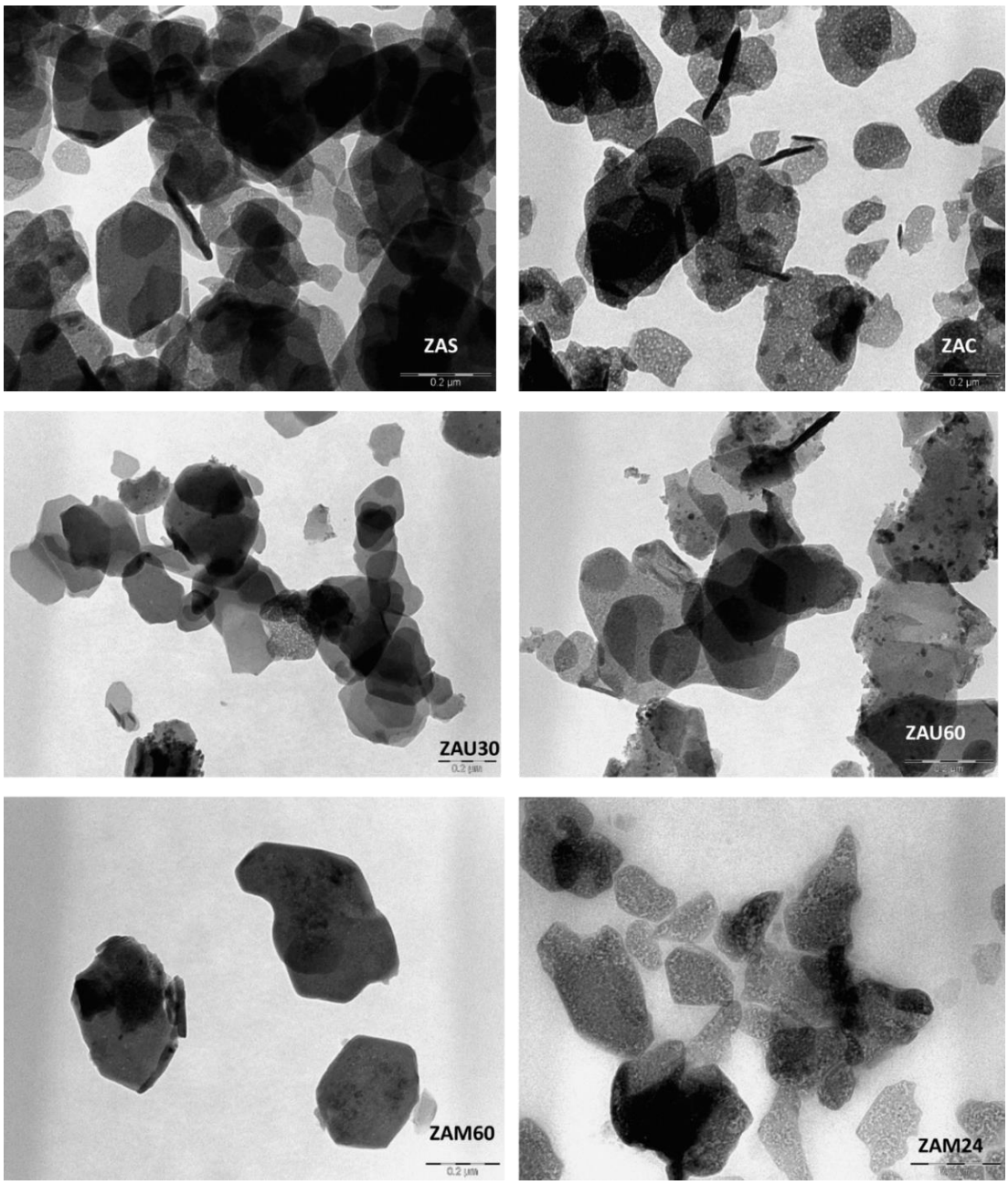

4.2.1.2 Activity of Zn/Al LDH and derived materials for glycerol oligomerization

Initially, reaction conditions were evaluated for ZAC, calcinated at 450 °C. Study of reaction temperature is presented in Figure 4.25a), for tests with 2% of catalyst within 24 hours, 220 °C led to small glycerol conversion (3%). By raising temperature to 230 °C, X_{Gly} achieved 12% with S_{di} of 43% and S_{tri} of 2% . On the contrary of the behavior exhibited with calcined Mg/Al LDH, in Section 4.1, higher temperature (240 °C) had similar activity to that of 230 °C (12%X_{Gly}, 44%S_{di} and 2%S_{tri}). Thus 230 °C was used in the following tests. For catalyst load evaluation, Figure 4.25 b), the activity increased with the higher amounts of ZAC. By using 3% of catalyst, X_{Gly} reached 18%, with similar S_{di} (41%). Further increasing to 4% of ZAC, de X_{Gly} was 23%, with 44% of S_{di}, such behavior is due to the larger number of base sites available.

For comparison with the Mg/Al mixed oxide, a test with shorter reaction time was performed as well, Figure 26 a). Within 8 hours of reaction, X_{Gly} was of 9% and the selectivity to diglicerol and to higher oligomers and other products (S_{ho}) were almost the same of the 24 hours test. This result suggests that with ZAC the conversion of glycerol was directed to the formation of diglycerol. The involvement of dimer in further oligomerization, resulting in higher selectivity to triglycerol and higher oligomers, takes more time due to the lower activity of this catalyst, in contrast with the Mg/Al catalyst.

To assess the activity of rehydrated solids, reaction conditions were 230 °C, 4% of catalyst and 8 hours, Figure 4.26 b). For mechanically stirred catalysts, ZAM60 had the same X_{Gly} of ZAC, with S_{di} of 43% and S_{tri} of 2%. Whereas the solid obtained after longer rehydration time, ZAM24, had 14% of X_{Gly}. These results can be correlated to the total basicity, Table 4.9, since ZAM24 presented 1.33 mmol.g^{-1}, ZAM60 0.74 mmol.g^{-1} and ZAC had 0.54 mmol.g^{-1}. The S_{di} was reduced to 29% for ZAM24 and S_{ho} reached 71%, suggesting that use of this catalyst favors diglycerol conversion into higher oligomers. For tests with the sonicated LDHs, ZAU30 had lower X_{Gly} (5%) and S_{di} of 36%.Conversely, ZAU60 had the highest X_{Gly} (25%), with S_{di} and S_{ho} similar to ZAC (42 and 54 %, respectively) and a higher S_{tri} (3.52%). Such result is consonant with the total basicity of ZAU60, which was the highest (1.47 mmol.g^{-1}).

Low selectivity to acrolein was observed in all tests performed with Zn/Al LDH derived catalysts, staying under 0.2%, Table 4.10, indicating that the material directed the conversion of glycerol to its oligomerization.

Figure 4. 25 - Catalytic evaluation of ZAC: a) Reaction temperature (reaction conditions: 2 wt% cat. and 24 h) b) Catalyst loading (reaction conditions: 230 °C and 24 h).

a)

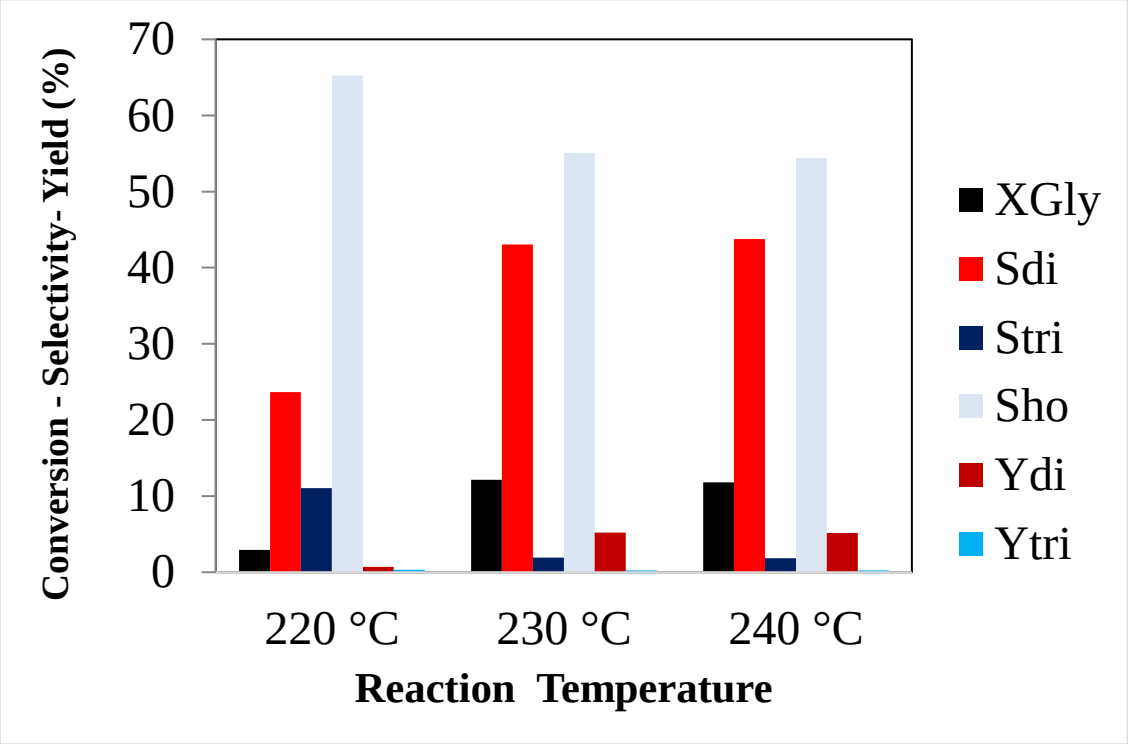

b)

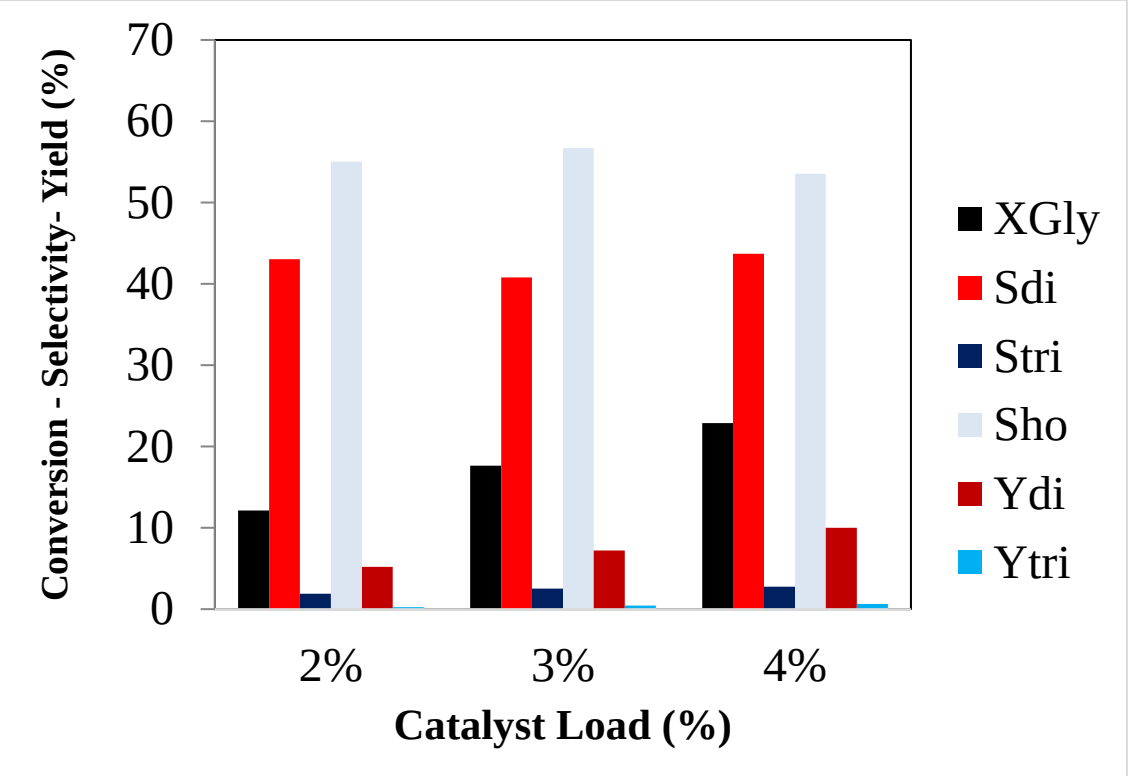

Figure 4. 26 - a) Evaluation of reaction time (reaction conditions: 4 wt% ZAC and 230 °C) and b) Rehydrated materials (reaction conditions: 4 wt% cat., 230 °C and 8 h).

a)

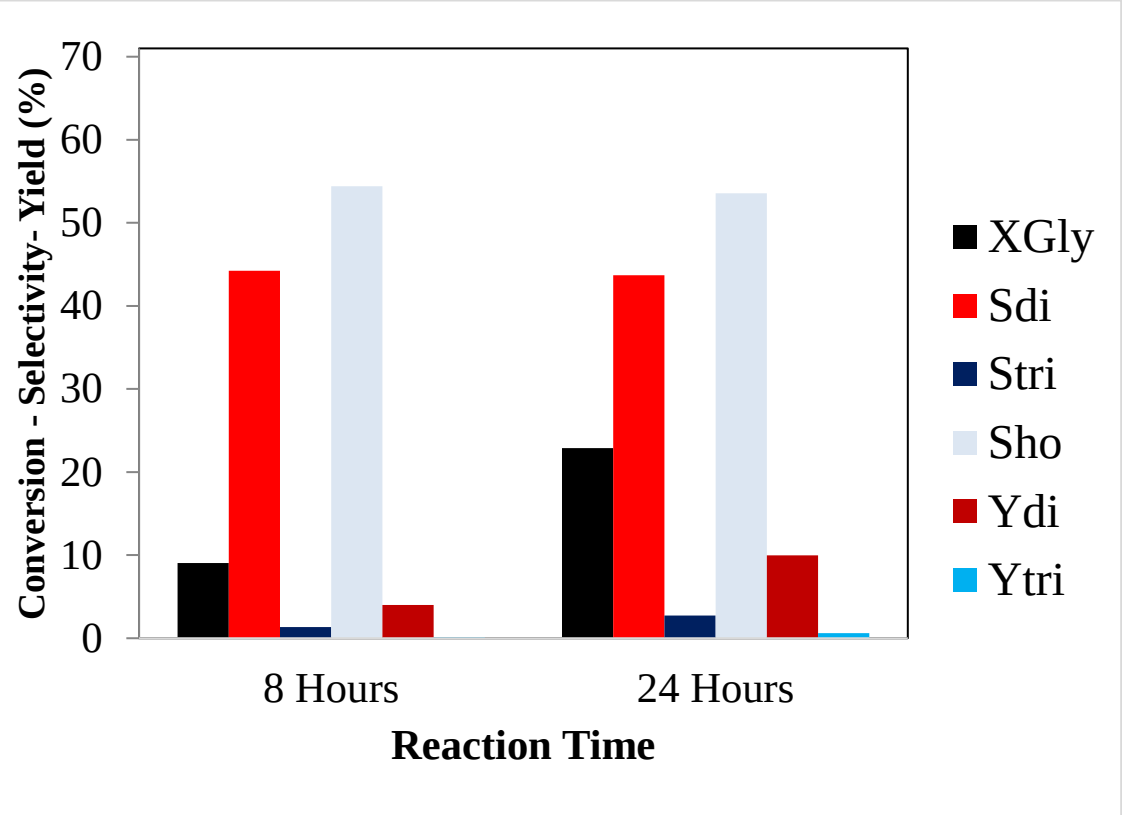

b)

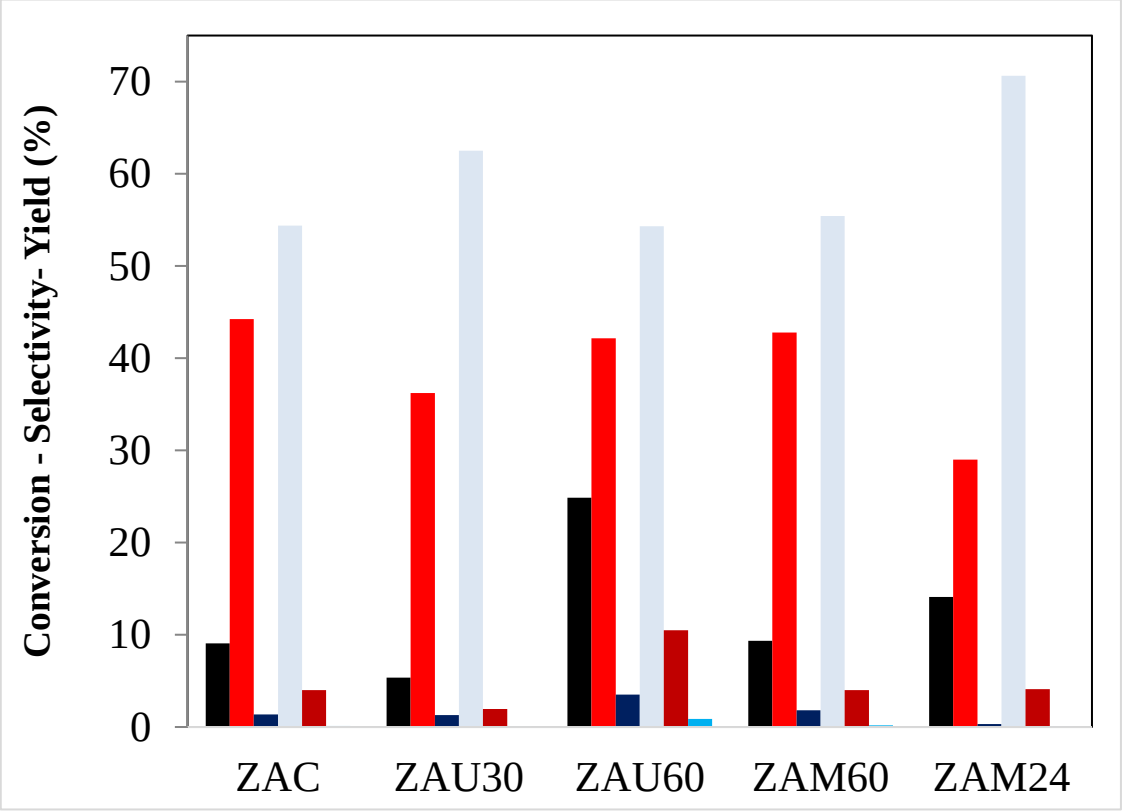

Table 4. 10 - Selectivity to acrolein for Zn/Al LDH tests.

Test	**Sample**	**S_{Acr} (%)**
Reaction Temperature	220 °C	0.14
(4 wt% cat. for 24 h)	230 °C	0.09
	240 °C	0.17
Catalyst Load	2%	0.09
(230°C for 24 h)	3%	0.03
	4%	0.22
Reaction Time	8 h	0.22
(4 wt% cat. and 230°C)	24 h	0.22
Rehydrated Zn/Al LDH	ZAC	0.22
(4 wt% cat., 230°C and 8 h)	ZAU30	0.12
	ZAU60	0.07
	ZAM60	0.06
	ZAM24	0.06

Comparison of physicochemical properties of ZAU60 and ZAM24 (Table 4.9) shows the same S_{BET} (57 m^2 g^{-1}), and their base sites distribution is markedly different for weak sites, ZAU60 has 1.31 $mmol.g^{-1}$ and ZAM24 1.19 $mmol.g^{-1}$.

For both Zn/AL and Mg/Al LDH (Figure 4.11a), the rehydration led to better activity than the use of mixed oxides. Considering the mechanism proposed by (RUPPERT *et al.*, 2008), Figure 2.2, first step of glycerol oligomerization is the proton extraction. The surface hydroxyl groups of rehydrated LDH lattice acts as Bronsted basic centres in this step, being more appropriate than the Lewis basic centres (O^{2-}) present in calcined materials, ZAC and MAC. Similar findings were observed by Jinesh, Antonyraj and Kannan (2010), assessing the catalytic activity of rehydrated Mg/Al LDH for the isomerization of allylbenzene.

4.2.2 Fluorine-containing catalysts

4.2.2.1. Catalysts characterizations

The ICP-OES results for as-synthesized samples, Table 4.12, confirmed that the M^{II}/Al molar ratio (where M^{II} is Mg, Zn, Co or Cu) is in good agreement with the theoretical amounts in the aqueous solution. Their molar ratio of K/Al was around 3.

Table 4. 11 - ICP - OES analysis for FPMAS, FPZAS, FPCoAS and FPCuAS.

Sample	M^{II}/Al^{a}	M^{II}/Al^{b}	K/Al
FPMAS	3	2.94	3.31
FPZAS	2	2.18	2.92
FPCoAS	3	2.76	3.47
FPCuAS	3	2.91	2.77

*M^{II} : Mg, Zn, Co or Cu;
[a] Theoretical molar ratio;
[b] Molar ratio in solid.

The coprecipitation methodology followed by thermal treatment has produced materials composed of several phases. Figure 4.27 presents the XRD patterns of the calcined materials (at 450 °C for 24 hours) . The diffractogram of FPMAC, Figure 4.27 a), exhibited intense peaks at 31.91°, 37.12°, 45.93°, 53.44°, 66.88° and 78.41° that can be ascribed to $KMgF_3$ (JCPDS 18-1033).

For Zn/Al material (FPZAC), Figure 4.2 b), the reflections were characteristic of the layered perovskite K_2ZnF_6 at 37.28 °, 40.28°, 42.27°, 49.93°, 66.95° and 74.68° (ICDS 100298). Diffraction peaks assignable to ZnO (JCPDS 01-075-1533) were observed at 56.02° and 81.4°.

The XRD pattern of FPCoAC, Figure 4.27 c), showed peaks at 44.61°, 52.42° and 57.35° that may be indexed to Co_3O_4 (JCPDS 43-1003). The peaks at 17.03°, 27.57° and 39.55 are assignable to K_3AlF_6 (JCPDS 03-0635).

FPCuAC, Figure 4.27 d), exhibited intense diffraction reflections at 38.07°, 41.60°, 45.51°, 57.42°, 62.81°, 69.21°, 72.87°, 78.68° and 86.72° that are characteristic of CuO (JCPDS 80-1917). Fluorine presence was confirmed by SEM-EDX, thus it may be in an amorphous phase.

Aluminium presence in FPMAC, FPZAC and FPCuAC, was confirmed by ICP (Table 4.11) and SEM-EDX, thus Al^{3+} can either be present in amorphous phases such as aluminates (K, Mg, Zn or Cu) or alumina (Al_2O_3).

Figure 4. 27 - XRD results for: a) FPMAC b) FPZAC c) FPCoAC and d) FPCuAC.

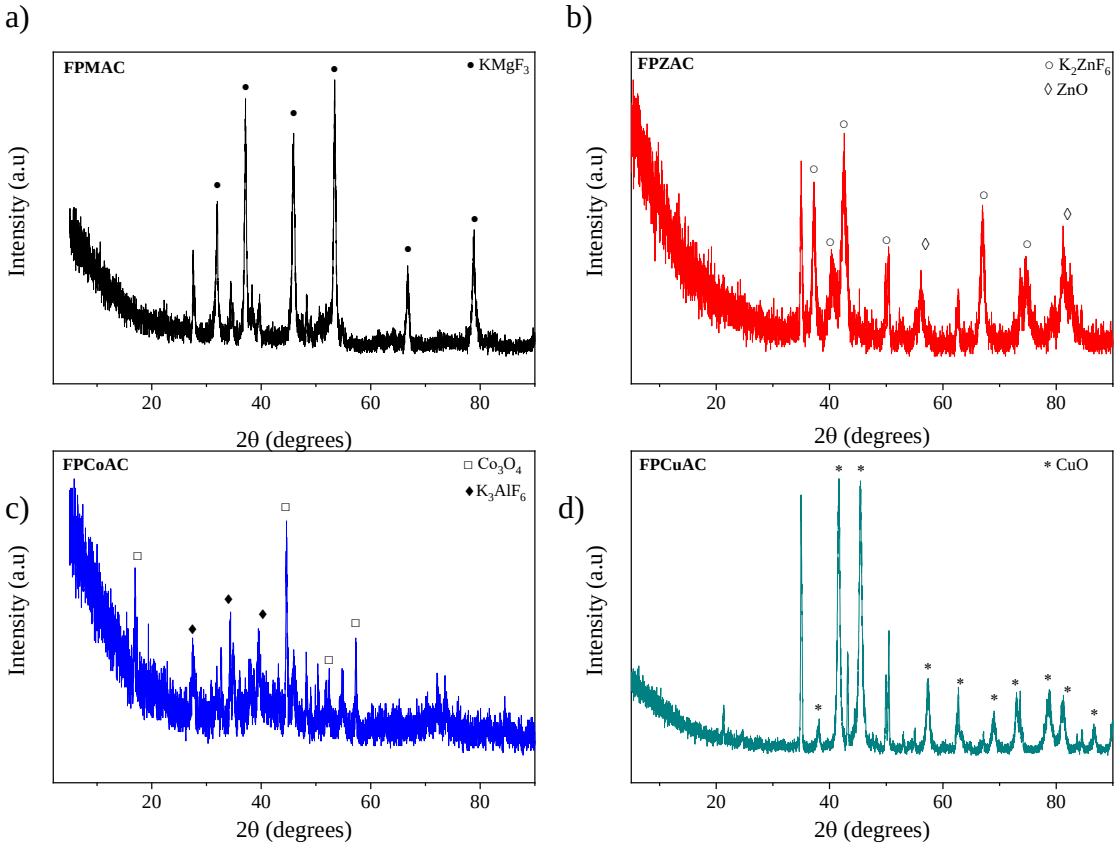

Thermogravimetric analysis, Figure 4.28 and Table 4.13, was performed to explain the effect of calcination in FPMAS, FPZAS, FPCoAS and FPCuAS. All materials displayed at least two weight losses, the first with maximum DTG peak at around 100 °C is related to the loss of adsorbed water. The second peak, bellow 400 °C, may be related to dehydroxylation and to the decomposition of CO_3^{-2}, arising from K_2CO_3 used in precipitating solution. FPZAS had a third step (T_M at 561°C) that can be related to the formation of oxides after further decomposition of carbonate. For FPCoAC, the final step (T_m at 589 °C) is ascribed to the reduction of Co_3O_4 to CoO (XABA *et al.*, 2018). The Cu/Al solid, FPCuAC, had the lowest total weight loss (5.56%).

Table 4. 12 - Thermogravimetric analysis of FPMAS, FPZAS, FPCoAS and FPCuAS.

Sample	**W_1(%)**	**T_{1M}(°C)***	**W_2(%)**	**T_{2M}(°C)**	**W_3(%)**	**T_{3M}(°C)**	**W_T(%)**
FPMAS	16.29	109	13.79	262	-	-	30.08
FPZAS	4.44	108	15.87	210	3.28	561	23.59
FPCoAS	9.61	136	17.07	239	4.83	589	31.51
FPCuAS	0.51	108	5.01	284	-	-	5.56

*Maximum DTG peak.

Figure 4. 28 - TGA/DTG for a) FPMAS, b) FPZAS, c) FPCoAS and d) FPCuAS.

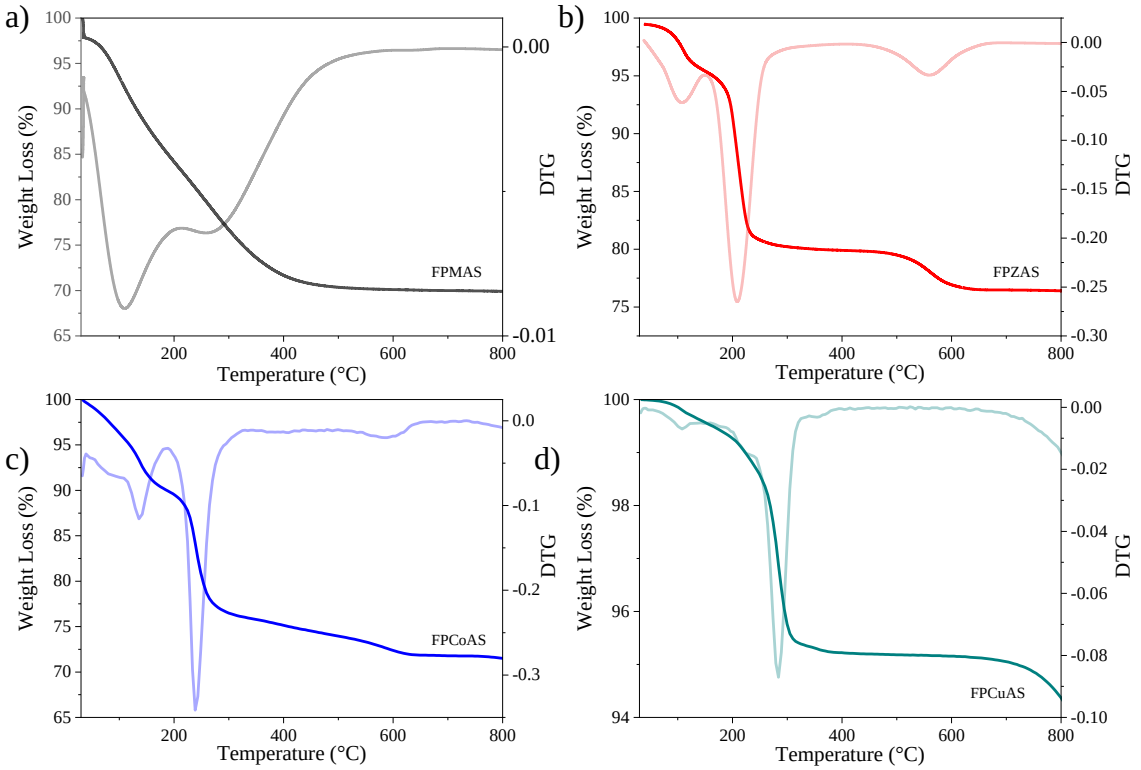

The BET surface area, average volume of pore and average pore diameter are summarized in Table 4.14. Comparison of S_{BET} shows the trend: FPMAC > FPCoAC > FPCuAC > FPZAC. The nitrogen isotherms of FPMAC and FPCoAC, Figure 4.29 , have the characteristics of type IV, according to IUPAC classification. FPMAC shows H1 hysteresis, typical of agglomerates arranged in a fairly uniform way, cylindrical pore geometry, relatively high pore size uniformity and facile pore connectivity. FPCoAC has H3 hysteresis, characteristic of aggregates of platelike particles forming slit-like pores. FPZAC (Fig. 4.29 b) and FPCuAC (Fig. 4.29 d) have isotherms type II with hysteresis H3. According to Rouquerol *et al.*(2013), due to delayed capillary condensation, multilayer adsorption can proceed on the particle surface until a high p/p_0.

The average pore diameters were typical of mesoporous materials , between 9.28 nm in FPCoAC and 46.98 nm in FPCuAC. The pore size distribution of FPZAC and FPMAC, Figure 4.30, presented only mesopores. For FPCoAC, this distribution was narrower than the others, Figure 4.30 c). Whereas for FPCuAC, Figure 4.30 d),there is a wide distribution centered at around 50 nm, showing a porosity composed of mesopores and macropores.

Table 4. 13 - Textural properties and surface basicity for FPMAC, FPZAC, FPCoAC and FPCuAC.

Sample	S_{BET} ($m^2\ g^{-1}$)	V_p ($cm^3\ g^{-1}$)	D_P (nm)	Base sites ($mmol.g^{-1}$)		
				Total [a]	Strong [b]	Weak [c]
FPMAC	94	0.33	10.42	1.70	0.17	1.53
FPZAC	29	0.22	31.67	1.54	0.07	1.47
FPCoAC	75	0.17	9.28	0.21	0.07	0.15
FPCuAC	33	0.19	46.98	0.54	0.03	0.51

[a] Acrylic acid was used as a probe molecule;
[b] Phenol was used as a probe molecule;
[c] Weak base site = Total base site − Strong base site.

Figure 4. 29 - N_2 isotherms for: a) FPMAC, b) FPZAC, c) FPCoAC and d) FPCuAC.

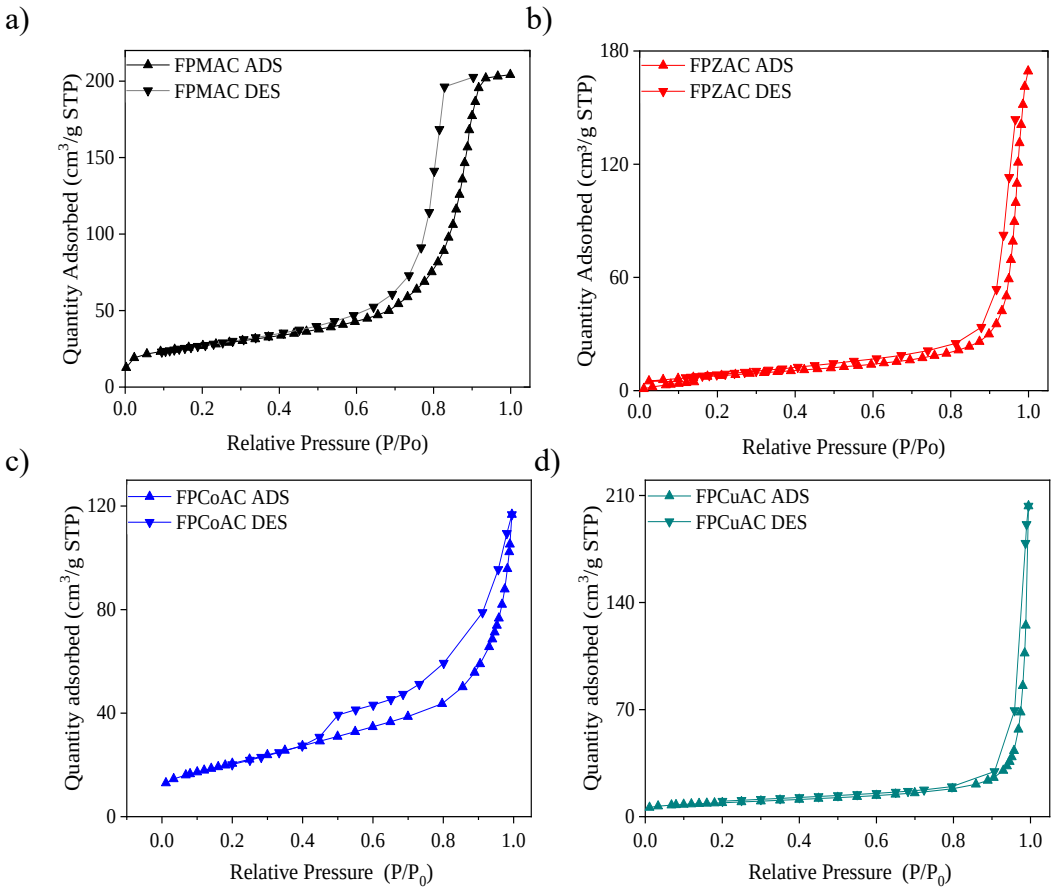

The surface basicity was investigated by the irreversible adsorption of acrylic acid and phenol, Table 4.13. FPMAC and FPZAC had higher total basicity (1.70 and 1.54 $mmol.g^{-1}$ respectively), comparing their base sites distribution, FPMAC has a slightly higher contribution of strong sites than FPZAC. Both FPCoAC and FPCuAC had lower total basicity (0.21 and 0.54 $mmol.g^{-1}$). All solids were mainly composed of weak base

sites. Number of weak sites on FPZAC was similar to that of ZAU60 (1.47 and 1.31 respectively) presented in Table 4.9.

Figure 4. 30 - BJH pore size distribution for: a) FPMAC, b) FPZAC, c) FPCoAC and d) FPCuAC.

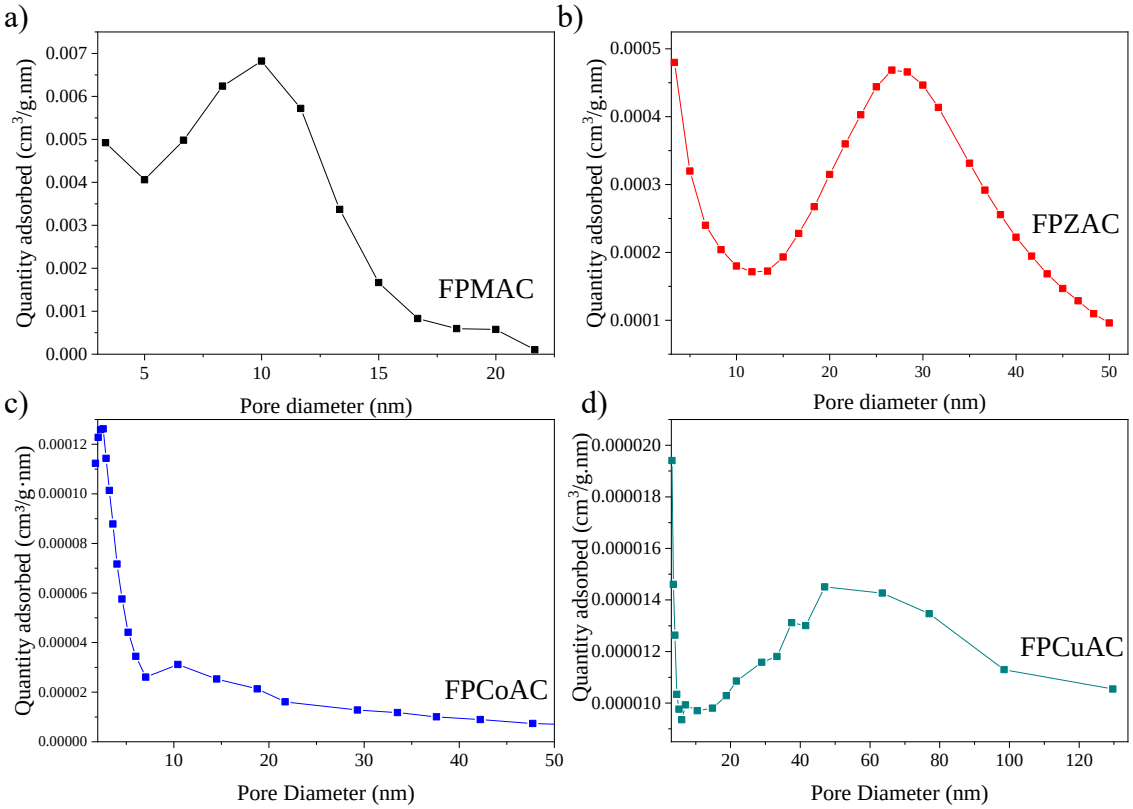

Figure 4. 31 - TEM images (scale bar 50 nm) for FPMAC, FPZAC, FPCoAC and FPCuAC.

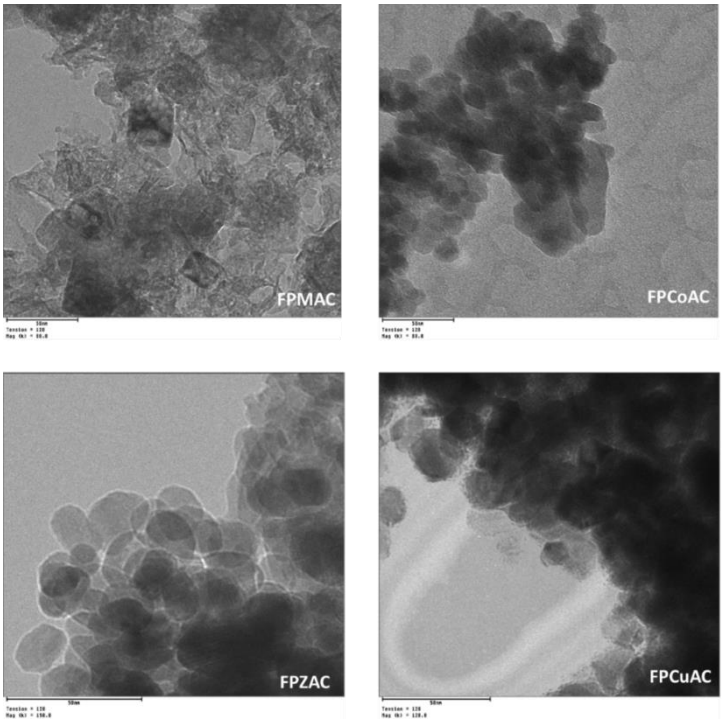

TEM micrographs for calcined materials are presented in Figure 4.31, FPCoAC, FPCuAC and FPZAC shows agglomerates with irregular shapes and sizes, whereas FPMAC presents cubic crystals (probably $KMgF_3$, according to XRD results).

Scanning electron microscopy, Figure 4.32, shows the formation of agglomerates of particles with irregular morphology. The presence of fluorine in calcined materials was confirmed by SEM-EDX analysis. Furthermore, samples can be arranged in decreasing order of F content (wt%) as follows: FPMAC (22.6 %) > FPZAC (19.6%) > FPCoAC (12.5%) > FPCuAC (5.1%).

Figure 4. 32 - SEM images (scale bar 4 µm) and EDX spectra for FPMAC, FPZAC, FPCoAC and FPCuAC.

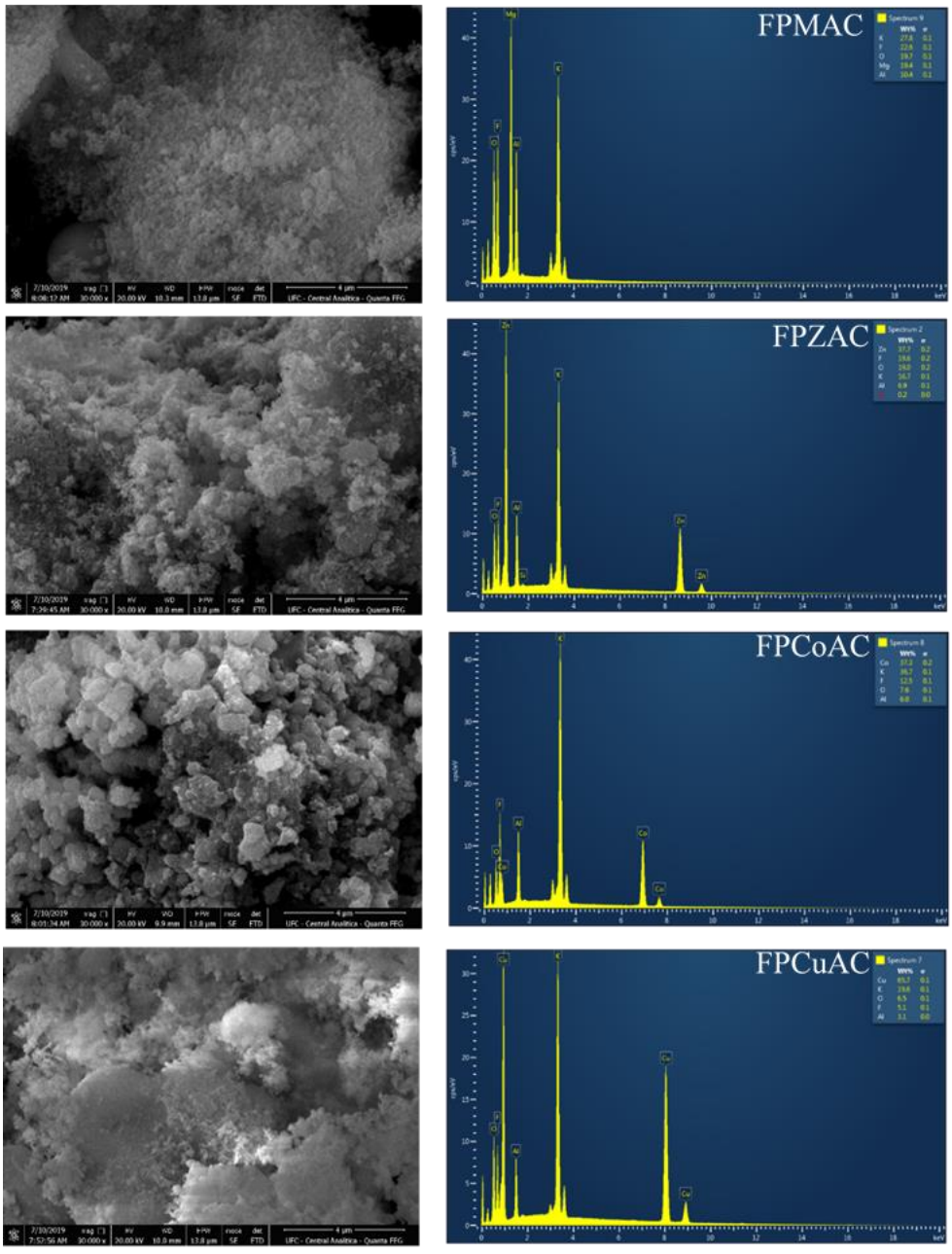

4.2.2.2 Catalytic performance of fluorine-containing materials

Figure 4.33 shows the catalytic results for fluorinated materials, in which, for 8 hours of reaction at 230 °C, 4% of FPCuAC led to the highest X_{Gly} (87%), followed by FPCoAC (51%), FPZAC (42%) and FPMAC (35%). Despite this, Cu/Al/F catalyst presented strong selectivity to high oligomers and other compounds (S_{ho} of 78%), forming a dark solid, as can be seen in Figure 4.34, the aspect of final product is also due to the interaction with metallic species (LEE, 2008). The lack of selectivity to the oligomers is probably coupled to secondary reactions, such as dehydration and oxidation (MARTIN; RICHTER, 2011; SIVAIAH *et al.*, 2012).

Figure 4. 33 - Glycerol oligomerization catalyzed by FPMAC, FPZAC, FPCoAC or FPCuAC (reaction conditions: 4 wt% cat ,230 °C and 8 h).

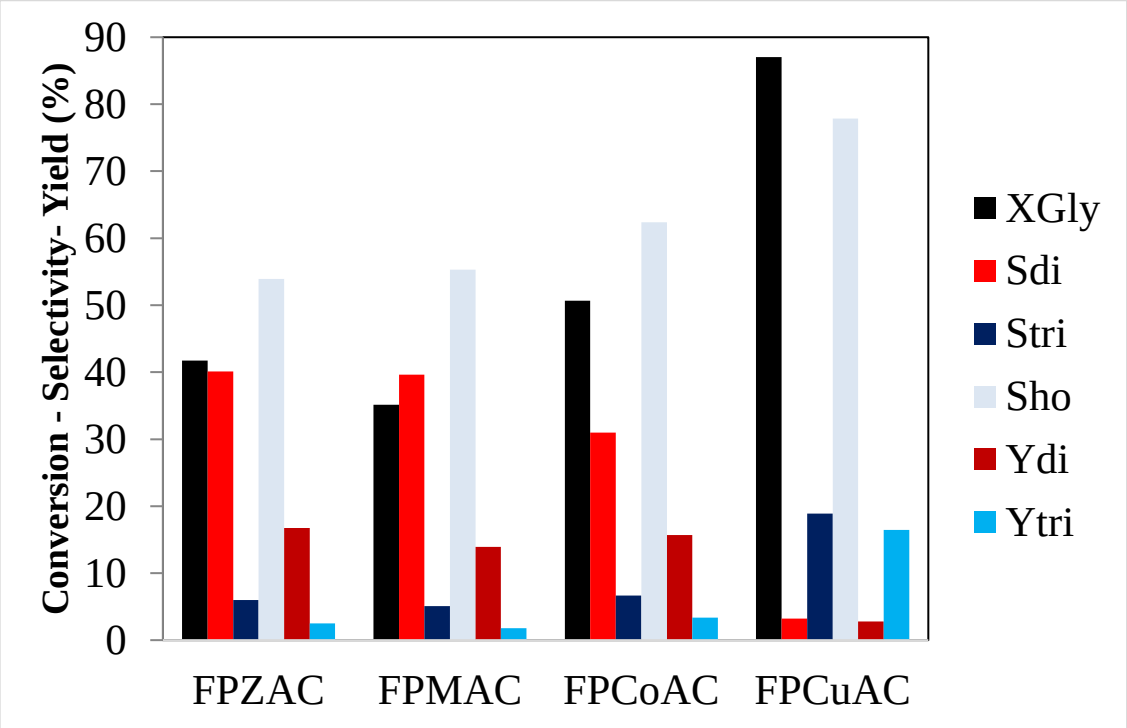

Comparing all four materials, FPZAC has interesting activity since has presented lower S_{ho} (54%) and good yield of di and triglycerol (17 and 3%, respectively). According to the XRD results, Figure 4.27,this solid consists of ZnO, fluoroperovskite K_3ZnF_6 and an amorphous Al phase. For the glycerol oligomerization mechanism proposed by Ruppert *et al.*(2008) , Figure 2.2, first Lewis basic site (oxygen anions from Zn-O) acts extracting a proton from a glycerol molecule. Then, the Lewis acid site (Zn-F) located on perovskites activates a hydroxyl group of another glycerol molecule, which is attacked by the nucleophilic oxygen obtained in the first step, leading to diglycerol.

Figure 4. 34 - Aspect of products from reactions catalyzed by FPCoAC, FPCuAC, FPMAC and FPZAC (reaction conditions: 4 wt% cat , 230 °C and 8 h).

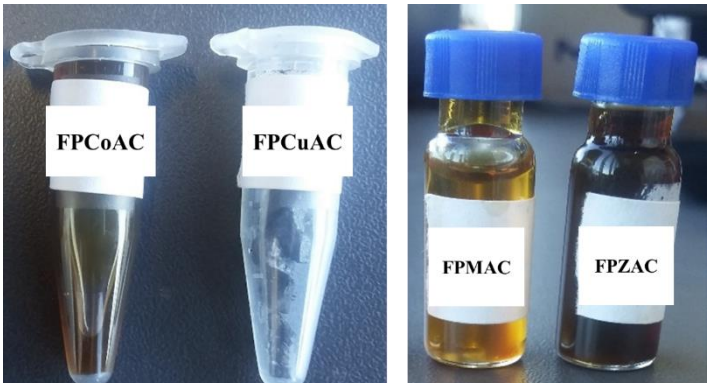

A good correlation can be observed between the selectivity to diglicerol and the fluorine content in the catalysts, Figure 4.32. FPMAC and FPZAC have similar amounts of fluorine (22.6 and 19.6%, respectively) and for both S_{di} was 40%. FPCoAC had 12.5 wt% of fluorine and S_{di} of 31%, despite having lower total basicity (0.21 mmol.g^{-1}) in contrast with FPMAC and FPZAC (1.70 and 1.54 mmol.g^{-1}). The F content on FPCuAC was only 3 wt%, with a S_{di} of 5.1%. Comparison of the activity of FPZAC with Zn/Al LDH catalysts shows that fluorine presence led to an enhancement of catalytic performance, considering that ZAC had a X_{Gly} of only 9% with Y_{di} of 4% and the best result from a rehydrated form was ZAU60 (X_{Gly} of 24% and Y_{di} of 11%).

The CO_2-TPD profile of FPZAC, Figure 4.35, can be deconvoluted into several peaks, corresponding to weak , moderate (metaloxygen and metal-fluorine pairs) and strong basic sites (coordinatively unsaturated O^{2-} and F^- ions) (GAO *et al.*, 2016).

Figure 4. 35 - CO_2 -TPD on set-up 2 for FPZAC, activated at 450 °C for 30 min.

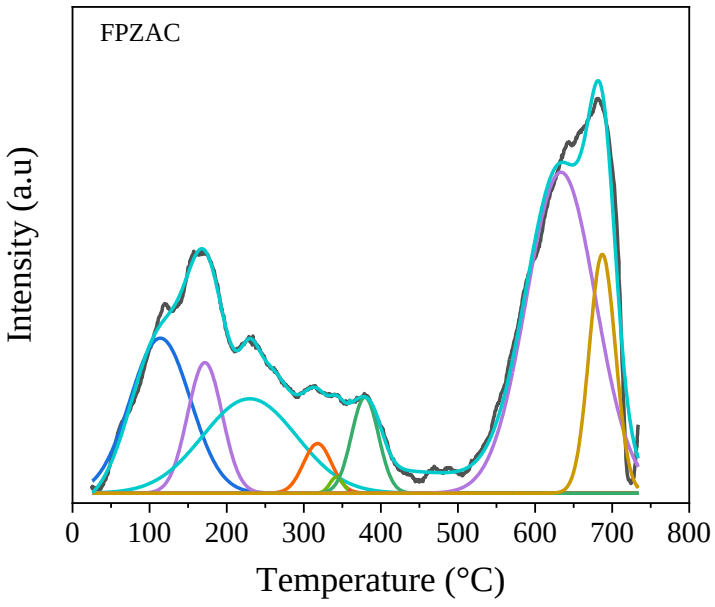

4.2.1.5 FPZAC reusability and stability

Due to the higher yield of di and triglycerol, FPZAC had its reusability and stability evaluated. Catalyst was recovered using the procedure described in Section 3.3. From Figure 4.36 a) is possible to notice a strong deactivation already in the first reuse, X_{Gly} was reduced from 35.45% to 12.32% in the second run. Diglycerol yield drops from 14.26 in the first run to 3.65% in the last. Since catalyst separation process was the same of MAU30P, from Section 4.1, adsorbed species may be blocking the active base sites.

Considering this and the findings in Section 4.1, some changes were tested for a new reusability study. First in reaction time, Figure 4.36 b) shows a comparison between 8 and 18 hours of reaction at 230 °C for 4 wt% of FPZAC. The X_{Gly} has grown 26%, despite the lower S_{di} this was enough to reach similar Y_{di}. In contrast, with the use of ZAC for 8 and 24 hours of reaction (4wt% cat., 230 °C as well), the X_{Gly} increased only 14%. Therefore, this is another positive effect of a catalyst with the combination of Zn/Al and fluorine presence against hydroxyls and carbonate as anions. The recycling procedure was modified as follows: after dissolution of reaction mixture/catalyst with ultrapure water and vacuum filtration, the solid was dried at 100 °C for one hour and then calcined at 450 °C for one hour. The new reaction cycle started right after thermal treatment, Figure 4.37.

The modification of recovery procedure was very effective in reducing the deactivation, which this time started on third run, with 54% of X_{Gly} compared to 68% in the previous cycles. Thus, the removal of organic species through catalyst calcination is probably responsible for this improvement. In the last reaction, S_{di} kept on the average of the other cycles, however X_{Gly} dropped to 43%.

The loss of active species by leaching from catalyst to the reaction mixture was monitored by ICP-OES, Table 4.14. the concentration of Al and Zn in products is very low. Whereas, potassium contents for the first reaction represents a loss of 18% in comparison to its amount in FPZAC, the second and third runs have each 10% of leaching and the last reaction 6%. The overall reduction of K content may help to explain the deactivation, since before the last cycle catalyst had lost at least 38% of metal. However, these values may not be high enough to indicate homogeneous contribution for catalysis. In our previous works, with calcined eggshells (CEG) and calcined dolomite (CD), both had X_{Gly} around 80% and high oligomers yield, however CEG had a significant homogeneous contribution, whereas dolomite had a marked deactivation over reusability

tests. Those behaviors are ascribed to Ca leaching, which reached 8920 and 7000 ppm for CEG and CD, respectively (BARROS *et al.*, 2017, 2018).

Figure 4. 36 - a) Reusability study of FPZAC (reaction conditions 4 wt% cat., 230 °C and 8 h) b) Comparison of reaction times (reaction conditions 4 wt% cat. and 230 °C).

a)

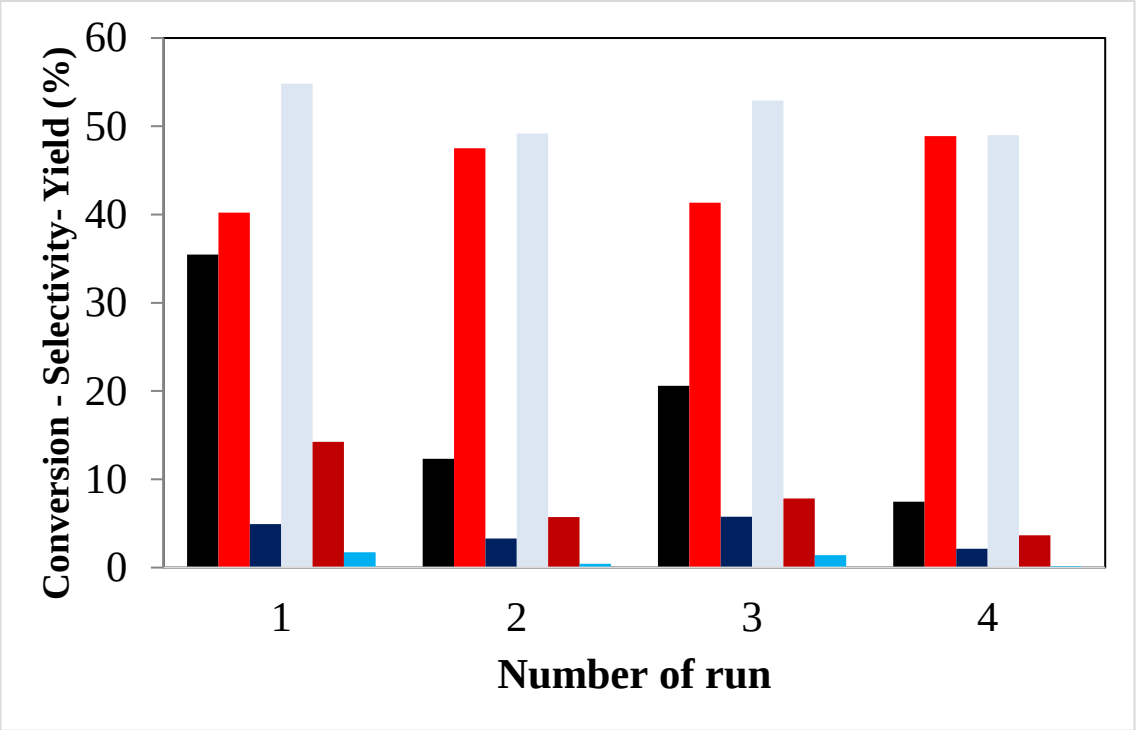

b)

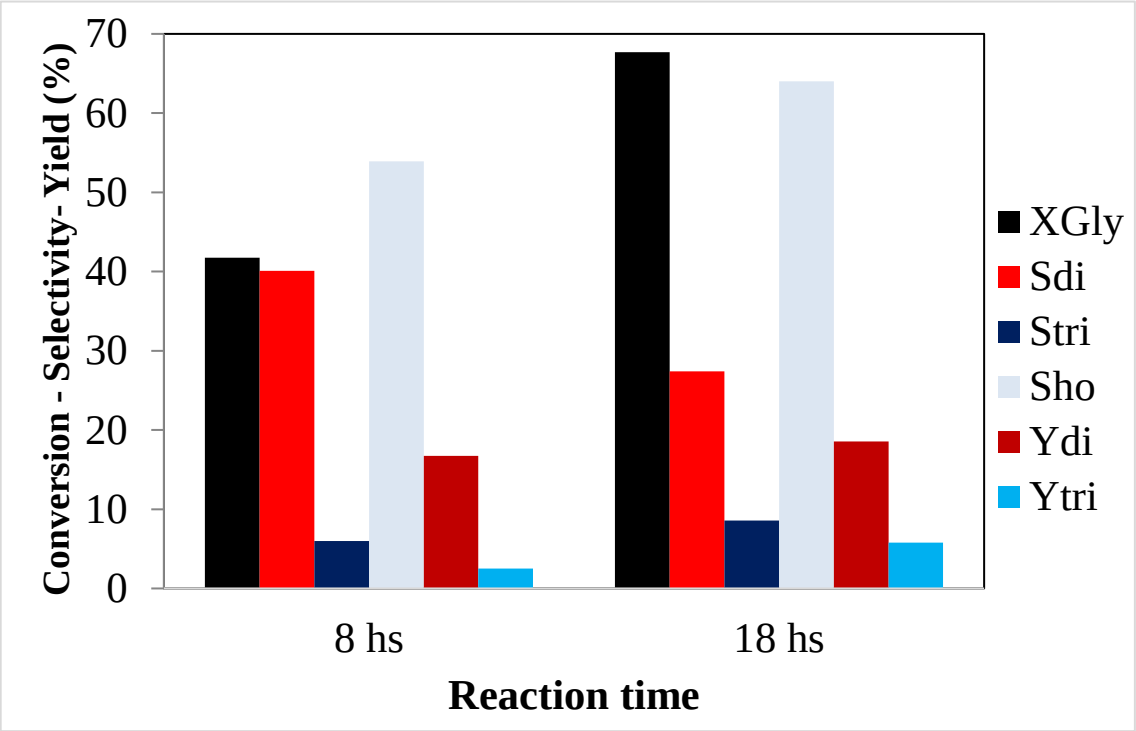

Figure 4. 37 - Reusability study for FPZAC (4 wt% cat., 230°C and 18 hrs).

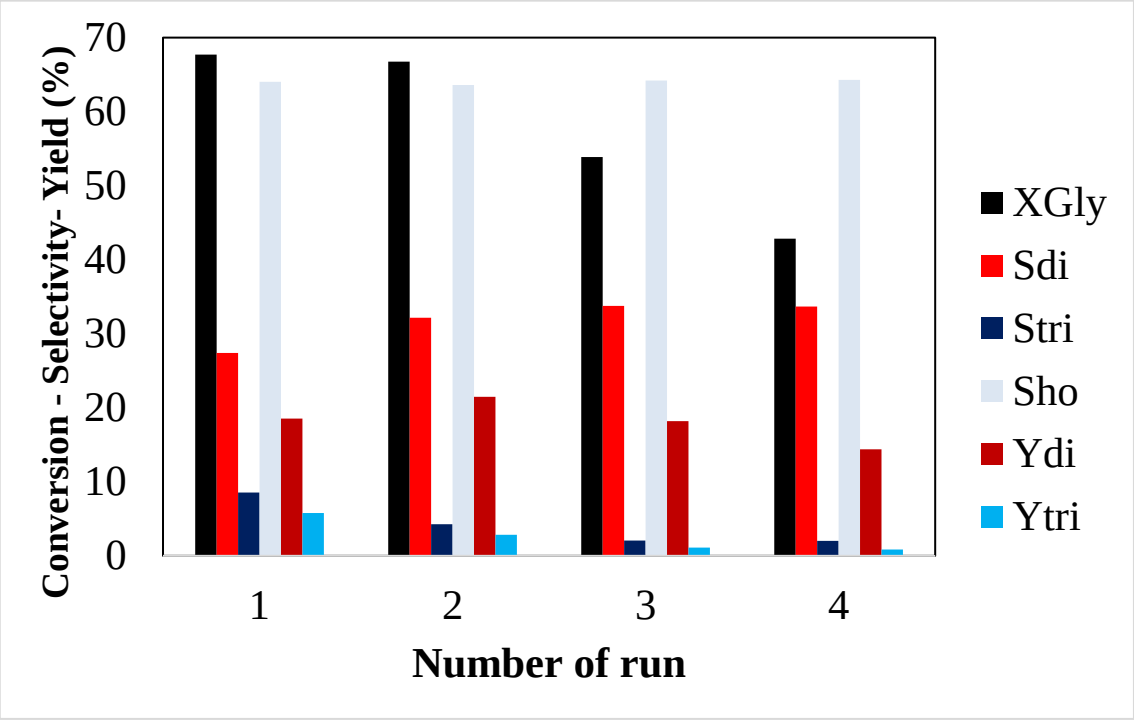

Table 4. 14 - Al, K and Zn amounts determined by ICP-OES in FPZAC, glycerol and reaction mixtures from catalyst reusability test.

Sample	Concentration (ppm)		
	Al	**K**	**Zn**
FPZAC	1.45	4.26	7.18
Glycerol	-	-	-
1st run	0.03	0.75	0.12
2nd run	0.05	0.41	0.12
3rd run	-	0.49	0.02
4th run	0.01	0.24	0.18

The XPS spectra of spent catalysts recovered from the first, second and third runs are presented in Table 4.15 and Figure 4.38. The presence of O, F, K, Zn, and Al was confirmed, in accordance with SEM-EDX results, Figure 4.32.

The C 1s signal, Figure 4.38a), exhibited an unique contributiion, 284.9 to 284.7 eV, characteristic of adventitious carbon C-C. The F 1s core level spectra shows a contribution around 685 eV, typical from metal fluorides, Zn-F and Al-F in this case.

Regarding the O 1s region, Figure 4.38c) , for the samples from the first and second runs signal could be decomposed in two contributions, around 529 and 531 eV, related to O^{2-} from metal oxide (ZnO, according to XRD results) and OH^- from superficial hydroxides, respectively. Both contributions have lowered the binding energy in the

second run. Conversely, the material from third run shows only one symmetric band at 531.3, pointing to some possible reduction on ZnO available on the surface.

The K 2p signal, displays an asymmetric band that could be decomposed in two contributions, around 293 and 296 eV, Figure 4.38 d), attributed to K $2p_{1/2}$ and K $2p_{3/2}$. For Zn $2p_{3/2}$ core level spectra the binding energy was 1020.8 eV for the samples from first and second runs and it has increase to 1021.6 eV for the third run, this value corresponding to chemical element state of Zn^{2+}, from either ZnO or K_2ZnF_4. Finally, for the Al 2p region, binding energy values ranged between 73.3 and 73.9 eV.

The atomic concentration of carbon, Table 4.15, was similar for the first and second runs, around 20%, whereas the third run had an increase to 46%. For oxygen, solids from initial runs had concentration of 42.7 and 45.77%, against 38.49 for the catalyst recovered from third run. The atomic concentration of potassium decreased from 3 to 0.66%, in accordance with ICP-OES results, that have shown the appearance of this metal in reaction products. For fluorine, the atomic concentration has decreased from 8 to 3%, which can be correlated to the reduction of X_{gly} observed from second to fourth run (67 to 43%) in Figure 4.37.

Table 4. 15 - XPS results for FPZAC recovered from 1st, 2nd and 3rd run.

Sample	**Binding energy (eV)**						**Atomic concentration (%)**					
	C 1s	**O1s**	**F 1s**	**K 2p**	**Zn $2p_{3/2}$**	**Al 2p**	**C**	**O**	**F**	**K**	**Zn**	**Al**
1st run	284.9	529.8 (62.77%) 531.5 (37.23%)	685.3	293.5 (64.53 %) 296.1 (35.47%)	1020.8	73.6	21.41	42.7	8.36	3.29	18.72	6.1
2nd run	284.6	529.7 (62,15%) 531.2 (37.85%)	684.4	292.5 (63.89%) 295.7 (36.11%)	1020.8	73.3	19.21	45.77	6.22	1.02	17.23	10.57
3rd run	284.7	531.3	685.5	293.8 (66.51%) 296.6 (33.49%)	1021.6	73.9	46.29	38.49	2.84	0.66	8.33	3.71

Surface concentrations of zinc was similar on spent catalyst from first and second run (around 18%), whereas aluminum exhibited an enrichment on the surface of solid from the second run, reaching 10%. On the catalyst recovered from the third run, both Zn and Al had a marked reduction on the atomic concentrations, which alongside with the reduction on fluorine, may explain the lowered activity for fourth run.

As in the case of Mg/Al and Zn/Al LDH catalysts, fluorine materials have led to low selectivity to acrolein (staying under 0.11%) as shown in Table 4.16. Over recycling these values have increased to 0.6%.

Figure 4. 38 - XPS spectra for spent FPZAC recovered from 1st, 2nd and 3rd run for: a) C 1s, b) F 1s, c) O 1s, d) K 2p, e) Zn 2p3/2 and f) Al 2p regions.

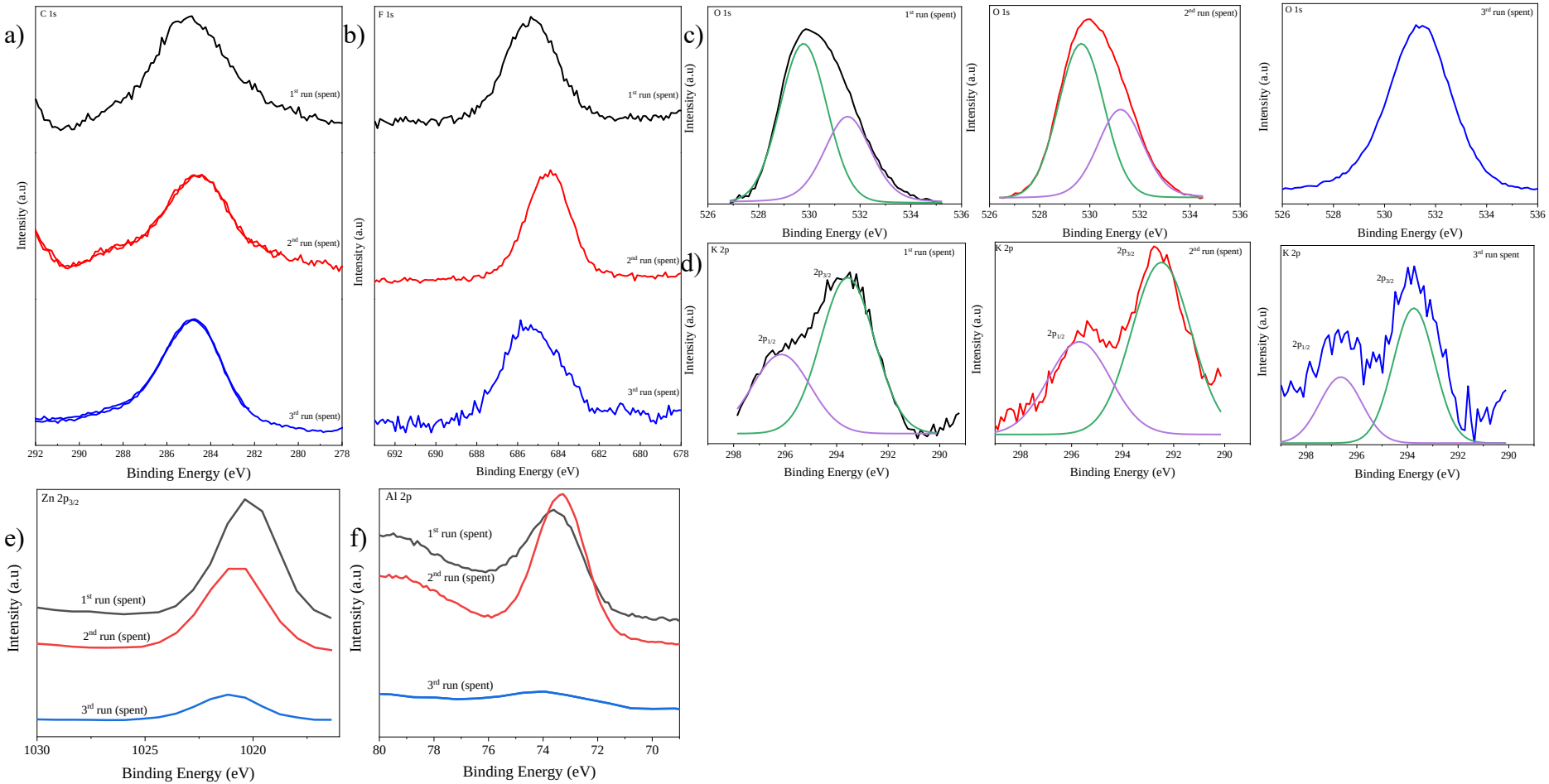

Table 4. 16 - Selectivity to acrolein for tests with fluorine-containing catalysts.

Test	Sample	S_{Acr} (%)
Fluorine catalysts	FPZAC	0.06
(4 wt% cat., 230°C and 8 h)	FPMAC	0.04
	FPCoAC	0.06
	FPCuAC	0.11
Reusability of FPZAC (8 hours)	1st run	0.06
(4 wt% cat. and 230°C)	2nd run	0.04
	3rd run	0.18
	4th run	0.44
Reusability of FPZAC (18 hours)	1st run	0.12
(4 wt% cat. and 230°C)	2nd run	0.58
	3rd run	0.54
	4th run	0.43

4.2.3 Partial Conclusion

The evaluation of rehydration of Zn/Al LDH has shown that both ultrasound and mechanical stirring were able to recover lamellar structure. However, the XRD, FTIR and TGA results pointed differences in the composition of lamellar interspace in comparison to ZAS. Sonication process favored the presence of weak base sites and ZAU60 had the highest basicity, 1.46 $mmol.g^{-1}$. Activity of rehydrated catalysts was evaluated for the best set of reaction conditions found with ZAC (8 hours at 230°C and 4 wt% of catalyst), and ZAU60 had the best response, 25% X_{Gly} and 10.5%Y_{di}.

According to XRD results, fluorine-containing materials were composed by the following phase: $KMgF_3$ for FPMAC; K_2ZnF_6 and ZnO for FPZAC; Co_3O_4 and K_3AlF_6 for FPCoAC and CuO for FPCuAC. Their BET surface area ranged between 94 $m^2\ g^{-1}$ (FPMAC) to 29 $m^2\ g^{-1}$ (FPZAC). The total basicity was 1.70 $mmol.g^{-1}$ for FPMAC and 1.54 $mmol.g^{-1}$ for FPZAC. SEM-EDX has confirmed fluorine content (wt%): FPMAC (22.6 %), FPZAC (19.6%), FPCoAC (12.5%) and FPCuAC (5.1%).

Regarding catalytic activity, FPCuAC exhibited the highest X_{Gly} (87%) coupled with low selectivity to the oligomers. Whereas FPZAC had X_{Gly} of 42%, lowest S_{ho} (54%) and the highest Y_{di} (17%). Fluorine content was directed related to the selectivity to diglycerol and has enhanced the catalytic performance.

The FPZAC recycling was improved, reaction time went to 18 hours and the procedure for catalyst recycling was modified, with a calcination prior reaction. This modification has kept Y_{di} around 20% up to the third run, with decreases to 14.41% for the fourth run. The deactivation was related to the potassium leaching and loss of fluorine on the surface.

4.3 Oligomerization of glycerol catalyzed by Co/Al LDH and $Co(acac)_2$ supported on LDH and fluoroperovskites

4.3.1 Catalysts characterizations

4.3.1.1 Co/Al LDH

The ICP-OES measurements have confirmed the presence of Co and Al with a molar ratio of 3.2, which is in good agreement with the theoretical amount in the aqueous solution, 3.

The diffractograms obtained for CoAS and calcined materials (CoAC450 and CoAC700) are shown in Figure 4.39. CoAS exhibits the main LDH peaks, JCPDS 70-2151, with well-defined and symmetric peaks in (003) and (006), and asymmetric peaks at (110),(113), (012) and (015). Both calcination temperatures lead to the formation of a solid solution of cobalt spinels composed of Co_3O_4 (JCPDS 43-1003), $CoAl_2O_4$ (JCPDS 44-160) and Co_2AlO_4 (JCPDS 38-814) (PÉREZ-RAMÍREZ *et al.*, 2002).

Figure 4. 39 - XRD for CoAS, CoAC450 and CoAC700.

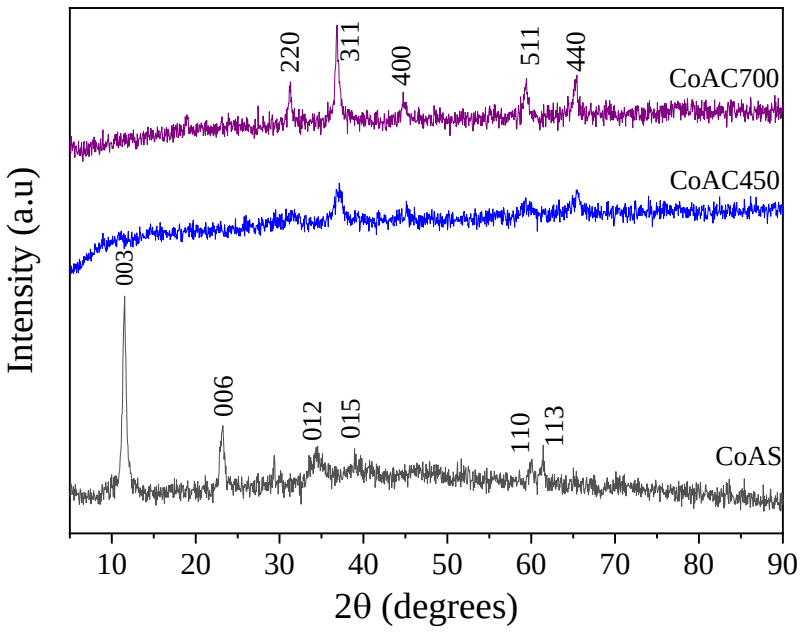

FTIR spectra of as-synthesized Co/Al LDH and its calcined forms are presented in Figure 4.40. For CoAC700 spectrum, there is an absence of the hydroxyl and carbonate bands (3500 and 1350 cm^{-1}, respectively), whereas in CoAC450 they are quite similar to the ones in CoAS, which implies that only the calcination at 700 °C led to the formation of spinels without carbonate presence. Both CoAC700 and CoAC450 have an intense and sharp peak around 655 cm^{-1} which indicates Co–O bonds of cobalt spinel

(Co_3O_4) (BASKARAN *et al.*, 2014). For CoAS, the band at around 735 cm^{-1} is ascribed to the overlap of Co-O and Al-O vibration modes of LDH and to Co-OH bonds (GENNEQUIN *et al.*, 2010; GUOXIANG *et al.*, 2014).

Figure 4. 40 - FTIR for CoAS, CoAC450 and CoAC700.

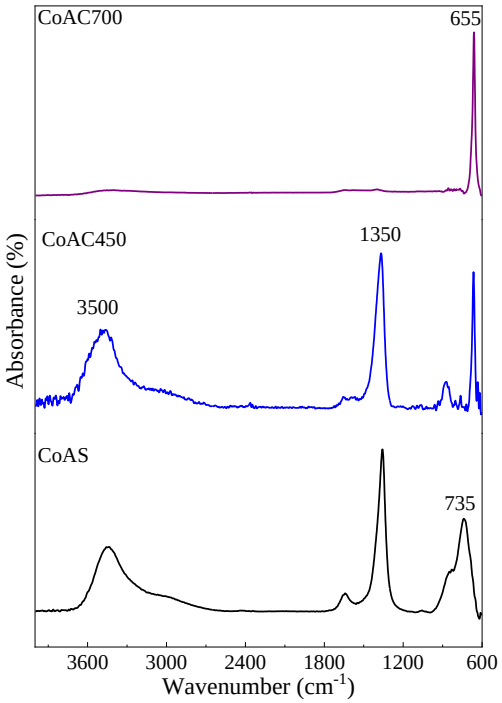

The TGA/DTG of CoAS, Figure 4.41, shows a total weight loss of 32%, in three steps. As in the case of Zn/Al LDH from Section 4.2, loss of adsorbed and interlamellar water and the decomposition of OH^- and CO_3^{-2} from the brucite-like layers takes place on the first step, maximum DTG peak (T_M) at around 225 °C. Two minor weight losses can be seen above 500 °C, T_M at 520 and 683 °C , which are related to the

Figure 4. 41 - TGA /DTG curves for CoAS.

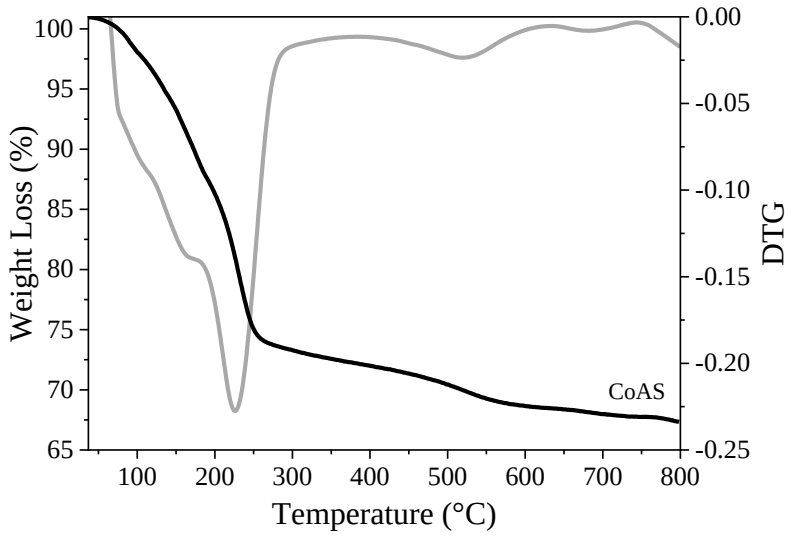

reduction of Co_3O_4 to CoO (SHI *et al.*, 2015). According to García-Sancho *et al.* (2011) this weight loss at temperatures higher than 450 °C can be related to the decarbonation process of an amorphous phase, inferred from FTIR.

Table 4.17 summarizes the textural properties of Co/Al LDH and its mixed oxides. For calcination at 700 °C, the surface area went from 62 to 96 m^2g^{-1}. And the average volume of pores has increased to 0.51 cm^3g^{-1} The nitrogen adsorption–desorption isotherms and BJH pore size distribution are shown in Figure 4.42. All isotherms are type IV, according to IUPAC classification, corresponding to multilayer adsorption followed by capillary condensation in mesopores. They also present hysteresis H3, characteristic of aggregates of platelike particles forming slit-like pores. The pore size distribution indicates that materials are composed of mesopores and macropores. CoAC700 had wide distribution of pores, with D_P of 36.85 nm.

Table 4. 17 - Textural properties and surface basicity of CoAS, CoAC450 and CoAC700.

Sample	**S_{BET} (m^2 g^{-1})**	**V_p (cm^3 g^{-1})**	**D_P (nm)**	**Base sites (mmol.g^{-1})**		
				Total [a]	**Strong [b]**	**Weak [c]**
CoAS	62	0.25	13.24	0.86	0.14	0.72
CoAC450	80	0.32	13.16	0.57	0.09	0.48
CoAC700	96	0.51	36.85	0.65	0.13	0.53

[a] Acrylic acid was used as a probe molecule;
[b] Phenol was used as a probe molecule;
[c] Weak base site = Total base site − Strong base site.

The surface basicity was investigated with irreversible adsorption of acrylic acid and phenol, Table 4.17. Both temperatures of calcination led to reduction on the total basicity, reaching 0.57 mmol.g^{-1} for CoAC560 and 0.65 mmol.g^{-1} for CoAC700 mmol.g^{-1}, these values are higher to that of fluorine-containing material from Section 4.2, FPCoAC (0.21 mmol.g^{-1}).

The basicity of CoAC700 and CoAC450 was also studied with CO_2-TPD (set-up 1, with the mass spectrometer detector), Table 4.18. The total of base sites was similar for both calcination temperatures, as noticed with UV-Vis method as well. However, their distributions of base sites are quite different, the desorption profiles are presented in Figure 4.43, CoAC450 has a lower intensity peak at 160 °C, ascribed to

Figure 4. 42 - N_2 isotherms and pore size distributions for: a) CoAS, b) CoAC450 and c) CoAC700.

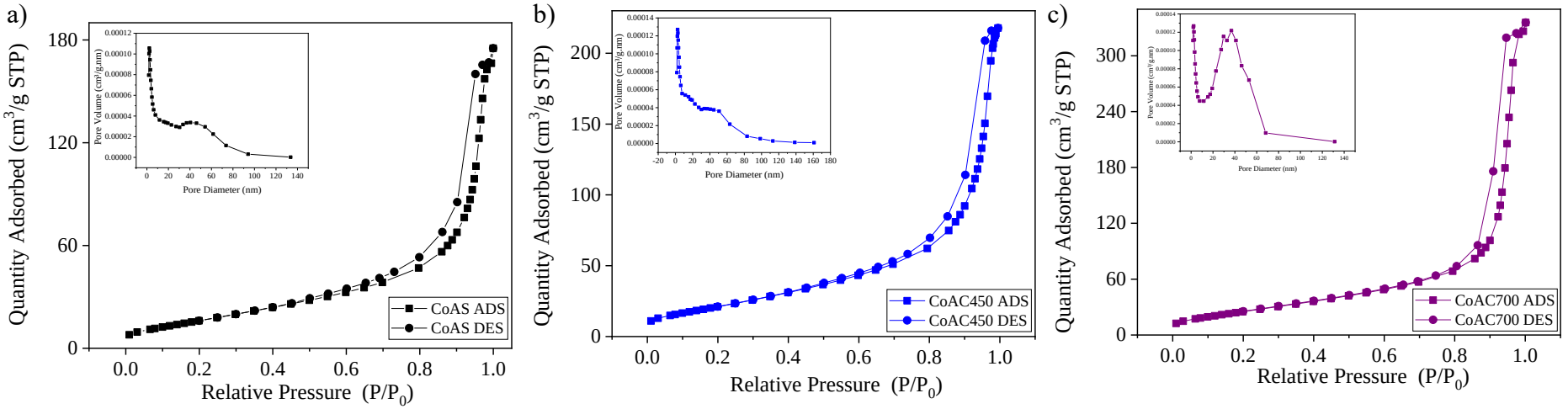

Figure 4. 43 - CO_2 -TPD (set-up 1) for a) CoAC450 and b) CoAC700.

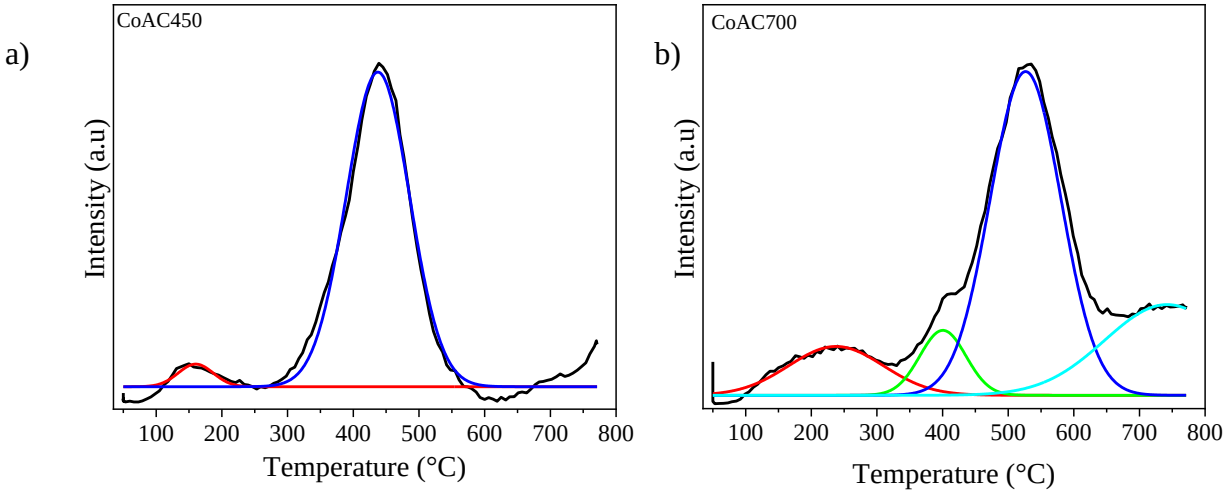

weak base sites, and a second one located at 441 °C which is related to strong base sites. Whereas the deconvolution of CoAC700 desorption profile shows three peaks, the first is in the region from weak to medium strength, maximum desorption temperature at 238 °C. The second peak is related to medium strength base sites, at 400 °C, and the last, at 526 °C, is ascribed to strong base sites.

Table 4. 18 - CO_2-TPD measurements for CoAC450 and CoAC700.

Sample	**Basicity (mmol.g^{-1})**						
	Total	**T (°C)**	**Weak**	**T (°C)**	**Medium**	**T (°C)**	**Strong**
CoAC450	6.60	160	0.52	-	-	441	6.08
CoAC700	5.46	-	-	238 400	1.03	526	4.43

The TEM micrographs for as-synthesized Co/Al LDH and calcined materials, Figure 4.44, shows irregular morphology with the presence of spheroidal particles as well as aggregates of thin plates, in accordance with nitrogen isotherms.

Figure 4. 44 - TEM images of CoAS, CoAC450 and CoAC700 (scale bar 0.1 µm).

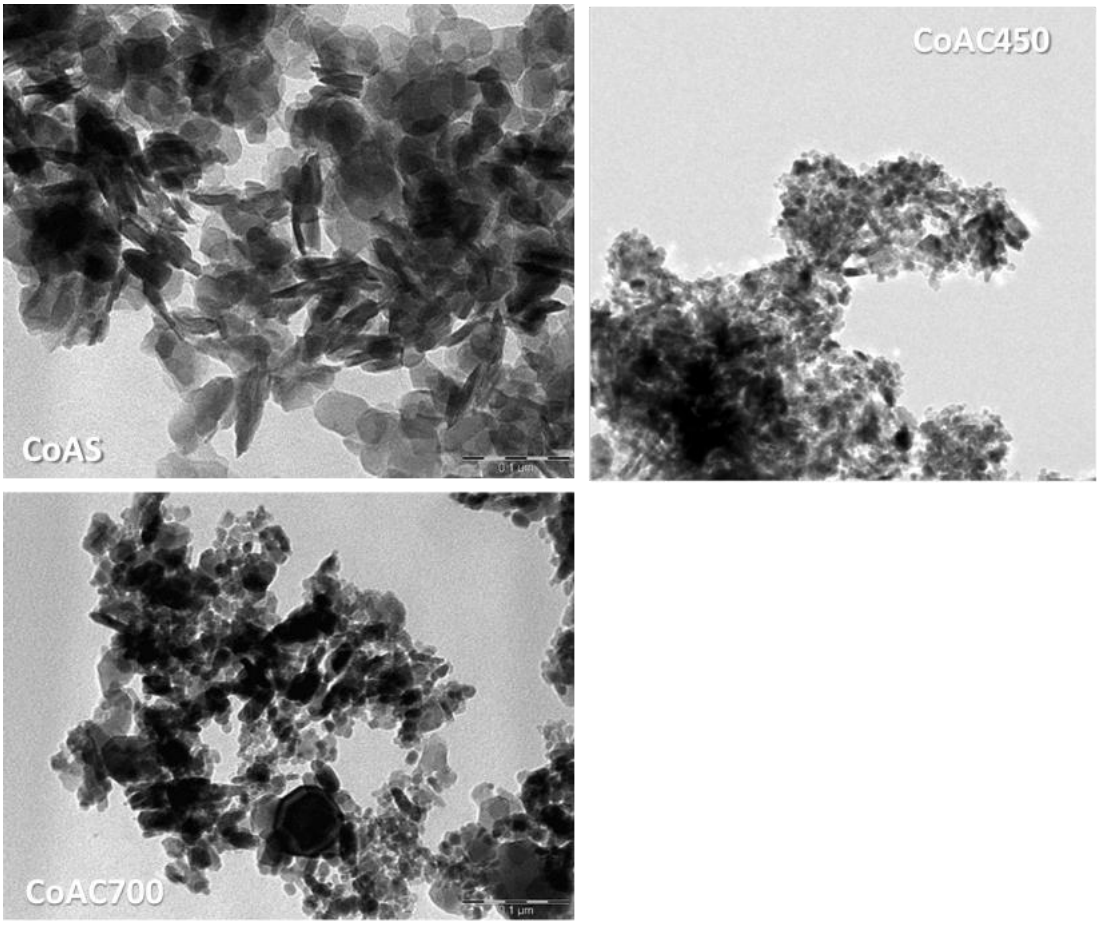

4.3.1.2 Co(acac)$_2$ supported on *LDH and Fluoroperovskites*

The content of cobalt arising from the impregnation of supports with Co(acac)$_2$/acetone solution was obtained with ICP-OES, Table 4.19. Mg/Al and Zn/Al molar ratios on LDH and fluoroperovskites (FPMAC and FPZAC) remained similar to their values prior impregnation, Tables 4.1 , 4.7 and 4.12.

Table 4. 19 - ICP - OES analysis for Co/MAS, Co/ZAC, Co/FPMAC and Co/FPZAC.

Sample	**Co/Al[a]**	**K/Al[a]**	**M^{II}/Al[a]**	**M^{II}/Al[b]**
Co/MAS	0.03	-	3.06	3
Co/ZAC	0.03	-	2.16	2
Co/FPMAC	0.04	2.38	2.90	3
Co/FPZAC	0.04	2.35	2.09	2

*M^{II} : Mg or Zn;
[a] Molar ratio in solid;
[b] Theoretical molar ratio.

The diffractograms of materials impregnated with Co(acac)$_2$, Figure 4.45, are very similar to that of their parental materials. Co/MAS presents the Mg/Al LDH pattern (JCPDS 70-2151). Co/ZAC has the typical ZnO reflections (JCPS 01-075-1533), in this case an extra reflection at 10° can be observed, being related to the cobalt acetylacetonates used to modify it. The peaks for Co/FPMAC are ascribed to $KMgF_3$ (JCPDS 18-1033). Co/FPZAC shows the presence of K_2ZnF_6 (ICDS 100298) and ZnO. This fact indicates a high dispersion of Co from Co(acac)$_2$ on the supports and can also be due to is low concentration (ZĂVOIANU *et al.*, 2010).

TGA/DTG results are presented in Figure 4.46 and Table 4.20. Co/MAS shows two steps of weight loss, as in the case of pure Mg/Al LDH, figure 4.3. In the first one, maximum DTG T_M at 247 °C, the loss of adsorbed and interlamellar water occurs. The second event consists of two reactions that are partially overlapping, T_M at 640 and 756 °C, being related to the removal of hydroxyls and carbonate in interlayer space. Since the supports of Co/ZAC, Co/FPMAC and Co/FPZAC are materials calcined at 450 °C, there is a lower weight loss, which takes place in two steps. First, removal of adsorbed water takes place bellow 300 °. The second event is from 450 to 800 °C and is ascribed to the formation of oxides after further decomposition of carbonate (arising from Na_2CO_3 or K_2CO_3 used for precursors).

Figure 4. 45 - XRD for $Co(acac)_2$, Co/MAS, Co/ZAC, Co/FPMAC and Co/FPZAC.

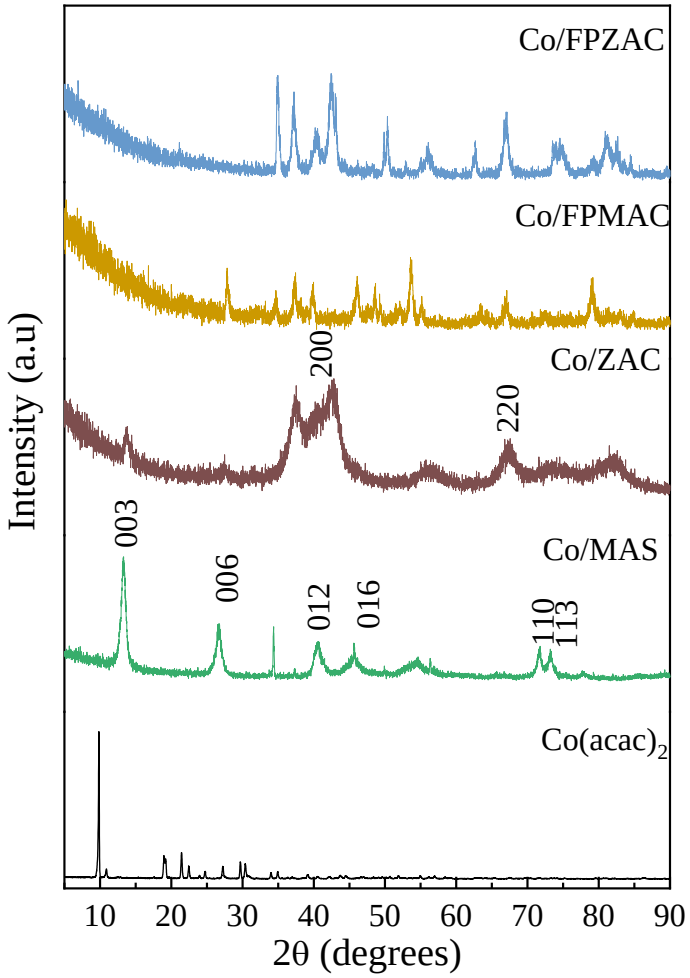

Table 4. 20 - Thermogravimetric analysis of $Co(acac)_2$ impregnated catalysts.

Sample	**W_1(%)**	**T_{1M}(°C)***	**W_2(%)**	**T_{2M}(°C)**	**W_3(%)**	**T_{3M}(°C)**	**W_T(%)**
Co/MAS	8.41	247	18.31	640	756	13.68	40.46
Co/FPMAC	5.78	269	19.24	678	-	-	25.02
Co/ZAC	6.46	227	14.27	640	-	-	20.73
Co/FPZAC	1.08	243	10.97	653	-	-	12.05

*Maximum DTG peak.

The impregnation with Cobalt(II) acetylacetonate has modified the textural properties of supports, Table 4.21. All materials presented lower S_{BET}, Co/FPZAC had the most expressive reduction, from 29 to 9 $m^2\ g^{-1}$. Nitrogen isotherms, Figure 4.47 , have the same aspect of bare supports, being type IV for Co/FPMAC, Co/MAS and type II for Co/ZAC and Co/FPZAC, according to IUPAC classification. The pore size distributions are in the range of mesopores, 2-50 nm.

Figure 4. 46 - a) TGA b) DTG for Co/MAS, Co/ZAC, Co/FPMAC and Co/FPZAC.

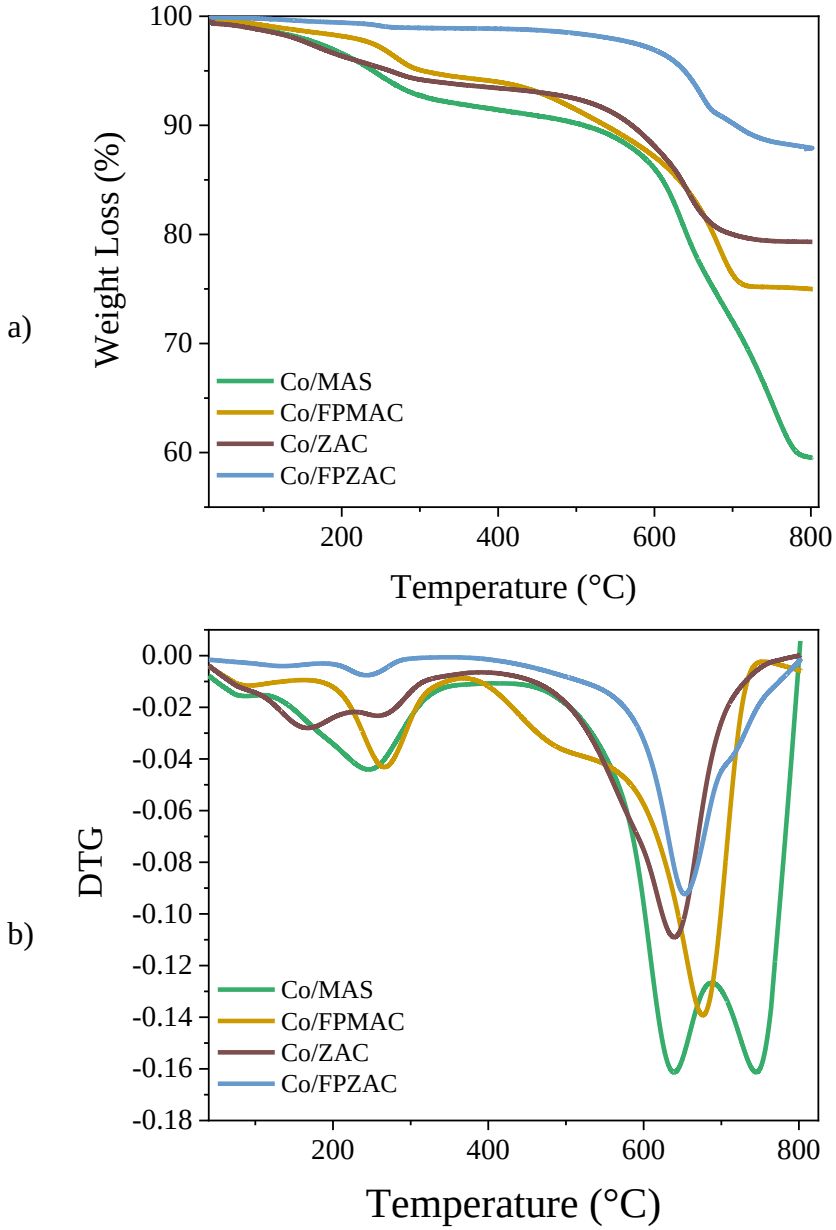

Table 4. 21 - Textural properties of Co/MAS, Co/ZAC, Co/FPMAC and Co/FPZAC.

Sample	**S_{BET} (m^2 g^{-1})**	**V_p (cm^3 g^{-1})**	**D_P (nm)**
Co/FPZAC	9	0.05	17.65
FPZAC	29	0.22	31.67
Co/ZAC	26	0.08	17.77
ZAC	59	0.15	2.28
Co/FPMAC	52	0.19	17.91
FPMAC	94	0.33	10.42
Co/MAS	40	0.14	9.97
MAS	58	0.13	19.57

Figure 4. 47 - N_2 isotherms and pore size distributions for a) Co/MAS, b) Co/FPMAC, c) Co/ZAC and d) Co/FPZAC.

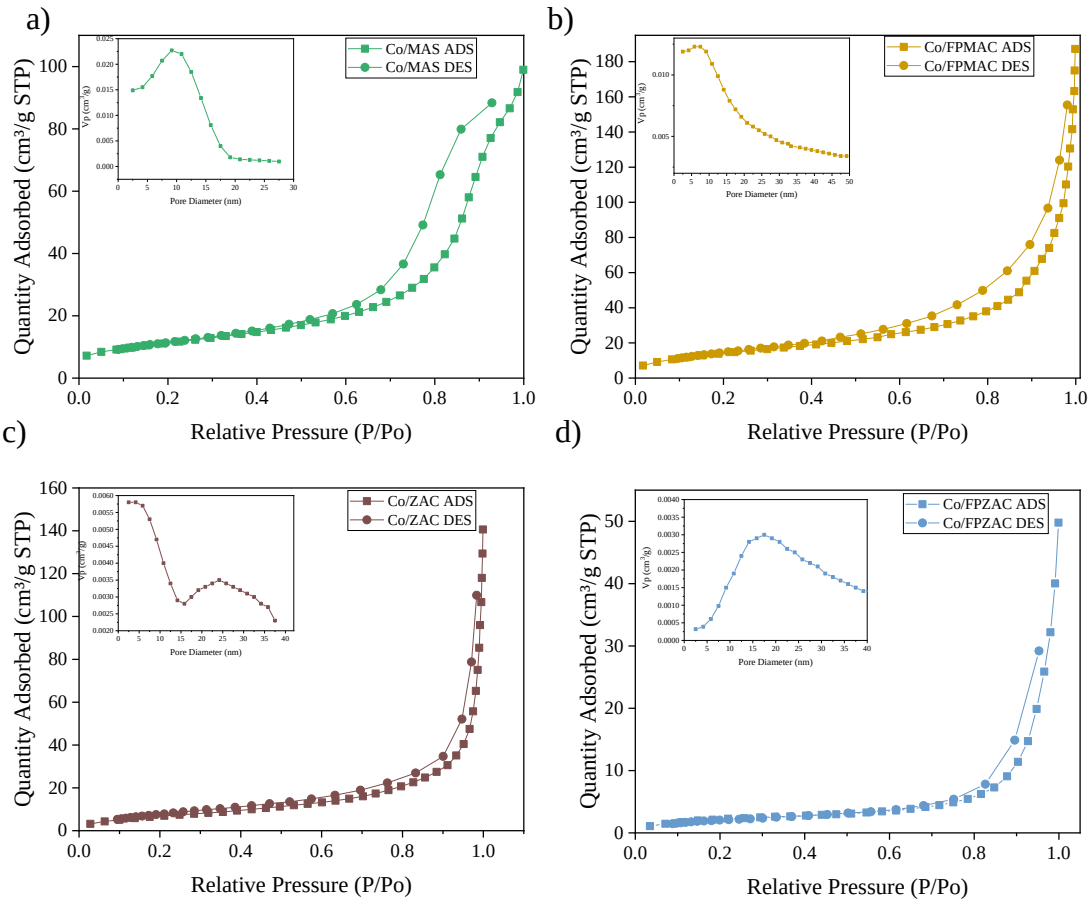

Table 4. 22 - Surface basicity for Co/MAS, Co/ZAC, Co/FPMAC and Co/FPZAC.

Sample	**Base sites (mmol.g^{-1})**		
	Total [a]	**Strong [b]**	**Weak [c]**
Co/MAS	0.99	0.07	0.92
Co/FPMAC	0.41	0.25	0.15
Co/ZAC	0.92	0.12	0.81
Co/FPZAC	0.93	0.03	0.89

[a] Acrylic acid was used as a probe molecule;
[b] Phenol was used as a probe molecule;
[c] Weak base site = Total base site − Strong base site.

Surface basicity was determined by irreversible adsorption of acids, Table 4.22. Except for Co/FPMAC, materials with $Co(acac)_2$ impregnation had higher number of basic sites than CoAC450 and CoAC700 (0.57 and 0.65 mmol.g^{-1}, respectively) , Table 4.17. Co/ZAC had an expressive change of its base sites distribution, since prior impregnation the solid had 0.03 mmol.g^{-1} of strong base sites and 0.51 mmol.g^{-1} of weak base sites. Conversely, Co/FPMAS and Co/FPZAC have reduced their total of bases sites,

which were initially 1.7 and 1.54 mmol.g^{-1},respectively. The following trend was observed for the total of base sites: Co/MAS > Co/FPZAC > Co/ZAC > Co/FPMAC.

For Cobalt(II) acetylacetonate modified catalysts, Figure 4.48, no change on morphology was noticeable for materials supported on MAS, FPMAC and FPZAC, in comparison with the images of each support presented in Figures 4.8 and 4.31. The $KMgF_3$ crystals noticed in FPMAC remained after impregnation. Co/ZAC exhibited compact agglomerates with irregular distribution, in contrast with the hexagon-like crystals observed in Figure 4.24. This behavior can explain the expressive drop on S_{BET} in comparison with ZAC presented in Table 4.21.

Figure 4. 48 - TEM images (scale bar 50 nm) of Co/MAS, Co/ZAC, Co/FPMAC and Co/FPZAC.

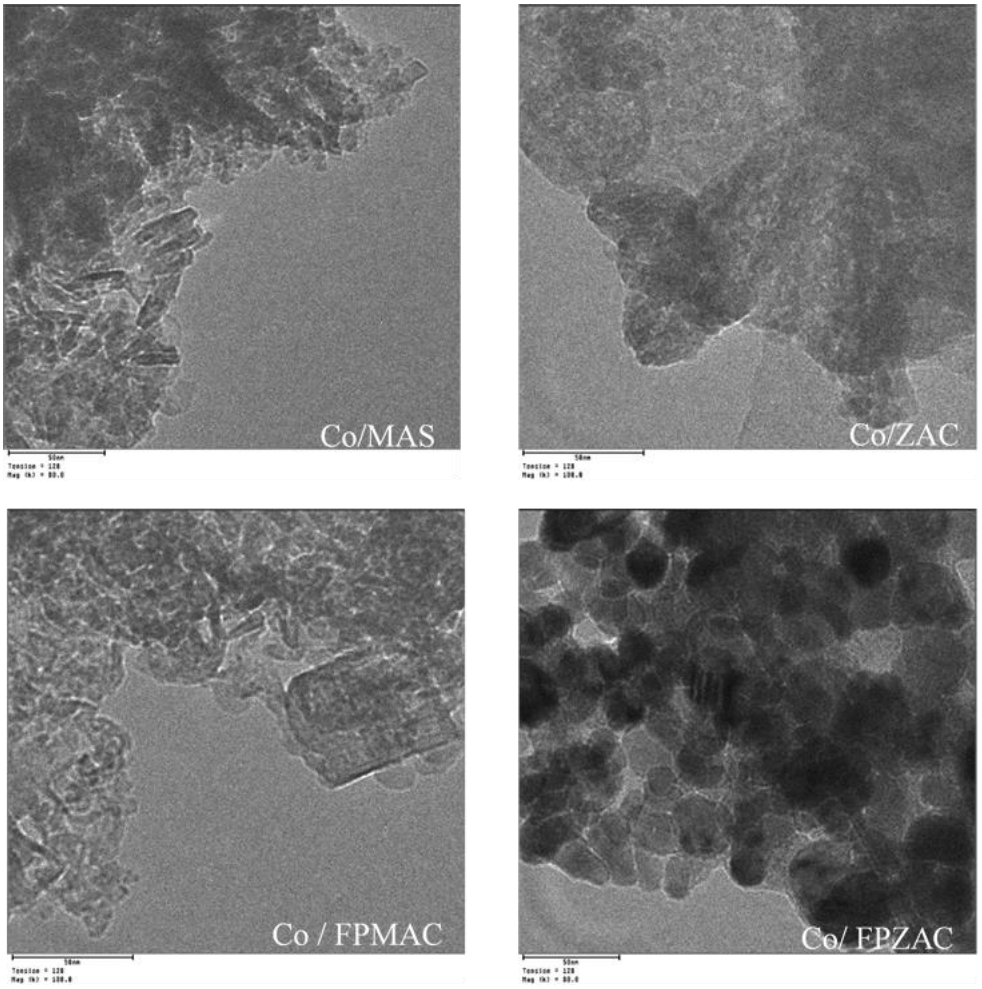

4.3.2 Catalytic study

4.3.2.1 Co/Al LDH

The catalytic application started with the study of calcination temperature, Figure 4.49, for tests with 2% of catalyst, reactions at 220 °C for 24 hours. CoAS activated at 700 °C for 6 hours had a better activity than calcined at 450 °C for 24 hours, reaching 16% of X_{Gly} against 9% of CoAC450, besides the higher yield of oligomers. Both CoAC450 and CoAC700 are formed by cobalt spinels, however TGA and FTIR analysis have point out the absence of carbonate on the latter. Such difference in activity can be related to the pore size distribution of CoAC700 since this textural property affects diffusion. Furthermore, the base sites distribution may explain the improved activity as well, since CoAC700 presented higher amounts of weak to medium strength base sites, which have a good correlation with the production of di and triglycerol, as noticed in Section 4.2 for both rehydrated Zn/Al LDHs and fluorine containing catalysts.

Figure 4. 49 - Influence of calcination temperature (reaction conditions: 2 wt% cat., 220 °C and 24 h).

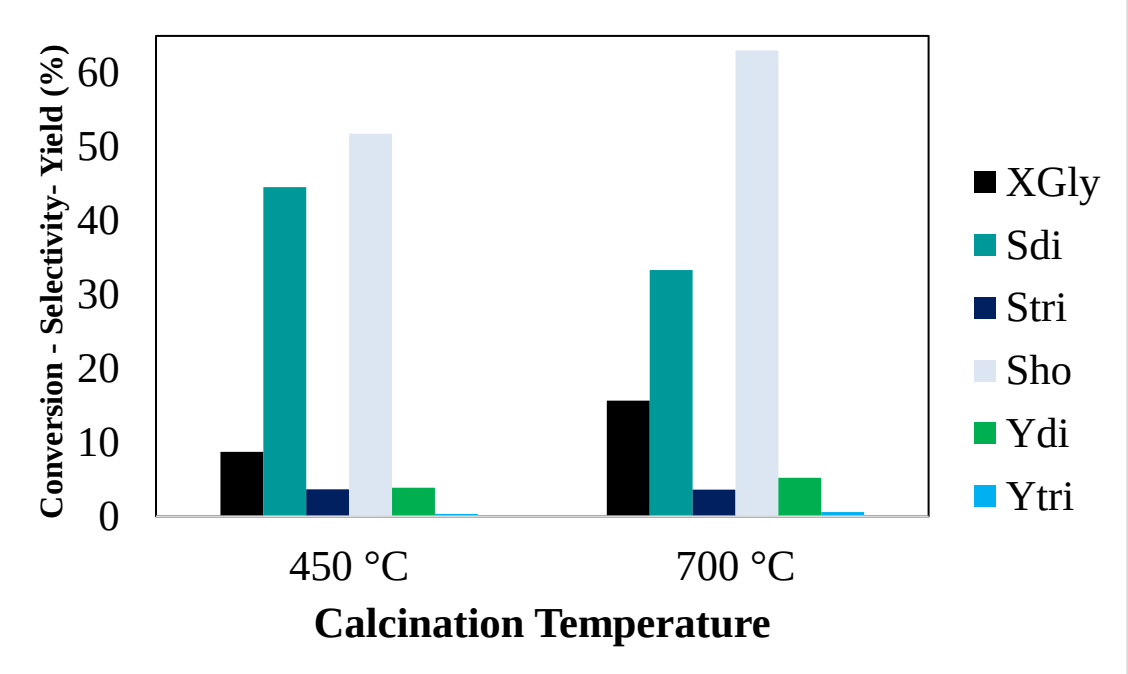

Reaction temperature and catalyst loading were evaluated using 2 wt% of CoAC700, Figure 4.50. Increasing temperature to 230 °C, Figure 4.50 a), led X_{Gly} to reach 38% and S_{di} went from 33 to 39%. As in Zn/Al LDH case, Figure 4.25, further temperature increasing did not improve activity. On catalyst loading section, Figure 4.50

b), is possible to notice that change to 3% led to similar catalytic response, while 4% has brought glycerol conversion to 69% on similar S_{di} and S_{tri} levels. At this stage, Co/Al had

Figure 4. 50 - Evaluation of reaction parameters for CoAC700: a) Reaction temperature (reaction conditions:2 wt% cat. and 24 h) b) Catalyst loading (reaction conditions: 230 °C and 24 h).

a)

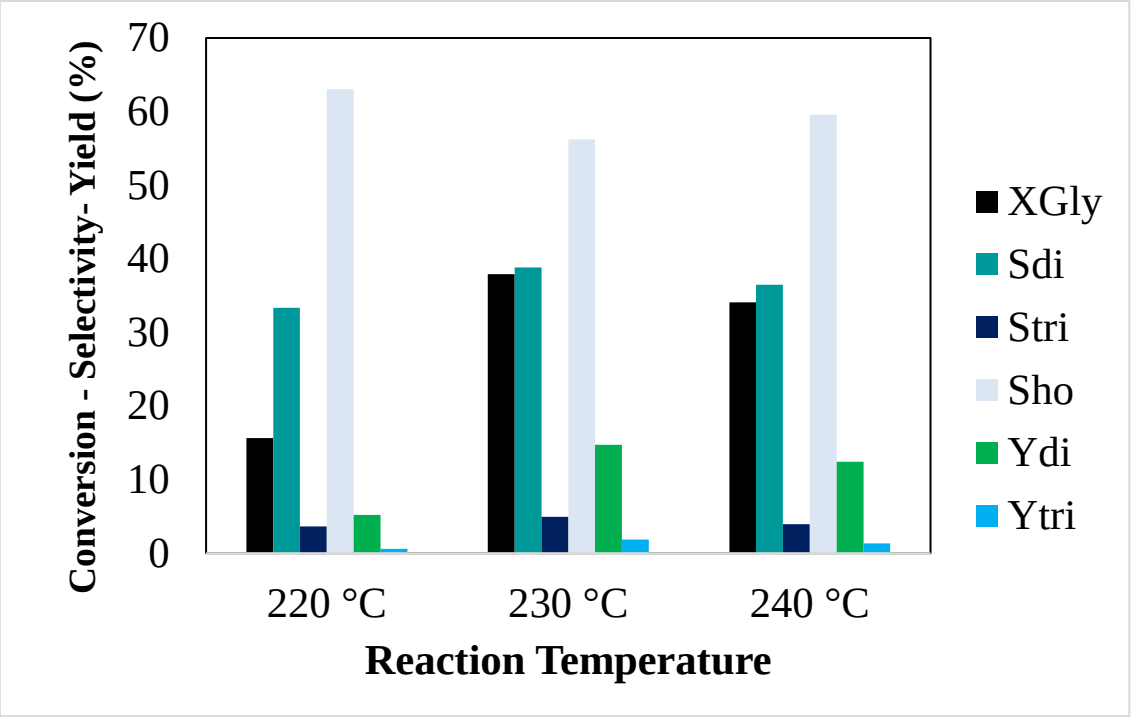

b)

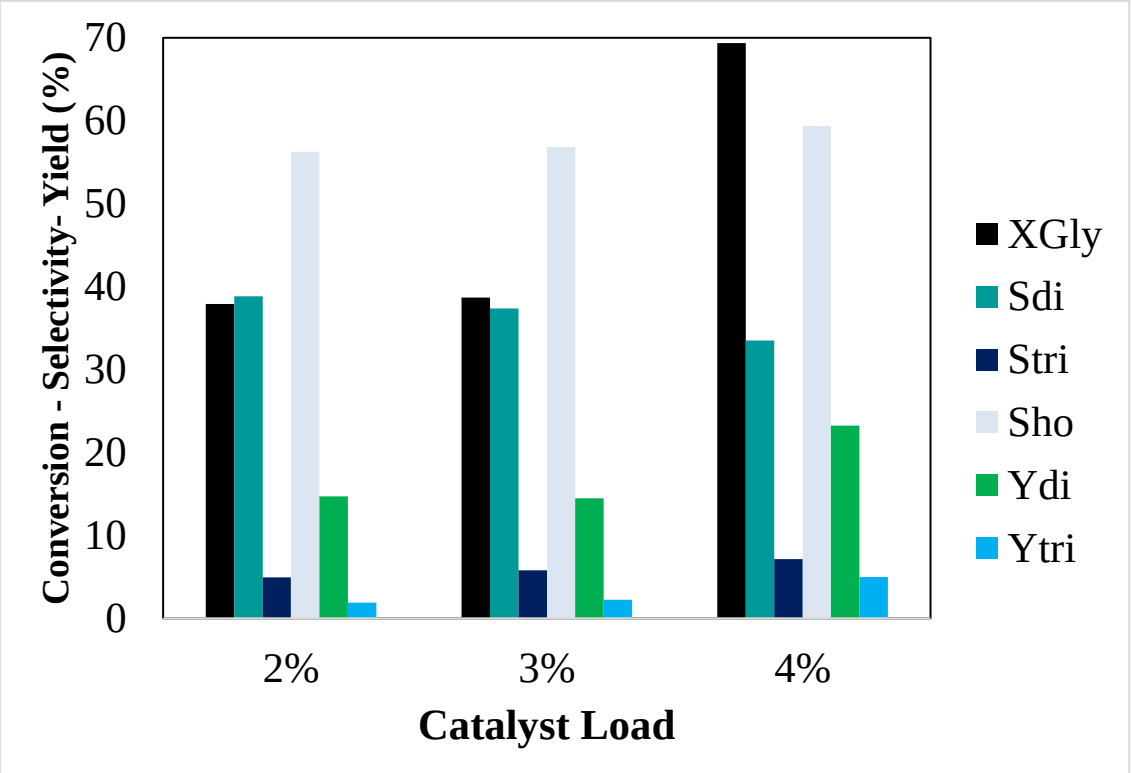

better response than Zn/Al, which reached just 9% of X_{Gly} but still under the performance of the catalyst derived from Mg/Al LDH, MAU30P, since it had X_{Gly} of 64%, S_{di} of 37% and S_{tri} of 5.4% for a 8 hours reaction at 240 °C with 4 wt% of catalyst.

As in previous Sections, the effect of reaction time on the selectivity to the oligomers was evaluated and an 8 hours test was performed, Figure 4.51. Glycerol conversion dropped to 23.5%. and S_{di} was 5% higher. Moreover, fluorine catalyst FPCoAC under the same reaction conditions, Figure 4.33, had higher activity: X_{Gly} of 51% and of S_{di} of 31% and S_{tri} of 7%.

Figure 4. 51 - Evaluation of reaction time for CoAC700 (reaction conditions: 4 wt% cat. at 230 °C).

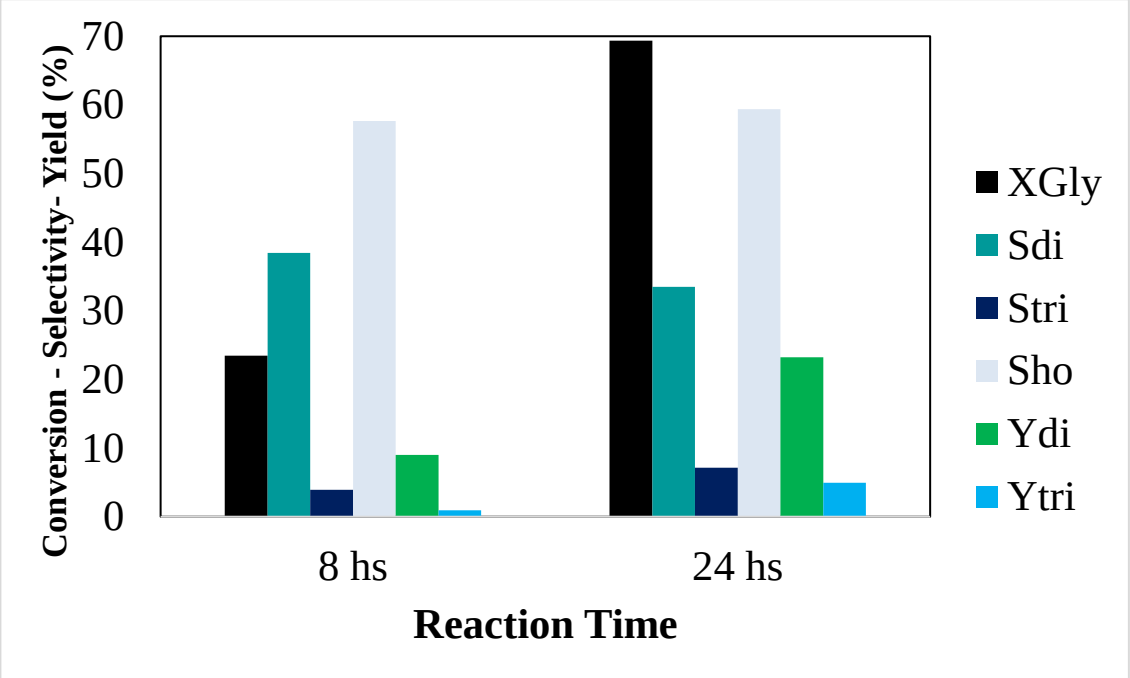

To investigate the influence of cobalt as a promoter of glycerol oligomerization, cobalt (II) acetylacetonate supported on Mg/Al LDH, calcined Zn/Al LDH and the fluorine-containing materials FPMAC and FPZAC were used as catalysts.

4.3.2.2 Cobalt (II) acetylacetonate supported on LDH and fluoroperovskite

The activity for glycerol oligomerization of Cobalt(II) acetylacetonate supported on LDH and fluoroperovskite was tested under optimal reaction temperature and catalyst loading found in the previous section. Initially, reaction time was of 4 hours, Figure 4.52 a). Yield of diglycerol exhibited the following trend: Co/FPZAC< Co/ZAC < Co/FPMAC < Co/MAS. In comparison with the reaction catalysed by the bare supports, Co/FPMAC had similar activity in a lower reaction time than FPMAC (X_{Gly} of

35% for a reaction with 4 wt% of catalyst at 230 °C for 8 hours). Conversely, Co/ZAC has increased the conversion from 9% with ZAC (same temperature and catalyst amount for 8 hours of reaction) to 33%. Co/FPZAC had 18% of X_{Gly} against 41% for the reaction with FPZAC for 8 hours. Glycerol conversion with Co/MAS was of 45%, whereas MAU30P had 64% (reaction at 240 °C for 8 hours).

Additional tests were performed for Co/MAS and Co/FPMAC to clarify the influence of reaction temperature and time, these catalysts were chosen due to their higher Y_{di} and low formation of high oligomers and other products (S_{ho}), Figure 4.52 b). For Co/MAS, increasing temperature to 240 °C has improved the activity, with 50% of X_{Gly} and similar S_{ho}, Y_{di} and $Y_{tri.}$ In contrast, Co/FPMAC has led to lower conversion, around 15%. Regarding the 8 hours reactions, both materials led to higher than for 4 hours, X_{Gly} reaching similar Y_{di} and Y_{tri}, around 18 and 7% as well as S_{ho} (around 60%).

To compare the basicity of Co/MAS with the as-synthesized Mg/Al LDH, CO_2-TPD was carried out (set-up 2), with activation for 1 hour at 100 °C, Figure 4.53. Deconvolution of Co/MAS shows multiple active sites and a different profile from the bare support (Figure 4.6), with the presence of two desorption peaks of low intensity at 112 and 226 °C, related to weak base sites. The high intensity peak at 362 °C shows that the material has several medium strength sites. For MAS, main peak was desorbed at 450°C. The last peak of Co/MAS, at 553 °C, is ascribed to strong sites.

Considering the difficulties in the separation of glycerol and oligoglycerol mixtures pointed by Martin and Richter (2011), the catalyst with higher glycerol conversion, Co/MAS, was chosen for the evaluation of stability and recycling.

The profile of glycerol conversion and yield of oligomers versus reaction time is presented in Figure 4.54 a). In the first hour, there is a X_{Gly} of 10%, with production of diglycerol and a small amount of triglycerol (Y_{di} of 7% and Y_{tri} of 0.14%). The induction period that was previously observed in our study with calcined dolomite (CD) is not noticed for Co/MAS, Figure 4.54b) (BARROS *et al.*, 2018). Considering the mechanism proposed by Ruppert *et al.* (2008), adapted in Figure 2.2 , the oligomerization of glycerol consists in two steps: first, a basic site extracts a proton of glycerol, and in the second step, an unsaturated site favors the attack of deprotonated glycerol by another glycerol molecule. For reaction with CD, the formation of deprotonated glycerol species could be limited. Within the first 4 hours, CD catalyzed reaction reaction had 5% of $X_{Gly,}$ whereas

Figure 4. 52 - Catalysts impregnated with cobalt(II) acetylacetonate, reactions conditions: a) at 230 °C with 4 wt% cat. for 4 h b) at 240 °C with 4 wt% cat.

a)

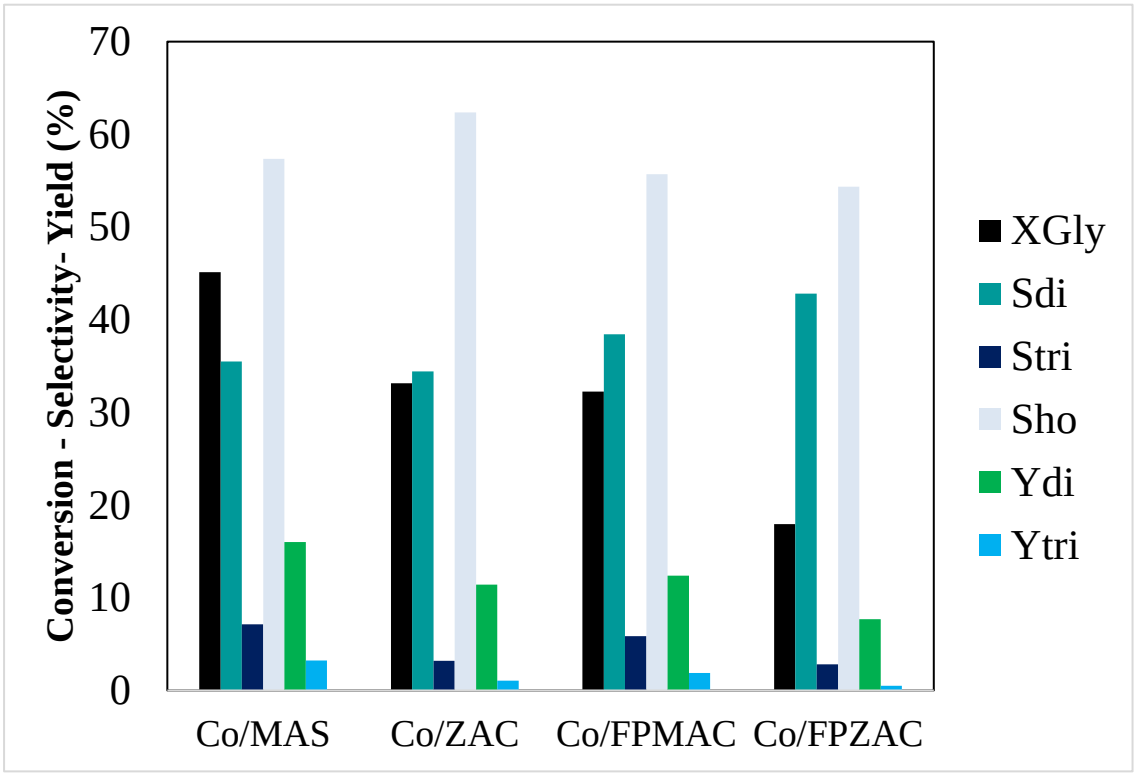

b)

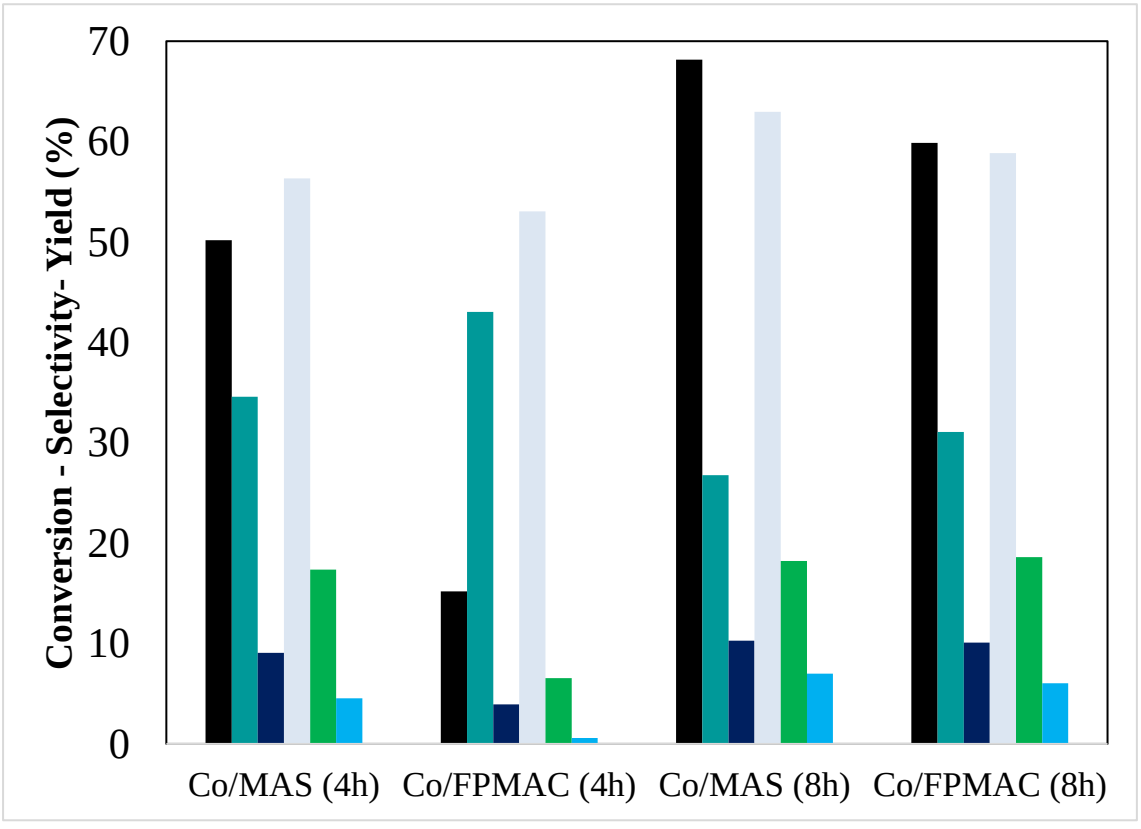

Figure 4. 53 - CO_2 -TPD (set-up 2) profile for Co/MAS activated for 1 hour at 100 °C

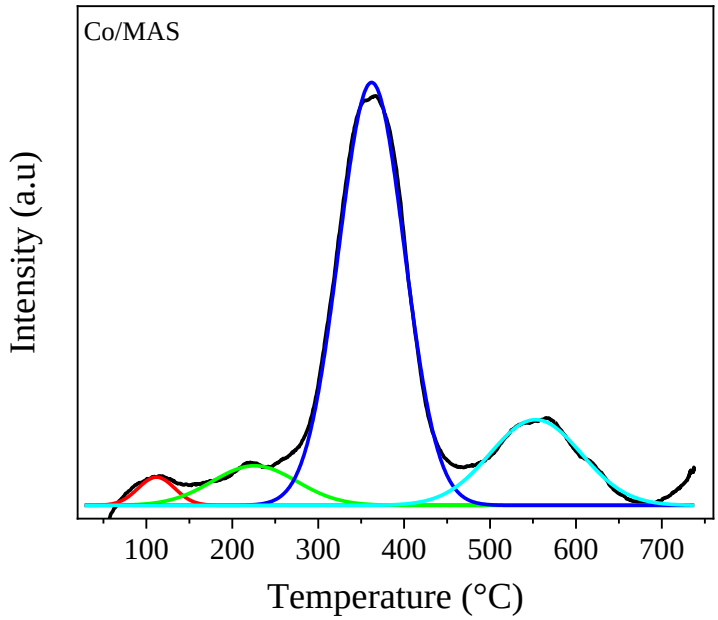

CaO from calcined eggshells (CEG, from BARROS *et al.*, 2017) had 9% and Co/MAS 27%. As shown in Figure 4.18,test with MAU30P had in comparison to Co/MAS, similar X_{Gly} (56 and 59%) and Y_{di} (19 and 18%), whereas Y_{tri} was 0.83% for MAU30P and 5% for Co/MAS (for 8 hours of reaction, under the same conditions).

According to Richter *et al.* (2008), glycerol oligomerization is best described by a first order equation. Considering the mechanism mentioned previously, due to the abundance of neutral glycerol, its concentration can be viewed as unchanged. Thus, reaction is observed as of pseudo first order. The initial glycerol concentration is formally contained in the values of rate constant. Their study, consisted on a kinetic treatment for the oligomerization of glycerol using $CsHCO_3$ as catalyst, in a batch reactor at 260 °C for 0.1, 0.2 and 0.4 wt% of $CsHCO_3$.

In their comprehensive review article, Martin and Richter (2011), mentioned the work of Zajic (1966), which determined rate constants for thermal glycerol oligomerization and for experiments with Na_2O added at loadings of 0.1, 0.3 and 1 wt%. They also translated the rate constant from the study of Zajic from 220 to 260 °C using the activation energy of 47.3 kJ/mol for 0.3 wt% Na_2O.

The rate constants for Co/MAS, MAU30P (Section 4.1) and our previous works with CEG and CD were calculated for a first order reaction. For comparative purposes, we have translated the rate constant from Zajic to 240 °C, results are shown in Table 4.23. The rate constants of Co/MAS and MAU30P are quite similar, being higher

Figure 4. 54 - a) XGly and oligomers yield versus time for Co/MAS (reaction conditions: 4 wt% and 240 °C) b) Comparison of profiles with CEG (reaction conditions: 2 wt% and 220 °C), CD (reaction conditions: 2 wt% and 220 °C) and MAU30 (reaction conditions: 4 wt% and 240 °C).

a)

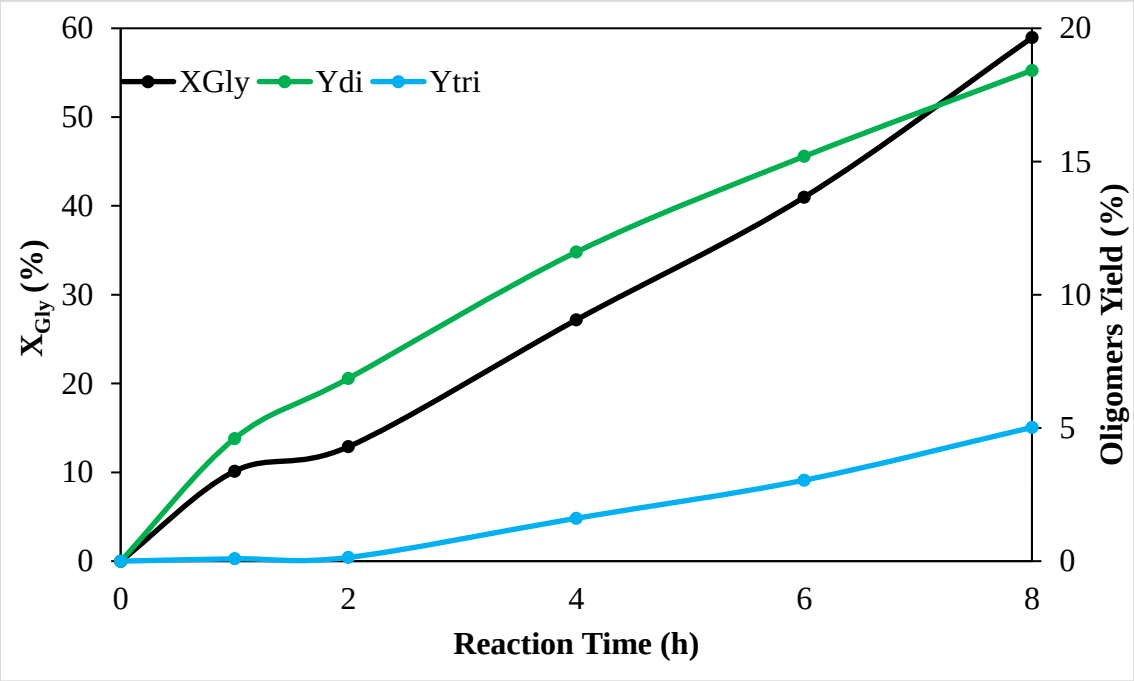

b)

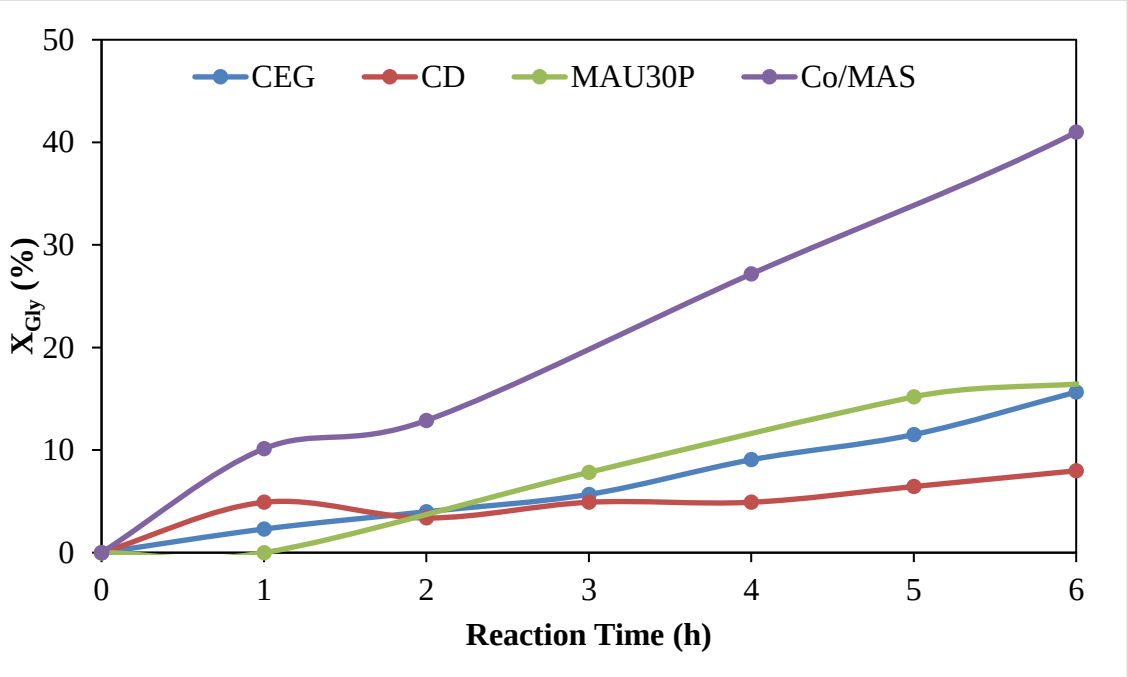

than for Na_2O, at same temperature. Martin and Richter (2011) highlighted that the rate constant changes with concentration of Cs points to mechanistic modifications and that

the reaction does not obey a strict consecutive formation of the oligomers by reaction with glycerol, because diglycerol reacts preferentially with itself to form tetraglycerol.

Table 4. 23 - Reaction constants for glycerol oligomerization with MAU30P, Co/MAS, CEG, CD, $CsHCO_3$ and Na_2O.

Catalyst	**wt%**	**T (°C)**	**k (h^{-1})**
MAU30P	4	240	0.099
Co/MAS	4	240	0.105
CEG (BARROS *et al.*, 2017)	2	220	0.082
CD (BARROS et al, 2018)	2	220	0.070
$CsHCO_3$(RICHTER *et al.*, 2008)	0.1	260	0.058
	0.2	260	0.101
	0.4	260	0.121
Na_2O (ZAJIC, 1966 apud MARTIN and RICHTER, 2011)	0.3	220	0.025
	0.3	260	0.059[a]
	0.3	240	0.039[b]

* CEG: CaO from calcined eggshell; CD: Calcined dolomite
[a] Estimated by Martin and Richter (2011)
[b] Estimated by the author

4.3.2.3 Co/MAS reuse and stability

The reuse of Co/MAS followed the procedure in Section 4.3, in which catalyst is recovered from reaction medium by decanting, followed by water addition, filtration and drying at 80 °C overnight prior new cycle. The catalysts deactivation is present already from the first to the second reaction cycle, X_{Gly} went from 68 to 26%, third run had 21% and increased to 28% on the last reaction, Figure 4.55 a). The selectivity to higher oligomers and other products (S_{ho}) increased from 49 to 56%.

A comparison of the reusability studies of Co/MA, FPZAC (Section 4.2) and MAU30P (Section 4.1) is shown in Figure 4.56. With the recovery procedure of drying spent catalyst, Y_{di} for Co/MAS reuses was constantly around 10%. Whereas, MAU30P had higher diglycerol yield over the first three cycles and decreased to around 3% for the last reaction. By changing recovery procedure (and a longer reaction time), FPZAC with calcined spent catalyst had 14% of Y_{di} in the last reaction.

Production of acrolein for Co/Al LDH and catalysts impregnated with Cobalt(II) acetylacetonate is shown in Table 4.24. Selectivity to acrolein was bellow 0.12% for the evaluation of reaction parameters and the screening of catalysts. However, S_{Acr} has increased over the reuses of Co/MAS, reaching a maximum of 0.73% in the last

reaction. This trend was also observed for the recycling of MAU30P and FPZAC in previous sections.

Figure 4. 55 - Reusability of Co/MAS (reaction conditions: 4 wt% cat., 240 °C and 8 h).

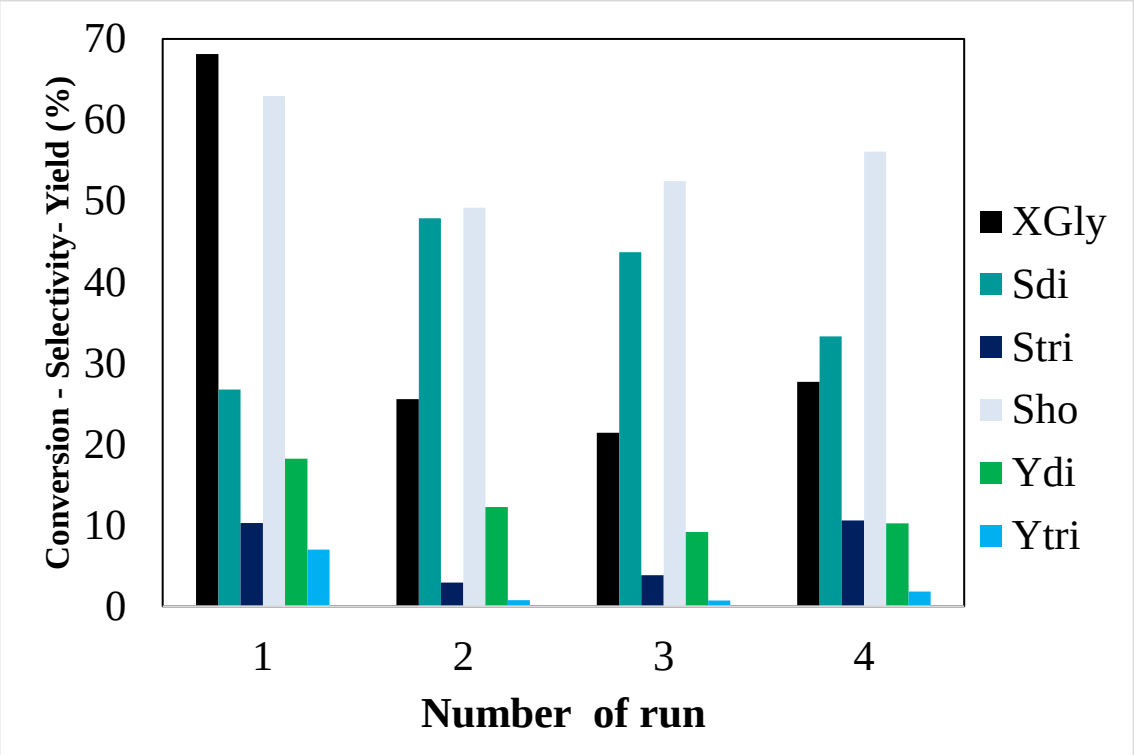

Figure 4. 56 - Reusability studies for MAU30P (dried spent catalyst, reaction conditions: 4 wt% cat., 240 °C, 8 h), FPZAC (dried spent catalyst, reaction conditions: 4 wt% cat., 230 °C, 8 h), FPZAC(calcined spent catalyst, reaction conditions: 4 wt% cat., 230°C, 18 h), Co/MAS (dried spent catalyst, reaction conditions: 4 wt% cat., 240 °C, 8 h).

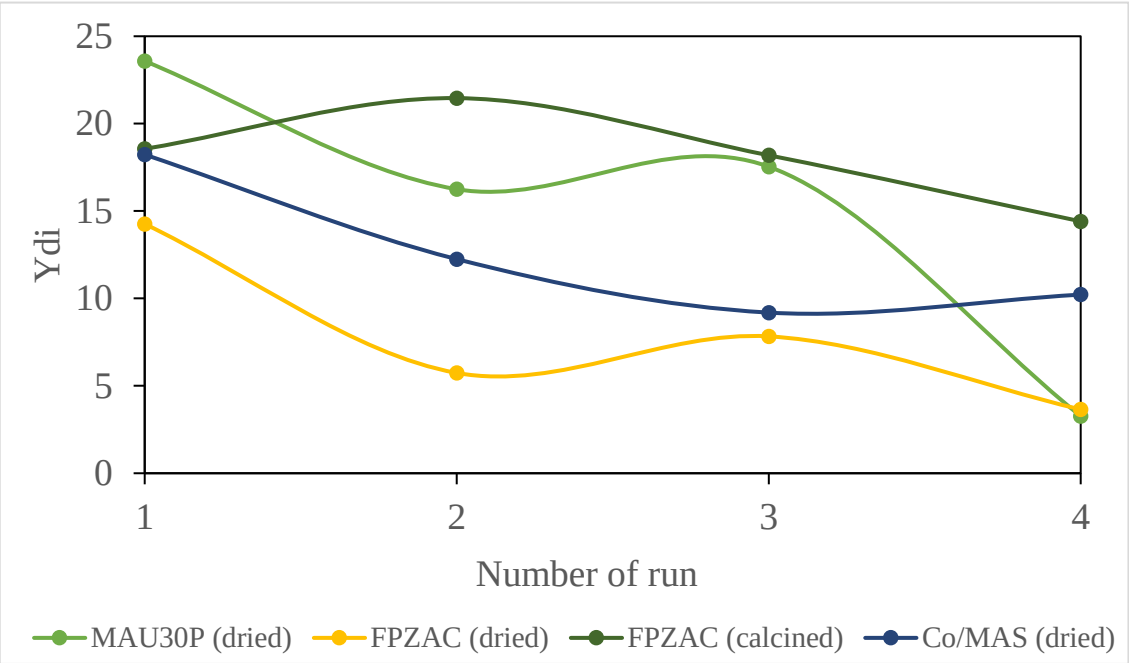

Table 4. 24 - Selectivity to acrolein for Co/Al LDH and $Co(acac)_2$ tests.

Test	Sample	S_{Acr} (%)
Calcination Temperature	CoAC700	0.51
(2 wt% cat., 220 °C and 24 h)	CoAC450	NI
Reaction Temperature	220 °C	NI
(2 wt% cat. and 24 h)	230 °C	0.02
	240 °C	0.02
Catalyst Loading	2%	0.02
(230 °C and 24 h)	3%	0.04
	4%	0.08
Reaction time	8 h	0.02
(4 wt% cat. and 230 °C)	24 h	0.06
$Co(acac)_2$	Co/MAS	0.01
(4 wt% cat., 230 °C and 4 h)	Co/ZAC	0.01
	Co/FPMAC	0.06
	Co/FPZAC	0.11
(4 wt% cat., 240 °C and 4 h)	Co/MAS	0.06
	Co/FPMAC	0.06
4 wt% cat., 240 °C and 8 h)	Co/MAS	0.06
	Co/FPMAC	0.13
Co/MAS reuse	1st run	0.03
4 wt% cat., 240 °C and 8 h)	2nd run	0.55
	3rd run	0.56
	4th run	0.73

ICP-OES analysis was performed in the products to verify occurrence of leaching of metallic species from Co/MAS. The results have pointed out absence of Co, Al and Mg. In Section 4.1, reaction products from recycling of MAU30P did not have Mg and Al as well. FPZAC, Section 4.2, had absence of Al and Zn, however, the loss of potassium over three cycles represented 38% of its concentration in the solid prior reaction. Leaching is observed in other studies in glycerol oligomers production as well. Sivaiah *et al.*(2012) has reported leaching of the basic element with the use of Cs-exchanged (X and Y) zeolites and mesoporous silica, as well as Cs impregnated on MCM-41 in its purely siliceous form or with Al.

Thermogravimetric analysis of fresh and spent catalysts, Figure 4.57 has indicated the presence of adsorbed species, either glycerol, oligomers or other reaction products, that were not removed by dissolution/filtration. This weight loss can be seen in the DTG event located from around 200 to 450 °C. After the first reaction, spent Co/MAS had 4% of impurities in comparison to its fresh form, followed by 2.6 and 3.09 % for recovered catalysts from 2nd and 3rd runs, respectively. The impurities can explain the

reduction of conversion by the blocking of the base sites. The solid recovered from last run had 12.27% of impurities.

Figure 4. 57 - Co/MAS fresh and spent forms from reusability study a) TGA b) DTG.

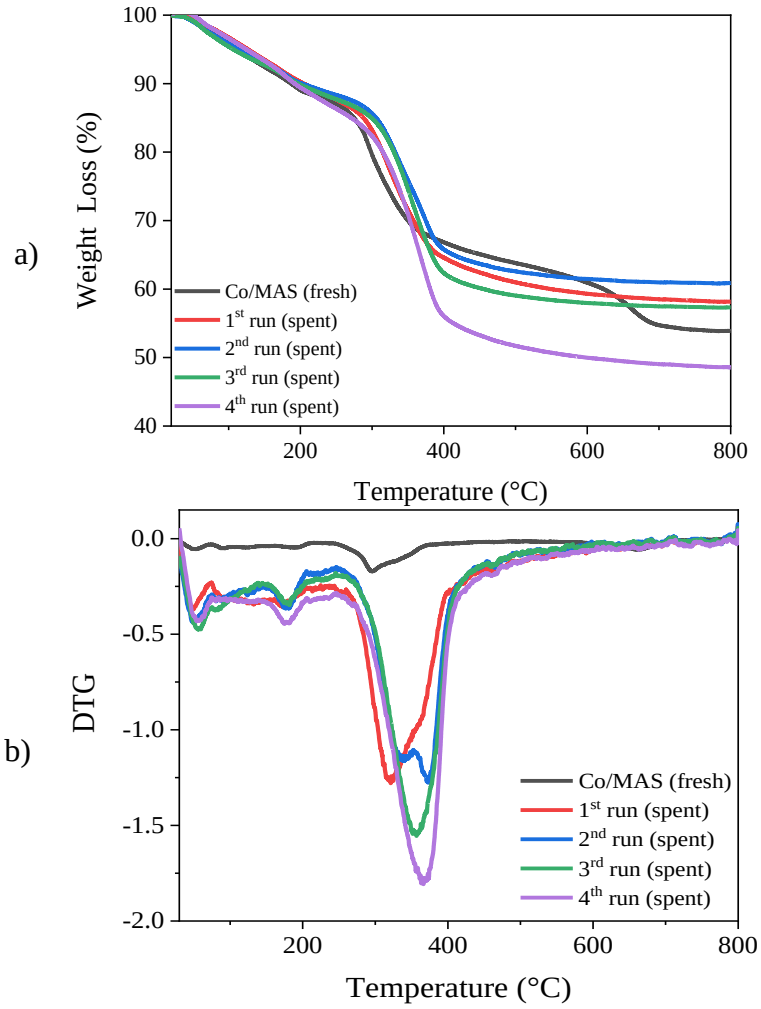

The surface composition and metal oxidation states of Co/MAS (fresh and spent forms) were investigated by XPS, Table 4.25. The XPS spectra of C 1s, O 1s, Co 2p, Mg 2s and Al 2p are shown in Figure 4.58.

The C 1s region of fresh catalyst can be deconvoluted into four components. The first contribution at 283.3 eV corresponds to carbon in C-metal bonding, probably related to cobalt carbide, this peak was not present in Figure 4.17, MAU30P spectra, which is derived from the same solid used as support. The main contribution at 284.9 eV and the third peak at 286.9 eV are attributed to adventitious carbon: C-C and C-O, respectively. The fourth peak, at 289 eV, is related to C=O. The spent catalyst from the first run has the same peaks, with a reduced carbide contribution, Table 4.25. The material recovered from fourth run had only the contributios of C-C (284.8 eV), C-O (286.5 eV) and C=O (288.8 eV) (GAUTAM *et al.*, 2018).

Table 4. 25 - XPS results for fresh and spent Co/MAS recovered from 1st and 4th runs.

Sample	Binding energy (eV)					Atomic concentration (%)					Molar ratio	
	C 1s	O 1s	Co 2p	Mg 2p	Al 2p	C	O	Co	Mg	Al	Mg/Al	Co/Al
Co/MAS (fresh)	283.3 (22.16%) 284.9 (67.6%) 286.9 (6.62%) 289.1 (3.62%)	532	783.4 (59.91%) 787.2 (27.66%) 795.3 (12.43%)	50.4	74.4	56.3	30.67	0.29	7.07	5.39	1.44	0.03
1st run (spent)	283.3 (15.87%) 284.8 (61.64%) 286.6 (17.15%) 289.2 (5.24%)	532	783.1 (57.84%) 786.4 (28.80%) 800.4 (13.36%)	50.3	74.4	55.04	33.49	0.16	5.71	4.26	1.48	0.02
4th run (spent)	284.8 (81.31%) 286.5 (9.43%) 288.8 (9.26%)	531.5	-	49.7	73.9	30.04	49.06	-	12.31	8.6	1.59	-

The high-resolution XPS spectrum of O 1s for Co/MAS fresh and recovered from the first reaction shows a single contribution at 532 eV, ascribed to OH^-. Spent catalyst from fourth run shows lower binding energy (531.5 eV), Figure 4.58 b).

The Co 2p core level, Figure 4.58 c), exhibits a broad peak that was curve fitted in two main peaks and a satellite peak. The presence of a peak at around 783 eV and a satellite at about 787 eV indicates that surface cobalt is a Co^{2+} species. The third peak is ascribed to Co^{3+} (TODOROVA *et al.*, 2010).

As shown in Figure 4.58 d), Mg 2p spectra for Co/MAS and the solid recovered from the first reaction presents a single contribution at 50.4 and 50.3 eV, respectively, typical from $Mg(OH)_2$. Whereas the binding energy of spent catalyst from fourth run exhibits a small shift toward lower binding energy (49.7 eV). Furthermore, the Al spectra for fresh and spent catalysts have a single contribution from 74.4 to 73.9 eV, ascribed to $Al(OH)_3$.

The surface composition obtained from XPS studies, Table 4.25, showed a Co/Al molar ratio of 0.03 for the fresh Co/MAS, which is the same value determined by ICP-OES, Table 4.19. Therefore, the distribution of Co/Al was even from the surface to the bulk. The Mg/Al molar ratio was lower than the value found for the bulk, as in MAU30P (Section 4.1). The contents of carbon and oxygen were similar for fresh catalyst and its spent form from first reaction. However, Co, Mg, Al had lower amounts, and thus the Co/Al molar ratio has reduced as well. Such findings can be correlated to the reduction on X_{Gly} noticed in Figure 4.54. Cobalt was not detected for the spent catalyst of fourth run, which also displayed a surface enrichment of Mg and Al. The Mg/Al molar ratio was constant across recycling, unlike in MAU30P. The carbon content on the surface was reduced for the solid from the last reaction, in contrast with the amount of impurities observed in TGA/DTG results, Figure 4.56.

Figure 4. 58 - XPS spectra for fresh and spent Co/MAS recovered from 1st, 3rd and 4th run for a) C 1s, b) O 1s, c) Co 2p3/2, d) Mg 2p and e) Al 2p regions.

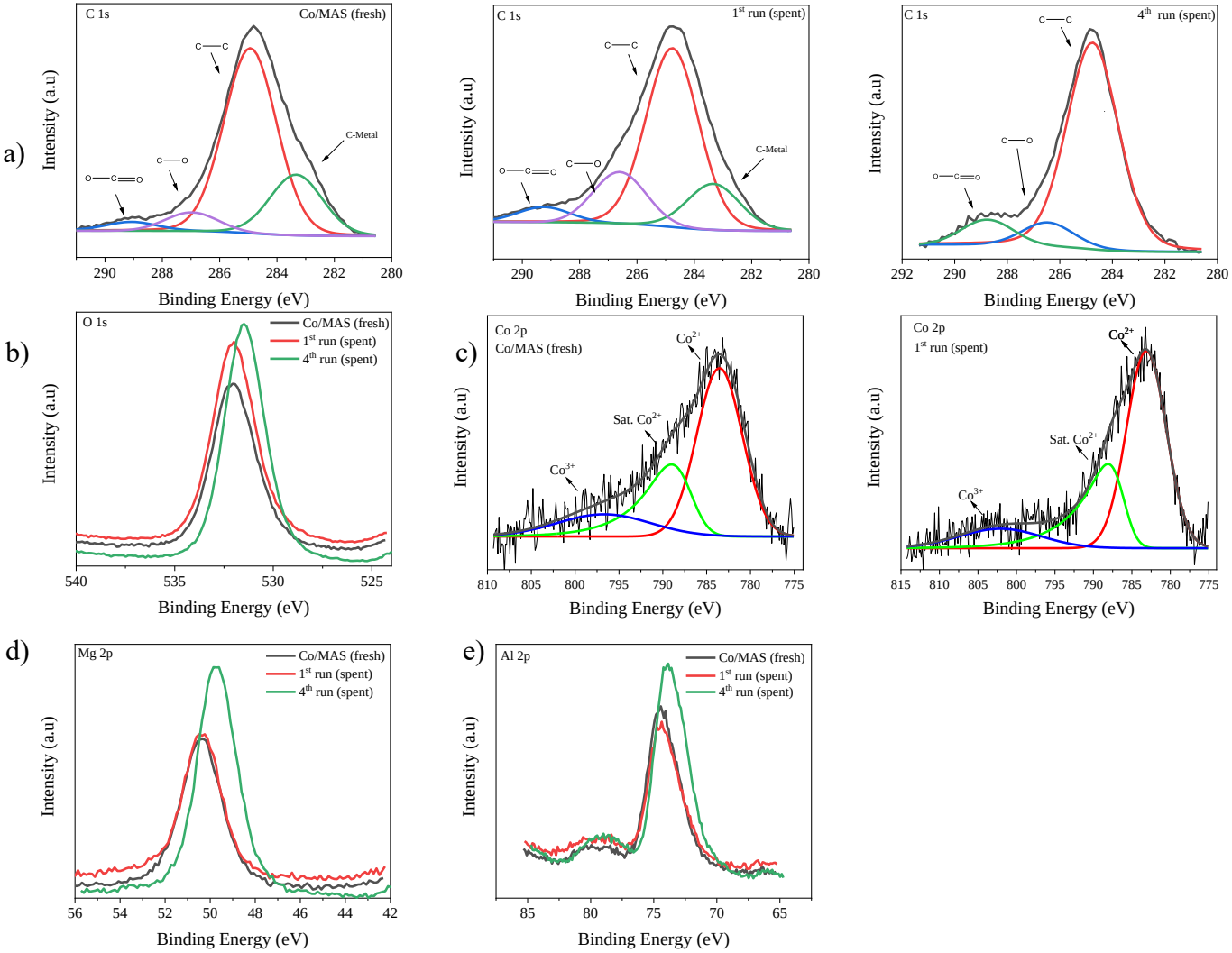

4.3.3 Partial Conclusion

The thermal treatment of Co/Al LDH at 450 and 700 °C produced a solid solution of cobalt/aluminum spinels. The total basicity was similar for both materials, as seen in UV-Vis and CO_2-TPD methods. However, the base sites distribution of CoAC700 had higher amounts of weak to medium strength base sites, assuring a better catalytic response. The best set of conditions for glycerol oligomerization were 4 wt% of catalyst and 24 h of reaction at 230 °C, with a conversion of 69% and yield of diglycerol of 23%.

After adjustments in reaction conditions, the best response among catalysts impregnated with Cobalt(II) acetylacetonate was from the material supported on Mg/Al LDH, which had 68% of glycerol conversion and yield of diglycerol of 18%, for reactions with 4 wt% of catalyst, at 240 °C for 8 hours. The impregnation with the cobalt complex has changed the base site distribution with addition of weak base sites.

The recycling of Co/MAS was possible up to fourth run. Metals were not detected in reaction products, discarding the occurrence of leaching. Growing amounts of impurities were quantified in the products via thermogravimetric analysis. The analysis of surface of fresh and spent catalysts revealed reduction in Co/Al molar ratio, whereas Mg/Al molar ratio was similar across recycling. Therefore, deactivation is related to the presence impurities in the bulk catalyst and to the loss of cobalt on its surface.

5 CONCLUSION

Regarding Mg/Al and Zn/Al LDHs, rehydration via ultrassound and mechanical stirring have sucessfuly recovered lamellar strcuture, with modifications in their textural and acid-base properties. Thus, this process has improved their activity for glycerol oligomerization, in comparison to mixed oxides.

To increase the production of oligomers with Mg/Al catalyst, a modification procedure was designed based on a correlation of basicity and selectivity to diglycerol. The treatment with acetic acid led to a surface enrichment of Mg on MAU30P and has increased the selectivity and catalyst stability.

The presence of higher amounts of weak to medium strength base sites had a good correlation with the production of diglycerol and triglycerol for Co/Al and Zn/Al, in the forms of rehydrated LDH, fluorine-containing solids, mixed oxides and $Co(acac)_2$ supported catalysts. Moreover, Zn/Al and Co/Al had higher activity for fluorine-containing materials, due to the enhancement in Lewis acidy, that plays a key role in the second step of reaction mechanism.

The harsh reaction conditions had influence in catalyst reusability and stability. Deactivation of MAU30P was atributed to the reduction in the molar ratio of Mg/Al on the surface and to the presence of glycerol and adsorbed products. For Co/MAS the amount of impurities was lower, but together with the loss of surface cobalt have contributed to the decrease of activity. Calcined spent FPZAC had its deactivation related to the potassium leaching and to the loss of fluorine on surface. All catalysts could be used up to 4 reaction cycles.

In addition , this study has shown that glycerol oligomerization is viable by heterogeneous catalysis. Thus, contributing to consolidate an alternative for the valorization of this by-product of biodiesel industries.

REFERENCES

ABELLÓ, S. *et al.* Aldol condensations over reconstructed Mg-Al hydrotalcites: Structure-activity relationships related to the rehydration method. **Chemistry - A European Journal**, v. 11, n. 2, p. 728–739, 2005.

ABELLÓ, S.; VIJAYA-SHANKAR, D.; PÉREZ-RAMÍREZ, J. Stability , reutilization , and scalability of activated hydrotalcites in aldol condensation. **Applied Catalysis A: General**, v. 342, p. 119–125, 2008.

ALGOUFI, Y. T.; KABIR, G.; HAMEED, B. H. Synthesis of glycerol carbonate from biodiesel by-product glycerol over calcined dolomite. **Journal of the Taiwan Institute of Chemical Engineers**, v. 70, p. 179–187, 2017.

ÁLVAREZ, M. G. *et al.* Tunable basic and textural properties of hydrotalcite derived materials for transesterification of glycerol. **Applied Clay Science**, v. 58, n. 2012, p. 16–24, 2012.

ÁLVAREZ, M. G. *et al.* Structure evolution of layered double hydroxides activated by ultrasound induced reconstruction. **Applied Clay Science**, v. 83–84, p. 1–11, 2013.

ANGELESCU, E. *et al.* The impact of the "memory effect" on the catalytic activity of Mg/Al; Mg,Zn/Al; Mg/Al,Ga hydrotalcite-like compounds used as catalysts for cycloxene epoxidation. **Applied Catalysis A: General**, v. 341, n. 1–2, p. 50–57, 2008.

ANITHA, M.; KAMARUDIN, S. K.; KOFLI, N. T. The potential of glycerol as a value-added commodity. **Chemical Engineering Journal**, v. 295, p. 119–130, 2016.

ANUAR, M. R.; ABDULLAH, A. Z.; OTHMAN, M. R. Etherification of glycerol to polyglycerols over hydrotalcite catalyst prepared using a combustion method. **Catalysis Communications**, v. 32, p. 67–70, 2013.

ARCANJO, M. R. A. *et al.* Conversion of glycerol into lactic acid using Pd or Pt supported on carbon as catalyst. **Catalysis Today**, v. 279, p. 317–326, 2017.

ATIA, H.; ARMBRUSTER, U.; MARTIN, A. Influence of alkaline metal on performance of supported silicotungstic acid catalysts in glycerol dehydration towards acrolein. **Applied Catalysis A: General**, v. 393, n. 1–2, p. 331–339, 2011.

BARROS, F. J. S. *et al.* Glycerol oligomers production by etherification using calcined eggshell as catalyst. **Molecular Catalysis**, v. 433, n. 2017, p. 282–290, 2017.

BARROS, F. J. S. *et al.* Glycerol Oligomerization Using Low Cost Dolomite Catalyst. **Waste and Biomass Valorization**, v. 0, n. 0, p. 1–14, 2018.

BASKARAN, T. *et al.* Silicate anion intercalated cobalt-aluminium alcohol oxidation. **RSC Advances**, v. 4, p. 11188–11196, 2014.

BEHR, A. *et al.* Improved utilisation of renewable resources : New important derivatives of glycerol. **Green Chemistry**, v. 10, p. 13–30, 2008.

BENÍCIO, L. P. F. *et al.* Layered double hydroxides : nanomaterials for applications in

agriculture. **R. Bras. Ci. Solo**, v. 39, n. 1, p. 1–13, 2015.

BERGADÀ, O. *et al.* Adsorption of Carbon Dioxide in Several Aged Hydrotalcites and Calcined Hydrotalcites : Influence of Microwave Irradiation during the Ageing Step on their Basic Properties. **Adsorption Science and Technology**, v. 25, p. 143–154, 2006.

BOOKONG, P.; RUCHIRAWAT, S.; BOONYARATTANAKALIN, S. Optimization of microwave-assisted etherification of glycerol to polyglycerols by sodium carbonate as catalyst. **Chemical Engineering Journal**, v. 275, p. 253–261, 2015.

CARVALHO, D. C. *et al.* Ni – Fe and Co – Fe binary oxides derived from layered double hydroxides and their catalytic evaluation for hydrogen production. **Catalysis Today**, v. 250, n. 2015, p. 155–165, 2015.

CECILIA, J. A. *et al.* V and V – P containing Zr-SBA-15 catalysts for dehydration of glycerol to acrolein. **Catalysis Today**, v. 254, n. 2015, p. 43–52, 2015.

CHEN, L. *et al.* Glycerol acetalization with formaldehyde using heteropolyacid salts supported on mesostructured silica. **Applied Catalysis A, General**, v. 549, p. 207–215, 2017.

CHEN, Z.; LIU, D. Toward glycerol biorefinery: metabolic engineering for the production of biofuels and chemicals from glycerol. **Biotechnology for Biofuels**, v. 9, n. 205, p. 1–15, 2016.

CHIMENTÃO, R. J. *et al.* Defect-induced strategies for the creation of highly active hydrotalcites in base-catalyzed reactions. **Journal of Catalysts**, v. 252, p. 249–257, 2007.

CIRIMINNA, R. *et al.* Glycerol-Derived Renewable Polyglycerols: A Class of Versatile Chemicals of Wide Potential Application. **Organic Process Research & development**, v. 19, p. 748–754, 2015.

CREPALDI, E. L.; VALIM, J. B. Hidróxidos duplos lamelares: síntese, estrutura, propriedades e aplicações. **Química Nova**, v. 21, n. 3, 1998.

DAS, D. P.; DAS, J.; PARIDA, K. Physicochemical characterization and adsorption behavior of calcined Zn/Al hydrotalcite-like compound (HTlc) towards removal of fluoride from aqueous solution. **Journal of Colloid and Interface Science**, v. 261, n. 2, p. 213–220, 2003.

ELHALI, A. *et al.* Effects of molar ratio and calcination temperature on the adsorption performance of Zn / Al layered double hydroxide nanoparticles in the removal of pharmaceutical pollutants. **Journal of Science : Advanced Materials and Devices**, v. 3, p. 188–195, 2018.

ELHALIL, A. *et al.* Photocatalytic degradation of ca ff eine by ZnO-ZnAl 2 O 4 nanoparticles derived from LDH structure. **Journal of Environmental Chemical Engineering**, v. 5, n. 4, p. 3719–3726, 2017.

GALY, N. *et al.* Glycerol oligomerization in continuous flow reactor. **Journal of Industrial and Engineering Chemistry**, v. 51, p. 312–318, 2017.

GAO, P. *et al.* Fluorinated Cu / Zn / Al / Zr hydrotalcites derived nanocatalysts for CO2

hydrogenation to methanol. **Journal of CO2 utilization**, v. 16, p. 32–41, 2016.

GARCÍA-SANCHO, C. *et al.* Etherification of glycerol to polyglycerols over MgAl mixed oxides. **Catalysis Today**, v. 167, n. 2011, p. 84–90, 2011.

GARGALO, C. L. *et al.* Economic Risk Assessment of Early Stage Designs for Glycerol Valorization in Biorefi nery Concepts. **Industrial and Engineering Chemistry Research**, v. 55, p. 6801–6824, 2016.

GAUTAM, J. *et al.* Highly efficient electrocatalyst of N-doped graphene-encapsulated cobalt-iron carbides towards oxygen reduction reaction. **Carbon**, v. 137, p. 358–367, 2018.

GENNEQUIN, C. *et al.* Use and observation of the hydrotalcite " memory effect " for VOC oxidation. **Catalysis Today**, v. 157, p. 191–197, 2010.

GHOLAMI, Z.; ABDULLAH, A. Z.; LEE, K. T. Catalytic Etherification of Glycerol to Diglycerol over Heterogeneous Calcium-Based Mixed Oxide Catalyst: Reusability and Stability. **Chemical Engineering Communications**, v. 202, n. 10, p. 1397–1405, 2015.

GUOXIANG, P. *et al.* Preparation of CoAl layered double hydroxide nanoflake arrays and their high supercapacitance performance. **Applied Clay Science**, v. 102, p. 28–32, 2014.

HE, Q. S.; MCNUTT, J.; YANG, J. Utilization of the residual glycerol from biodiesel production for renewable energy generation. **Renewable and Sustainable Energy Reviews**, v. 71, n. November 2016, p. 63–76, 2017.

HEJNA, A. *et al.* Potential applications of crude glycerol in polymer technology – Current state and perspectives. **Renewable and Sustainable Energy Reviews**, v. 66, p. 449–475, 2016.

HU, R. *et al.* Synthesis of perovskite KMgF3 with microemulsion for photocatalytic removal of various pollutants under visible light. **Catcom**, v. 40, n. 3, p. 71–75, 2013.

IIDA, H.; KAWAGUCHI, R.; OKUMURA, K. Production of diethyl carbonate from ethylene carbonate and ethanol over supported fl uoro-perovskite catalysts Intensity / cps. **Catalysis Communications**, v. 108, n. September 2017, p. 7–11, 2018.

JINESH, C. M.; ANTONYRAJ, C. A.; KANNAN, S. Allylbenzene isomerisation over as-synthesized MgAl and NiAl containing LDHs : Basicity-activity relationships. **Applied Clay Science**, v. 48, n. 1–2, p. 243–249, 2010.

KIRBY, F. *et al.* CaO as Drop-In Colloidal Catalysts for the Synthesis of Higher Polyglycerols. **Chemistry - A European Journal**, v. 21, n. 13, p. 5101–5109, 2015.

KUBICEK, M.; BORK, H.; RUPP, J. L. M. Perovskite oxides ; a review on a versatile material class for solar-to-fuel conversion processes. **Journal of Materials Chemistry A: Materials for energy and sustainability**, v. 5, p. 11983–12000, 2017.

LEE, G. *et al.* Sonication assisted rehydration of hydrotalcite catalyst for isomerization of glucose to fructose. **"Journal of Molecular Catalysis. A, Chemical"**, v. 393, n. 2014,

p. 289–295, 2014.

LEE, J. D. **Concise inorganic chemistry**. 5th ed. [s.l]: John Wiley & Sons, 2008.

LEE, J. H. *et al.* Solventless Catalytic Etheri fi cation of Glycerol Using Acetate Salts as Efficient Catalysts. **Bulletin of the Korean Chemical Society**, v. 39, p. 722–725, 2018.

LENG, Y. *et al.* POSS-derived solid acid catalysts with excellent hydrophpboicity for hydrophobicity for highly efficient transformations of glycerol. **Catalysis Science & Technology**, v. 6, p. 875–881, 2016.

LIMA, E. *et al.* Fluorinated Hydrotalcites: The Addition of Highly Electronegative Species in Layered Double Hydroxides To Tune Basicity. **Inorganic Chemistry**, v. 51, p. 7774–7781, 2012.

LIU, Q. *et al.* Basicities and transesterification activities of Zn-Al hydrotalcites-derived solid bases. **Green Chemistry**, v. 16, p. 2604–2613, 2014.

MARQUES, F. L. *et al.* Synthesis of lactic acid from glycerol using a Pd / C catalyst. **Fuel Processing Technology**, v. 138, p. 228–235, 2015.

MARTIN, A.; RICHTER, M. Oligomerization of glycerol – a critical review. **European Journal of Lipid Science and Technology**, v. 113, n. 1, p. 100–117, 2011.

MEHER, L. C. *et al.* Catalytic Hydrogenolysis of Glycerol to Propylene Glycol over Mixed Oxides Derived from a Hydrotalcite-Type Precursor. **Ind. Eng. Chem. Res.**, v. 48, p. 1840–1846, 2009.

MITTA, H. *et al.* Efficient Vapor-Phase Selective Hydrogenolysis of Bio-Levulinic Acid to γ -Valerolactone Using Cu Supported on Hydrotalcite Catalysts. **Global Challanges**, v. 2, p. 1–12, 2018.

MONTEIRO, M. R. *et al.* Glycerol from biodiesel production : Technological paths for sustainability. **Renewable and Sustainable Energy Reviews**, v. 88, p. 109–122, 2018.

PADMASRI, A. H. *et al.* Calcined Mg – Al , Mg – Cr and Zn – Al hydrotalcite catalysts for tert -butylation of phenol with iso -butanol — a comparative study. **Journal of Molecular Catalysis A: Chemical**, v. 188, p. 255–265, 2002.

PARIDA, K.; DAS, J. Mg /Al hydrotalcites: preparation , characterisation and ketonisation of acetic acid. **Journal of Molecular Catalysis A: Chemical**, v. 151, p. 185–192, 2000.

PAVEL, O. D. *et al.* The activity of Mg / Al reconstructed hydrotalcites by ‘‘ memory effect ” in the cyanoethylation reaction. **Catalysis Communications**, v. 9, p. 1974–1978, 2008.

PÉREZ-BARRADO, E. *et al.* Influence of acid–base properties of calcined MgAl and CaAl layered double hydroxides on the catalytic glycerol etherification to short-chain polyglycerols. **Chemical Engineering Journal**, v. 264, n. 2014, p. 547–556, 2015.

PÉREZ-RAMÍREZ, J. *et al.* Magnetic properties of Co-Al, Ni-Al, and Mg-Al

hydrotalcites and the oxides formed upon their thermal decomposition. **Journal of Materials Chemistry**, v. 12, n. 8, p. 2370–2375, 2002.

PÉREZ-RAMÍREZ, J.; ABELLÓ, S.; PERS, N. M. VAN DER. Memory Effect of Activated Mg – Al Hydrotalcite : In Situ XRD Studies during Decomposition and Gas-Phase Reconstruction. **Chemistry European Jounal**, v. 13, p. 870–878, 2007.

POLO-GARZON, F.; WU, Z. Acid–base catalysis over perovskites: a review. **Journal of materials chemistry A**, v. 6, p. 2877–2894, 2018.

POPOVA, M. *et al.* Glycerol acetylation supported sulphated zirconia catalysts. **Catalysis Science & Technology**, v. 4, p. 3993–4000, 2014.

PRAKRUTHI, H. R.; PRAKASH, B. S. J.; BHAT, Y. S. Journal of Molecular Catalysis A : Chemical Microwave assisted synthesis of glycerol carbonate over LDH catalyst : Activity restoration through rehydration and reconstruction. **"Journal of Molecular Catalysis. A, Chemical"**, v. 408, p. 214–220, 2015.

REYERO, I. *et al.* Structured catalysts based on Mg – Al hydrotalcite for the synthesis of biodiesel. **Catalysis Today**, v. 216, p. 211–219, 2013.

RICHTER, M. *et al.* Homogeneously catalyzed batch reactor glycerol etherification by CsHCO 3. **Catalysis Communications**, v. 9, n. 2008, p. 2112–2116, 2008.

ROUQUEROL, J. *et al.* **Adsorption by powders and porous solids: principles, methodology and applications**. 2nd. ed. London: Academic Press, 2013.

RUPPERT, A. M. *et al.* Glycerol Etherification over Highly Active CaO-Based Materials : New Mechanistic Aspects and Related Colloidal Particle Formation. **Chemistry European Jounal**, p. 2016–2024, 2008.

SANCHO, C. G. *et al.* Influence of the niobium supported species on the catalytic dehydration of glycerol to acrolein. **Applied Catalysis B, Environmental**, v. 179, n. 2015, p. 139–149, 2015.

SAYOUD, N. *et al.* Homogeneously-acid catalyzed oligomerization of glycerol. **Green Chemistry**, v. 17, p. 4307–4314, 2015.

SHARMA, S. K.; PARIKH, P. A.; JASRA, R. V. Reconstructed Mg / Al hydrotalcite as a solid base catalyst for synthesis of jasminaldehyde. **Applied Catalysis A, General**, v. 386, n. 1–2, p. 34–42, 2010.

SHI, P. *et al.* Influence of calcination temperature on the catalytic performance of Co3O4/GO nanocomposites for Orange II degradation. **RSC Advances**, v. 5, p. 34125–34133, 2015.

SIVAIAH, M. V. *et al.* Recent developments in acid and base-catalyzed etherification of glycerol to polyglycerols. **Catalysis Today**, v. 198, n. 1, p. 305–313, 2012.

SONAR, S. K. *et al.* Solvent free acetalization of glycerol with formaldehyde over hierarchical zeolite of BEA topology. **Environmental Progress & Sustainable Energy**, v. 37, p. 797–807, 2017.

STARUKH, G.; ROZOVIK, O.; ORANSKA, O. Organo / Zn-Al LDH nanocomposites for cationic dye removal from aqueous media. **Nanoscale Research Letters**, v. 11, p. 228, 2016.

STEFANUS, F. *et al.* CaO-catalyzed synthesis of glycerol carbonate from glycerol and dimethyl carbonate : Isolation and characterization of an active Ca species. **Applied Catalysis A, General**, v. 401, n. 1–2, p. 220–225, 2011.

SUTTER, M. *et al.* Glycerol Ether Synthesis : A Bench Test for Green Chemistry Concepts and Technologies. **Chemical Reviews**, v. 115, n. 16, p. 8609–8651, 2015.

TAKEHIRA, K. Recent development of layered double hydroxide-derived catalysts − Rehydration , reconstitution , and supporting , aiming at commercial application −. **Applied Clay Science**, v. 136, p. 112–141, 2017.

THOMAS, G. S. *et al.* Thermally induced polytype transformations among the layered double hydroxides (LDHs) of Mg and Zn with Al. **J. Phys. Chem. B**, v. 110, p. 12365–12371, 2006.

TODOROVA, S. *et al.* Complete n -hexane oxidation over supported Mn – Co catalysts. **Applied Catalysis B : Environmental**, v. 94, p. 46–54, 2010.

WANG, Y. *et al.* Synergistic effect between strongly coupled CoAl layered double hydroxides and graphene for the electrocatalytic reduction of oxygen. **Electrochimica Acta**, v. 192, p. 196–204, 2016.

XABA, T. *et al.* Synthesis and characterization of cubic structured cobalt oxide nanoparticles capped with topo through the decomposition of Bis(N-Cyclohexyl-1-Naphtaldeydato) Cobalt (II) complex as a single source precursor. **Digest Journal of Nanomaterials and Biostructures**, v. 13, n. 4, p. 1141–1147, 2018.

YIN, W. *et al.* Oxide perovskites , double perovskites and derivatives for electrocatalysis, photocatalysis and photovoltaics. **Energy & Environmental Science**, 2018.

ZAJIC, J. Polyglycerol, IV." Kinetics of the polymerisation of glycerol. **Sbornik Vysoké Skoly Chemicko-Technologické V Praze**, v. 9, p. 91–101, 1966.

ZĂVOIANU, R. *et al.* Comparison between Me II Mg / Al hydrotalcites and hydrotalcite-supported Me (II) acetylacetonates (Me (II) = Co , Cu or Ni) catalysts for the epoxidation of cyclohexene with molecular oxygen. **Applied Clay Science**, v. 52, n. 2011, p. 1–10, 2010.

ZENG, J. H. *et al.* Monodispersed nanocrystalline fluoroperovskite up-conversion phosphors. **Crystal Growth & Design**, v. 7, p. 2774–2772, 2007.

ZHANG, X. *et al.* Catalytic behavior of combine oxides derived from Mg / Al x Fe 1 − x – Cl layered double hydroxides for H2S selective oxidation. **Catalysis Science & Technology**, v. 5, p. 4991–4999, 2015.

ZHOU, C.-H. C. *et al.* Chemoselective catalytic conversion of glycerol as a biorenewable source to valuable commodity chemicals. **Chemical Society Reviews**, v. 37, n. 3, p. 527–49, 2008.